Chapter 3A

A SERIES OF PIVALIC ACID BASED MULTI-COMPONENT SYSTEMS – GELATION BEHAVIOR, SOLVENT PARAMETER STUDY AND TEMPLATE DIRECTED NANOPARTICLE SYNTHESIS

Partially published in *Journal of Molecular Liquids*, 322 (2021) 114520.

3.1 INTRODUCTION

Two-component supramolecular gelators, a member of the vast family of LMOGs, represent a special position in the ever-growing list of compounds displaying gelation properties, mainly due to: (i) simplicity of the system to understand the mechanism of gelation, especially when the number of non-bonded contacts are limited (ii) multiple functionalities can be envisaged in a single system by suitable choice of individual components and (iii) crystal engineering approach can be applied successfully to design a new two-component gelator.[1–3] They offer an edge in terms of designing and manipulating the self-assembly process by providing exquisite tunability and control – which is impossible in conventional one-component systems.[4] That is because, a simple variation of one of the components can significantly modify the gelation behavior of a known gelator species. This corresponds to structural modification in either of the components and enables the introduction of functional behavior in the self-assembly of nanostructured materials.

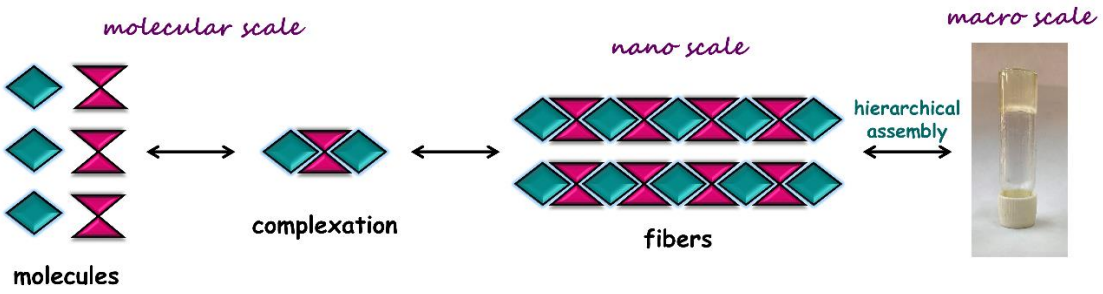

Figure 3.1 An illustration of the self-assembly of two-component gels

In a first, Hanabusa and coworkers reported a two-component gel based on the interaction of barbituric acid and pyrimidine units and introduced the concept of self-assembly of small molecules.[5] This study further inspired many research groups worldwide and led to the discovery of many well-known two-component gelators. Since then, various types of such systems have been reported based on acid-amine systems[6], cholesterol derivatives[7], ester linkages[8], host-guest interactions[9], donor-acceptor interactions[10], etc.

In recent years, crystal engineering has been proved to be an inevitable tool for designing new gelators, using the concept of supramolecular synthons.[11–13] Crystal engineering strategy can help us to design a molecule with a preferential 1-D hydrogen bonded network, a prerequisite for supramolecular gelation. This happens to be one of the *a priori* rules which has led to the development of many organogelators with the assistance of X-ray crystallography. The anisotropic growth of molecular assemblies results in the formation of a continuous network of ribbons, fibers, rods, tubes, etc.[14–16] which further entangle among themselves through weak non-covalent interactions forming a three-dimensional network, thereby trapping bulk solvents, as a result of capillary forces and surface tension. In that regard, a combination of single crystal X-ray diffraction and powder X-ray diffraction techniques can be successfully employed to obtain atomic-level resolution of the SAFiN structure.[17] If the theoretically determined/simulated X-ray diffraction pattern obtained from single crystal structure matches with the experimentally determined powder pattern, we can confirm the molecular packing of the gelator in its crystalline form and SAFiN form.

3.2 BACKGROUND

We decided to work with simple two-component systems possessing the potential to show supramolecular gelation. Surprisingly, a simple acid molecule of *tert*-butyl carboxylic acid (pivalic acid), which lacks long aliphatic chain, but has multiple methyl groups that can induce steric hindrance and may contribute to various weak non-bonded interactions such as C-H…O, C-H…N, C-H…π, etc. has never been considered for supramolecular gelation studies. However, few pivalic acid salts have been reported in the literature due to its interesting hydrogen bonded network, and surprisingly, their gelation property was never explored.[18,19]

Primary ammonium monocarboxylate (PAM) salts have been known to show well-defined 1-D hydrogen bonded networks (Synthon 1) or 0-D (Synthon 2), which may be extended to 2-D due to additional non-bonded contacts such as C-H…O, C-H…N. etc. (Scheme 3.1). Furthermore, the salts of monocarboxylic acid with primary diamines may form 0-D charge assisted hydrogen bonded networks (Synthon 3, Scheme 3.1) that can be extended to 1-D by suitable choice of a functional group on acid/amine.

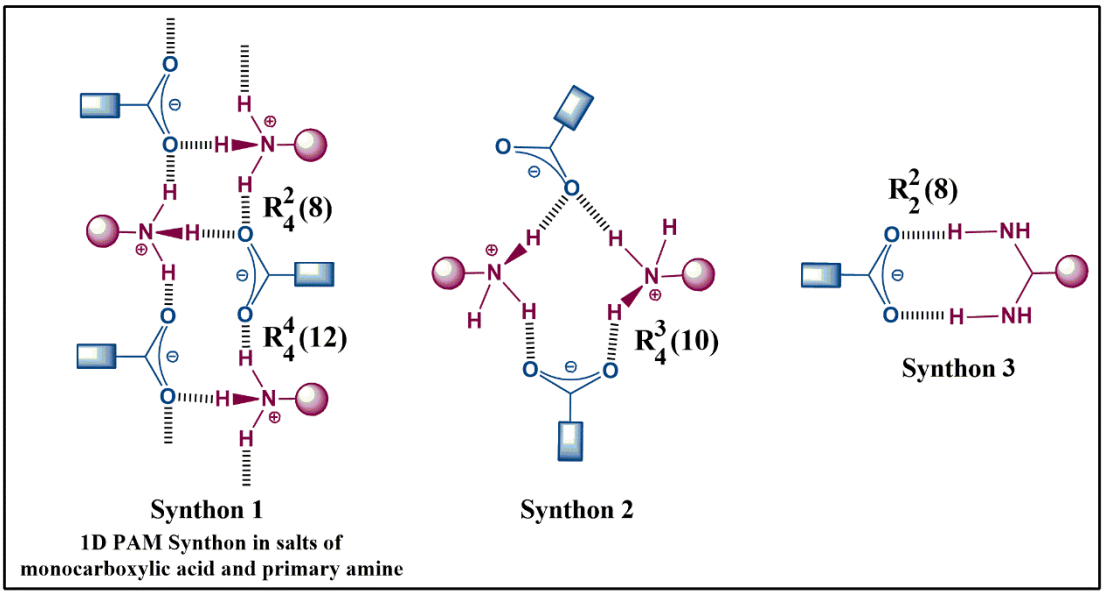

Scheme 3.1 Probable binding modes of Hydrogen bonding in PAM species

In the present work, a series of organic salts were designed and synthesized based on pivalic acid (**A1**) and primary amines (with aliphatic, alicyclic, and aromatic backbones) (**B1-B13**) to discover a new class of organogelators. Interestingly, out of 13 salts synthesized, 10 turned out to be organogelators. It was found that all the compounds chosen for this study (**A1**, **B1-B13**) were not capable of gelation in their own right, which proves that the acid-base complex formation was solely responsible for gelation behavior. We also directed our efforts to grow single crystals of these salts to understand their hydrogen bonding patterns and probe the mechanism of supramolecular gelation/non-gelation from the crystal engineering approach.

Additionally, supramolecular synthons present in the salts were assigned graph set representations to recognize, identify and quantify the hydrogen bonded networks.[20] Hirshfeld surface analysis were carried out on all crystal structures to compute the contribution of various non-covalent interactions present in them towards the stability and overall packing in the crystalline state.[21] To probe the correlation between packing of molecules in the thermodynamically stable crystalline state and semi-solid gel phase, various physicochemical techniques were employed such as FT-IR, NMR, Powder X-ray diffraction (PXRD), Scanning Electron Microscopy (SEM), etc. We have also tried to probe the role of solvent parameters such as dielectric constant, Hildebrand parameter, Hansen parameters, Kamlet-Taft parameters, etc. on the gel phase to get

complete idea about the role of solute and solvent molecules and their interactions on supramolecular gelation.

Surprisingly, the gelator fibers of **A1B12** in acetonitrile displayed rectangular fibers with well-defined pores, which prompted us to explore the application of the gel phase as a template for nanoparticle synthesis, where UV irradiation of gel sample containing silver salt led to the formation of silver metal nanoparticles with a size of approx. 38 nm.

3.3 EXPERIMENTAL PROCEDURES

3.3.1 Synthesis

3.3.1.1 Synthesis of salts A1B1-A1B13

All the salts were synthesized by refluxing pivalic acid and amine taken in equimolar amounts ((1:1) and (2:1) for diamine) in methanol for 1 hour (Scheme 3.2). The solutions were then kept at RT (25ºC) for few days so that slow evaporation of solvent could lead to formation of crystalline solids. These compounds were then kept for recrystallization in various solvents. The salts so obtained were subjected to various physico-chemical techniques (NMR, FT-IR), single crystal X-ray diffraction studies and gelation trials.

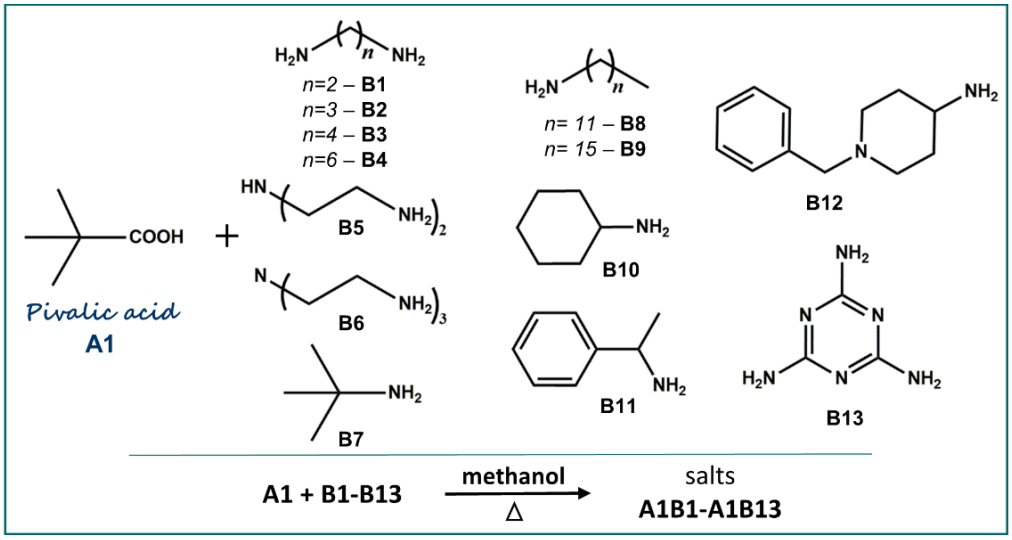

Scheme 3.2 Salts A1B1-A1B13 synthesized using pivalic acid and various amines

3.3.1.2 Synthesis of nanoparticles

Silver nanoparticles were synthesized by the simple method of reduction of silver salts using UV radiation. 1 mL aqueous solution containing 2 mg silver nitrate was added to 1 mL solution of acetonitrile and compound **A1B12** (75 mg) in a quartz cuvette and gently heated. After the formation of stable colorless gel at room temperature, it was irradiated with a mercury vapor UV lamp at 125 W for 1 hour. A visible color change from colorless to dark brown in the gel containing silver nanoparticles was observed.

3.3.2 Gelation trials

All the salts were tested for their gelation behavior in various solvents of different polarities. 50 mg of sample of was taken in a glass vial to which solvent was added gradually and the vial heated in a temperature-controlled water bath till the solute dissolved completely. The solution was cooled to room temperature (~25ºC) and allowed to stand overnight. The gel formation was confirmed by inverted vial method. The solvent was added till no more gelation was exhibited by the system.

T_{gel} (gel-to-sol conversion temperature) was also measured using the same inverted vial method. The vials containing the gels were heated in a temperature-controlled water bath at a steady rate of 0.5°C/min. The temperature at which first drop of gel melted was considered as $T_{gel.}$

3.3.3 Materials and Methods

All the chemicals were obtained from Sigma Aldrich and TCI and the solvents were obtained from SD Fine Chemicals, India and were used without any further purification.

3.3.3.1 NMR studies

NMR data was recorded on BRUKER AVANCE, 400 MHz spectrometer in $CDCl_3$ or DMSO-d6 with TMS as internal standard. The ^1H NMR spectra of all compounds can be found in Supplementary Data* at the end of the chapter.

3.3.3.2 FT-IR studies

FT-IR studies were performed on Bruker Alpha FT-IR spectrometer. The solid sample was ground together with anhydrous KBr using mortar pestle and the pellet so formed

was subjected to FT-IR analysis. The FT-IR spectra of all compounds can be found in Supplementary Data* at the end of the chapter. Comparative FT-IR spectra of samples in gel and solution phase (with acetonitrile as solvent) were recorded using CaF_2 discs.

3.3.3.3 Single crystal X-ray diffraction

Single crystal diffraction data for all compounds was collected on an Xcalibur, EOS, Gemini diffractometer with graphite monochromatic Mo Kα radiation (0.71073 Å). All structures were solved and refined using the Olex2[22] software and ShelXL[23] refinement package. Graphics were generated using MERCURY (version 4.3.1). All structures were solved by direct methods and refined in a regular pattern. In all the cases, non-hydrogen atoms were treated anisotropically. Whenever possible, the hydrogen atoms were refined by locating on a difference Fourier map. In other cases, hydrogen atoms were geometrically fixed. The crystallographic parameters and H-bond parameters are listed in Tables S3.1* and S3.2*.

3.3.3.4 Hirshfeld surface analysis

The 3D Hirshfeld surfaces[24,25] and two-dimensional Hirshfeld fingerprint plots of all the salts were obtained using Crystal Explorer 3.1[26,27] software. Intermolecular interaction energies of the salts were also measured for CE-HF model with HF/3-21G basis sets.

3.3.3.5 Polarizing Optical Microscopy studies

POM analyses were performed using LEICADM2500P polarizing microscope. Images were captured using LEICADFC295 camera which is attached with the instrument. Thin layer of gel was formed on glass slide and allowed to dry, forming xerogel whose images were captured.

3.3.3.6 SEM of gels

The samples for SEM were prepared by gently spreading the gel on the SEM stubs and freezing them under liquid nitrogen. These frozen gel samples were used directly for the viewing images using JEOL JSM-5610LV Scanning Electron Microscope instrument.

3.3.3.7 SEM of nanoparticles

The Ag nanoparticles were used to obtain a surface view using JEOL-JSM 7600F FEG-SEM instrument.

3.3.3.8 Rheology

Rheology studies of **A1B9** were performed on an Anton Paar MCR 102 Modular Compact Rheometer at 38°C. The instrument has a parallel plate geometry with a plate diameter of 50 mm, maintained at a gap of 0.5 mm; the gel samples were subjected to oscillatory amplitude sweep range of 0 to 100 rad/s and values of G' (storage modulus) and G" (loss modulus) were evaluated.

3.3.3.9 Powder X-ray diffraction studies

Powder diffraction patterns of bulk (crystalline) gelator and xerogel (Acetonitrile, slowly evaporated) of **A1B10-A1B12** were recorded on an XPERT (Cu Kα radiation, λ = 1.54056 Å) diffractometer on a continuous scanning mode at 2θ value 5-50^{o}. The silver nanoparticles recovered from the template of **A1B12** gel were also subjected to powder diffraction studies (2θ = 4-80^{o}) using the same instrument.

3.3.3.10 DLS (Dynamic Light Scattering) of nanoparticles

DLS studies were performed using BIC 90 plus Brookhaven instrument with a photodiode detector.

3.3.3.11 DRS (Diffuse Reflectance Spectroscopy) study of nanoparticles

The sample for DRS study was prepared by drying and calcining the gel containing silver nanoparticles at 200°C.

The powder was mixed with $BaSO_4$ and the spectrum was recorded using Perkin Elmer UV-Visible Spectrometer.

3.3.4 Analytical Data

The salt formation was confirmed by Fourier Transform-Infra Red spectroscopy (FT-IR). All the synthesized salts showed characteristic bands for C=O stretching of carboxylate groups at (1690–1740 cm^{-1}), (1400–1450 cm^{-1}) indicating the formation of carboxylate salts of pivalic acid and N-H stretch at (2700-2200 cm^{-1}), (3500-3300 cm^{-1}) indicating formation of primary ammonium cations for the respective bases.

A comparative study of bulk and xero gels was also carried out using FT-IR was carried out (Section 3.4.7). The FT-IR spectra of all salts were found to be nearly matching with those of bulk indicating that the chemical nature of all the salts was retained after gel formation.

The ^{1}H NMR studies also confirmed salt formation.

Compound A1B1 (ethan-1,2-diaminium pivalate). M.P.= 68°C, ^{1}H NMR (400 MHz, DMSO-d6, TMS) = δ (ppm) 3.989 (NH), δ 2.669 (*s*, 2H, CH_2), δ 1.062 (*s*, 9H, 3(CH_3)) x2.

FT-IR, cm^{-1} (KBr) – 3415, 3292, 2950, 2164, 1620, 1557, 1406, 1365, 1325, 1223, 1156, 1132, 1111, 1027, 884, 794, 593, 530.

Compound A1B2 (propan-1,3-diaminium pivalate). M.P.= 155°C, ^{1}H NMR (400 MHz, DMSO-d6, TMS) = δ (ppm) 4.8 (NH), δ 2.749 (*s*, 4H, 2(CH_2)), δ 1.697 (*s*, 2H, CH_2), δ 1.026 (*s*, 18H, 2 x 3(CH_3)).

FT-IR, cm^{-1} (KBr) – 3419, 2955, 2163, 1629, 1518, 1408, 1356, 1222, 1007, 884,796, 594, 533.

Compound A1B3 (butan-1,4-diaminium pivalate). M.P.= 200°C, ^{1}H NMR (400 MHz, DMSO-d6, TMS) = δ (ppm) 3.513 (*s*, 2H, CH_2), δ 2.748 (*s*, 2H, CH_2), δ 1.679 (*s*, 18H, 2 x 3(CH_3)), δ 1.536 (*m*, 2H, CH_2), δ 1.270 (*m*, 4H, 2(CH_2)).

FT-IR, cm^{-1} (KBr) – 3423, 2955, 2182, 1631, 1533, 1481, 1405, 1355, 1222, 1042, 883, 796, 772, 735, 593, 537, 453.

Compound A1B4 (hexan-1,6-diaminium pivalate). M.P.= 194°C, ^{1}H NMR (400 MHz, DMSO-d6, TMS) = δ (ppm) 2.195 (*s*, 4H, 2(CH_2)), δ 1.699 (*s*, 18H, 2 x 3(CH_3)), δ 1.271 (*m*, 8H, 4(CH_2)).

FT-IR, cm^{-1} (KBr) – 3420, 2953, 2178, 1633, 1539, 1409, 1365, 1221, 1156, 1088, 1003, 885, 839, 795, 729, 594, 535.

Compound A1B5 (2,2'-azanediyldiethanaminium pivalate). M.P.= 85°C, ^{1}H NMR (400 MHz, $CDCl_3$, TMS) = δ (ppm) 6.491 (2H, NH), δ 3.393 (*t*, 4H, 2(CH_2)), δ 2.005 (*s*, 9H, 3(CH_3)).

FT-IR, cm^{-1} (KBr) – 3258, 3195, 3036, 2491, 1905, 1681, 1570, 1444, 1371, 1334, 1279, 1223, 1173, 1069, 986, 880, 769, 713, 515.

Compound A1B6 (2,2',2''-nitrilotriethanaminium pivalate). M.P.= 160°C, ^{1}H NMR (400 MHz, $CDCl_3$, TMS) = δ (ppm) 2.196 (*s*, 6H, 3(CH_2)), δ 1.776 (*s*, 6H, 3(CH_2)), δ 1.268 (*s*, 9H, 3(CH_3)), δ 1.137 (*s*, 9H, 3(CH_3)), δ 1.043 (*s*, 9H, 3(CH_3)).

FT-IR, cm^{-1} (KBr) – 3422, 2956, 2921, 2361, 2168, 1632, 1561, 1411, 1357, 1222, 1099,884, 796, 533.

Compound A1B7 (2-methyl propan-2-aminium pivalate). M.P.= 55°C, ^{1}H NMR (400 MHz, $CDCl_3$, TMS) = δ (ppm) 5.728 (NH), δ 1.312 (*s*, 9H, 3(CH_3)), δ 1.16 (*s*, 9H, 3(CH_3)).

FT-IR, cm^{-1} (KBr) – 2976, 2632, 2550, 2207, 2019, 1633, 1404, 1315, 1225, 1025, 934, 883, 795, 592, 535, 470.

Compound A1B8 (dodecan-1-aminium pivalate). M.P.= 38°C, ^{1}H NMR (400 MHz, $CDCl_3$, TMS) = δ (ppm) 6.704 (3H, NH), δ 2.797-2.758 (*t*, 2H, CH_2), δ 2.635-1.580 (*m*, 2H, CH_2), δ 1.287-1.254 (*d*, 18H, 9(CH_2)), δ 1.117 (*s*, 9H, 3(CH_3)), 0.902-0.869 (*t*, 3H, CH_3).

FT-IR, cm^{-1} (KBr) – 3425, 2924, 2854, 2180, 1631, 1530, 1482, 1407, 1362, 1220, 1084, 1026, 885, 796, 771, 722, 594, 534.

Compound A1B9 (hexadecan-1-aminium pivalate). M.P.= 40°C, ^{1}H NMR (400 MHz, $CDCl_3$, TMS) = δ (ppm) 6.321 (3H, NH), δ 2.798-2.759 (*t*, 2H, CH_2), δ 2.187 (*s*, 2H, CH_2), δ 1.633-1.577 (*m*, 2H, CH_2), δ 1.291-1.256 (*d*, 23H, 12(CH_2)), δ 1.125 (*s*, 9H, 3(CH_3)), 0.906-0.872 (*t*, 3H, CH_3).

FT-IR, cm^{-1} (KBr) – 3430, 2919, 2851, 2607, 2361, 2181, 1630, 1530, 1482, 1407, 1363, 1220, 1080, 885, 796, 721, 594, 534.

Compound A1B10 (cyclohexyl aminium pivalate). M.P.= 175°C, ^{1}H NMR (400 MHz, $CDCl_3$, TMS) = δ (ppm) 6.130 (3H, NH), δ 2.882-2.828 (*m*, 2H, CH_2), δ 2.011-1.986 (*d*, 2H, CH_2), δ 1.797-1.766 (*t*, 2H, CH_2), δ 1.654-1.622 (*d*, 2H, CH_2), δ 1.363-1.207 (*m*, 4H, 2(CH_2)), δ 1.12 (*s*, 9H, 3(CH_3)).

FT-IR, cm^{-1} (KBr) – 3401, 2943, 2860, 2760, 2656, 2367, 2168, 1624, 1522, 1405, 1359, 1223, 1133, 1074, 1046, 883, 793, 590, 553, 450.

Compound A1B11 (1-phenylethanaminium pivalate). M.P.= 152°C, ^{1}H NMR (400 MHz, $CDCl_3$, TMS) = δ (ppm) 7.391-7.332 (*m*, 3H, 3(CH)), 7.300-7.257 (*m*, 2H, 2(CH)), δ 5.073 (*s*, 3H, NH), δ 4.223-4.172 (*m*, 1H, CH), δ 1.489-1.472 (*d*, 3H, CH_3), δ 1.158 (*s*, 9H, 3(CH_3)).

FT-IR, cm^{-1} (KBr) – 3430, 2958, 2867, 2555, 2190, 1608, 1566, 1520, 1404, 1361, 1220, 1148, 883, 796, 771, 700, 594, 532, 487.

Compound A1B12 (1-benzylpiperidin-4-aminium pivalate). M.P.= 72°C, ^{1}H NMR (400 MHz, $CDCl_3$, TMS) = δ (ppm) 7.346-7.296 (*m*, 4H, 4(CH)), 7.286-7.244 (*m*, 1H, CH), δ 4.517 (*s*, 3H, NH), δ 3.526 (*s*, 2H, CH_2), δ 2.914-2.802 (*m*, 3H, 3(CH)), δ 2.076-2.018 (*m*, 2H, 2(CH)), δ 1.902-1.876 (*d*, 2H, 2(CH)), δ 1.633-1.544 (*m*, 2H, 2(CH)), δ 1.210 (*s*, 9H, 3(CH_3)).

FT-IR, cm^{-1} (KBr) – 3291, 2658, 2232, 2027, 1826, 1643, 1567, 1480, 1404, 1316, 1216, 1133, 1053, 1020, 977, 930, 883, 843, 791, 738, 699, 631, 593, 537, 491, 462, 429.

Compound A1B13 (4,6-diamino-1,3,5-triazin-2-aminium pivalate). M.P >280°C, ^{1}H NMR (400 MHz, DMSO-d6, TMS) = δ (ppm) 5.994 (3H, 3(CH)), δ 3.505 (*s*, 3H, NH), δ 1.110 (*s*, 9H, 3(CH_3)).

FT-IR, cm^{-1} (KBr) – 3470, 3420, 3339, 3135, 1695, 1656, 1581, 1551, 1470, 1438, 1370, 1227, 1029, 814, 779, 606, 543, 464.

3.4 RESULTS AND DISCUSSION

All the salts were subjected to gelation tests in various solvents based on their polarity. Various solvents with varied polarities were utilized in gelation trials (Table 3.2) out of which, six solvents mainly yielded gelation.

Table 3.1 Classification of all salts according to their gelation/non-gelation behavior

Gelators	Non-gelators
A1B1-A1B3	**A1B4**
A1B5	**A1B6**
A1B8-A1B13	**A1B7**

3.4.1 Gelation studies and effect of amines on gelation

Out of all the salts synthesized in this study, ten salts turned out to be gelators. Compounds **A1B2** and **A1B10-A1B12** gave gels in maximum number of solvents (Table 3.1). Majorly, gels were observed in methanol, ethanol, acetone, DMSO, DMF and acetonitrile. Salts **A1B11** and **A1B12** gave gels in all six solvents. **A1B2** also gave gelation in *n*-butanol and **A1B13**, which is a salt of melamine and pivalic acid, turned out to be a good hydrogelator.

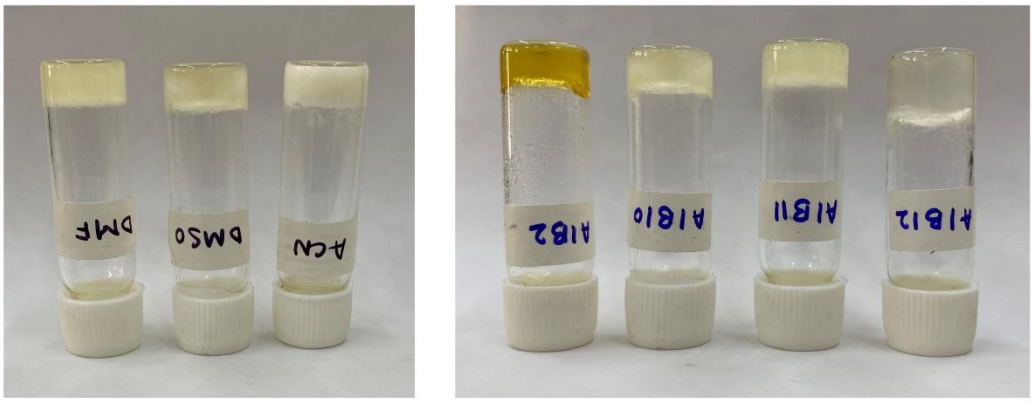

(a) (b)

Figure 3.2 (a) gels of A1B10 in different solvents, (b) clear DMSO gels of different compounds

Ethanol, DMF and DMSO were the most robust solvents in exhibiting gelation. Salts **A1B10-A1B12** gave stronger gels in acetonitrile, acetone, DMF and DMSO (with T_{gel} up to (~ 70°C) and mgc (minimum gelator conc.) ranging from 0.65-1 wt%.

Among **A1B1-A1B3**, it was discovered that **A1B2** could gel maximum number of solvents and the tendency to show gelation decreased with an increase in aliphatic chain length. **A1B1** and **A1B5** displayed better performance with methanol and ethanol. Among **A1B8** and **A1B9**, only the former showed gelation in DMSO as solvent, which coincides with the fact that a longer chain length could be detrimental to gelation performance.

Table 3.2 Solvents utilized in gelation trials; those in bold letters have given gelation for this series of compounds

Sr.	Solvent type	Nature	Solvents
1.	Oxygenated / Polar	Protic	**Water** **Methanol** **Ethanol** *iso*-propanol ***n*-butanol** *tert*-butanol propan-1,2-diol octan-2-ol decan-1-ol
		Aprotic	**Acetone** Ethyl acetate **Dimethyl Sulfoxide** **Dimethyl Formamide** **Acetonitrile** Tetrahydrofuran Diethyl ether Dibenzyl ether Diisopropyl ether
2.	Halogenated	Aprotic	Chloroform Dichloromethane Carbon tetrachloride
3.	Hydrocarbon		*n*-Hexane Cyclohexane *n*-Heptane *n*-Octane Decane Hexadecane Petrol Diesel Cooking oil Silicone oil Paraffin
4.	Aromatic		Toluene Chlorobenzene Nitrobenzene *m, p*-xylenes

It was carefully noted whether the gels were clear, translucent, or opaque in each solvent. We observed that clearer gels were obtained in DMF and DMSO, while solvents like acetone, acetonitrile, alcohols, and water gave opaque gels. Generally, opaque gels imply formation of larger aggregates/ stronger self-assembly, and low molecular weight gelators should be more inclined towards giving opaque gels as stronger interactions are required to immobilize the solvent molecules. However, clear gels might be a result of some specific solute-solvent interactions in the gel state, wherein some enhanced solvent-assisted forces might be causing this phenomenon.

Also, no gelation was observed in aromatic, hydrocarbon, and halogenated solvents.

Table 3.3 Gelation behavior of salts in various solvents

	ACN	Acetone	EtOH	MeOH	DMF	DMSO	*n*-BuOH	Water
A1B1	**S**	**S**	**G (1.1)**	**G (1.05)**	**S**	**S**	**S**	**I**
A1B2	**S**	**S**	**G (1.8)**	**G (2.0)**	**G (2.5)**	**G (2.3)**	**G (4.5)**	**I**
A1B3	**S**	**S**	**S**	**S**	**G (3.3)**	**G (2.9)**	**S**	**I**
A1B5	**I**	**I**	**G (1.17)**	**G (1.1)**	**S**	**S**	**S**	**I**
A1B8	**S**	**S**	**S**	**S**	**S**	**G (4.7)**	**S**	**I**
A1B9	**S**	**S**	**S**	**S**	**G (4.8)**	**G (4)**	**S**	**I**
A1B10	**G (0.65)**	**G (0.7)**	**G (1.3)**	**S**	**G (1.06)**	**G (1.05)**	**S**	**I**
A1B11	**G (0.7)**	**G (0.85)**	**G (1.4)**	**G (1.25)**	**G (1)**	**G (1)**	**S**	**I**
A1B12	**G (0.7)**	**G (0.8)**	**G (1.2)**	**G (1.2)**	**G (1)**	**G (1)**	**S**	**I**
A1B13	**I**	**I**	**I**	**I**	**I**	**I**	**I**	**G(5)**

G - gel, **S** - solution, **I** – insoluble.

Graph of T_{gel} vs. concentration was plotted for each gel (Figures 3.1, 3.2) which showed a gradual increase in the T_{gel} with increase in concentration, which proves that self-aggregation and stability of the supramolecular assembly increases with increase in gelator concentration.

Amines **B1-B3**, **B5**, **B8-B13** were capable of giving gelation, in a set of six solvents only. The gelation behavior was curbed by increasing the aliphatic chain length of the amine, majorly because of increase in the hydrophobicity of the system and such an architecture can hinder effective packing within the nanofibers. As the acid employed in the study itself consists of a bulky, aliphatic *tert*-butyl group, an increase in aliphatic chain length reduced the ability of the resultant salts to exhibit gelation behavior, as it

may have lacked the necessary balance between hydrophobic and hydrophilic interactions.

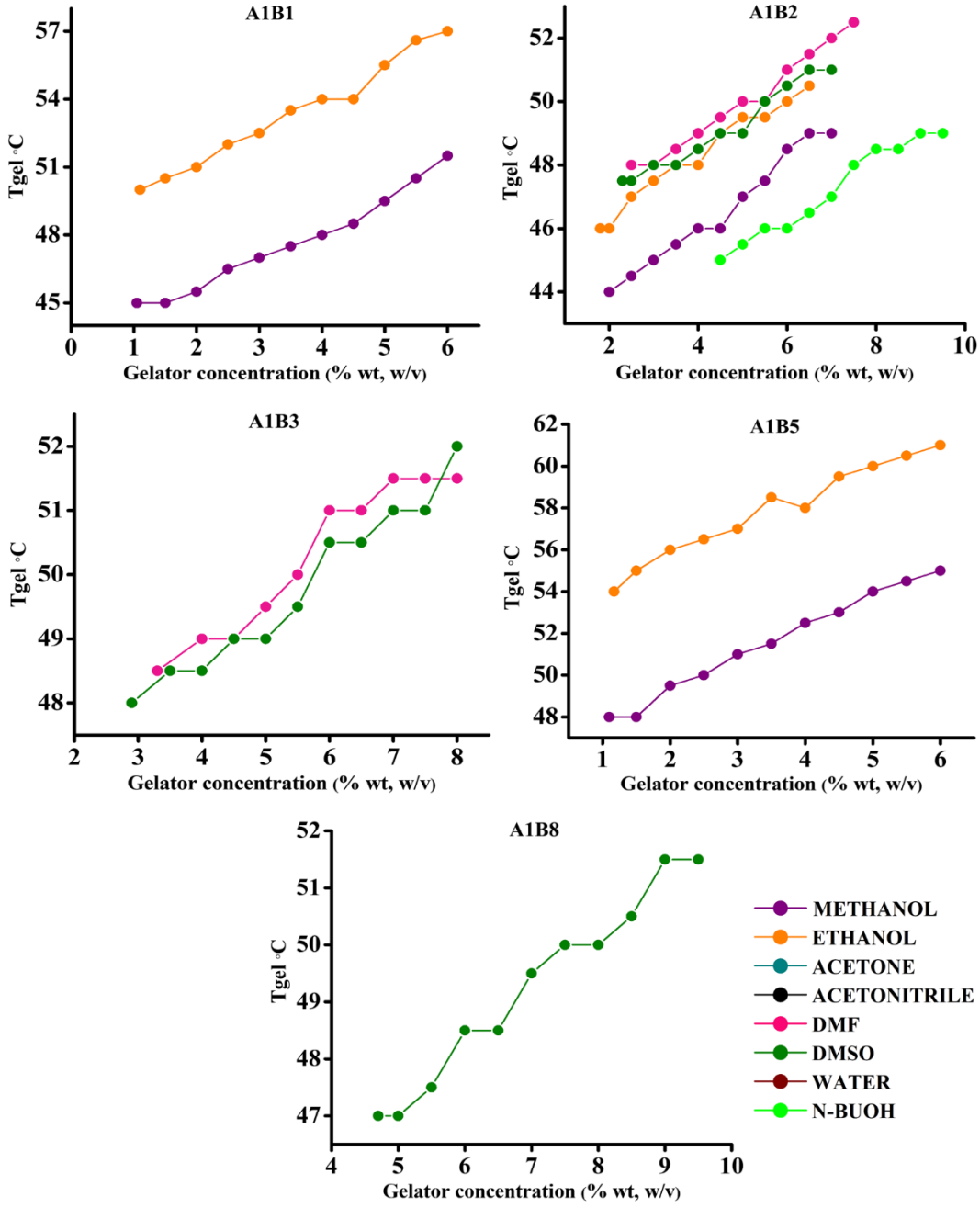

Figure 3.3 Effect of gelator concentration on gel-to-sol transition in various salts (I)

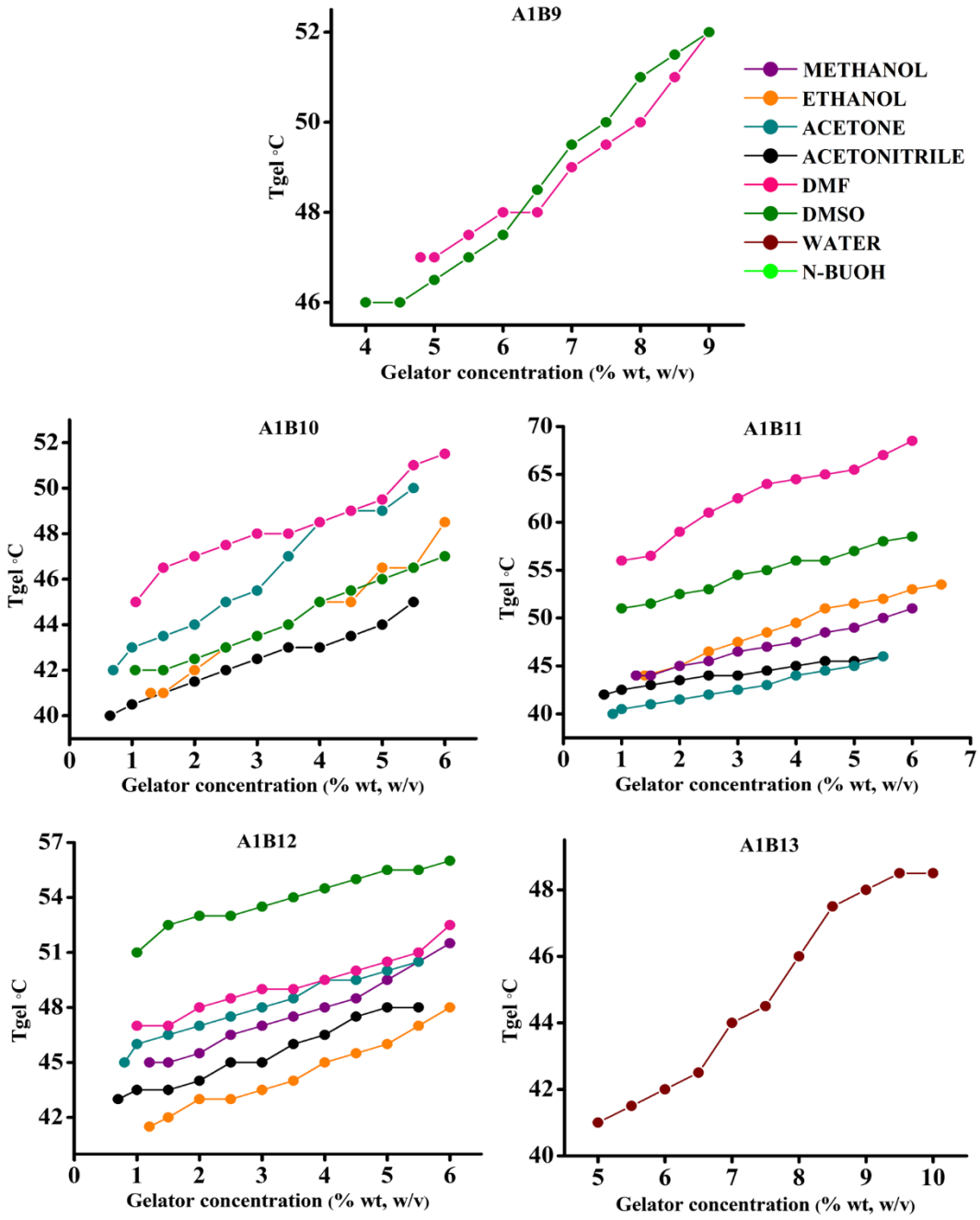

Figure 3.4 Effect of gelator concentration on gel-to-sol transition in various salts (II)

Fundamentally speaking, the process of gelation in multi-component acid-base systems begins with the proton transfer between the carboxylic acid and primary amine, which initiates the formation of hydrogen bonding interactions. These interactions, complemented by π-π interactions, van der Waals interactions and various solvophobic interactions lead to formation of 1D aggregates, which finally bundle up to trap solvents.

However, there can be fundamental differences in the mechanism of gelation in every different class of gelators and hence the optimal size of aliphatic chain to induce efficient gelation performance and the trends observed with increase/decrease in the hydrophobicity of any one component in such systems can be discreet for every new set of compounds.

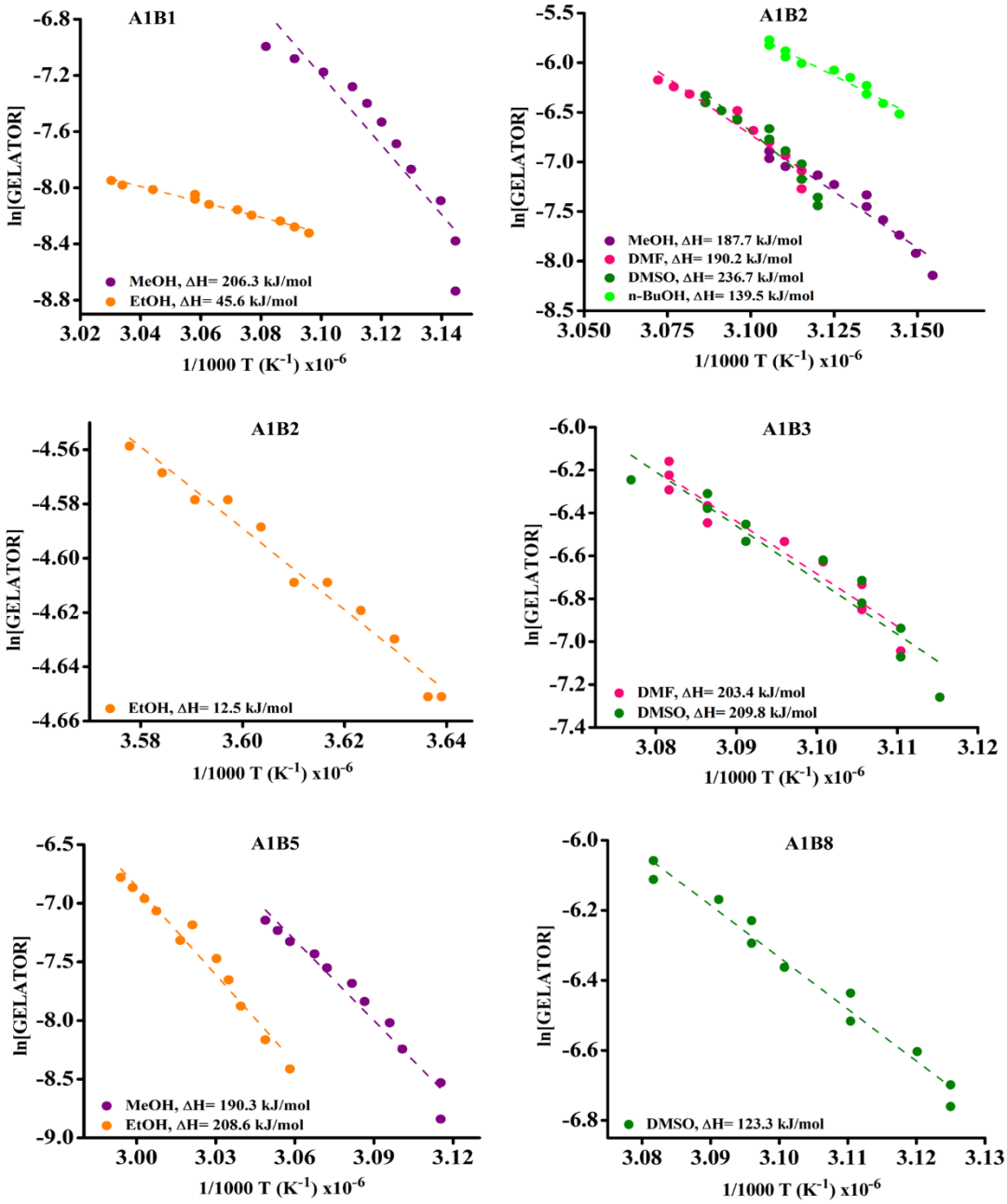

Figure 3.5 Semilog plots between the mole fractions of gelators against 1/1000T (K^{-1}) (I)

In this case, we believe that an increased chain length of amine drastically increased the hydrophobic interactions in the system, which caused less solubility and eventually, weaker gelation behavior. Salt of amine **B7**, which also contains a *tert*-butyl group did not give gelation, which further proves the above discussed hypothesis.

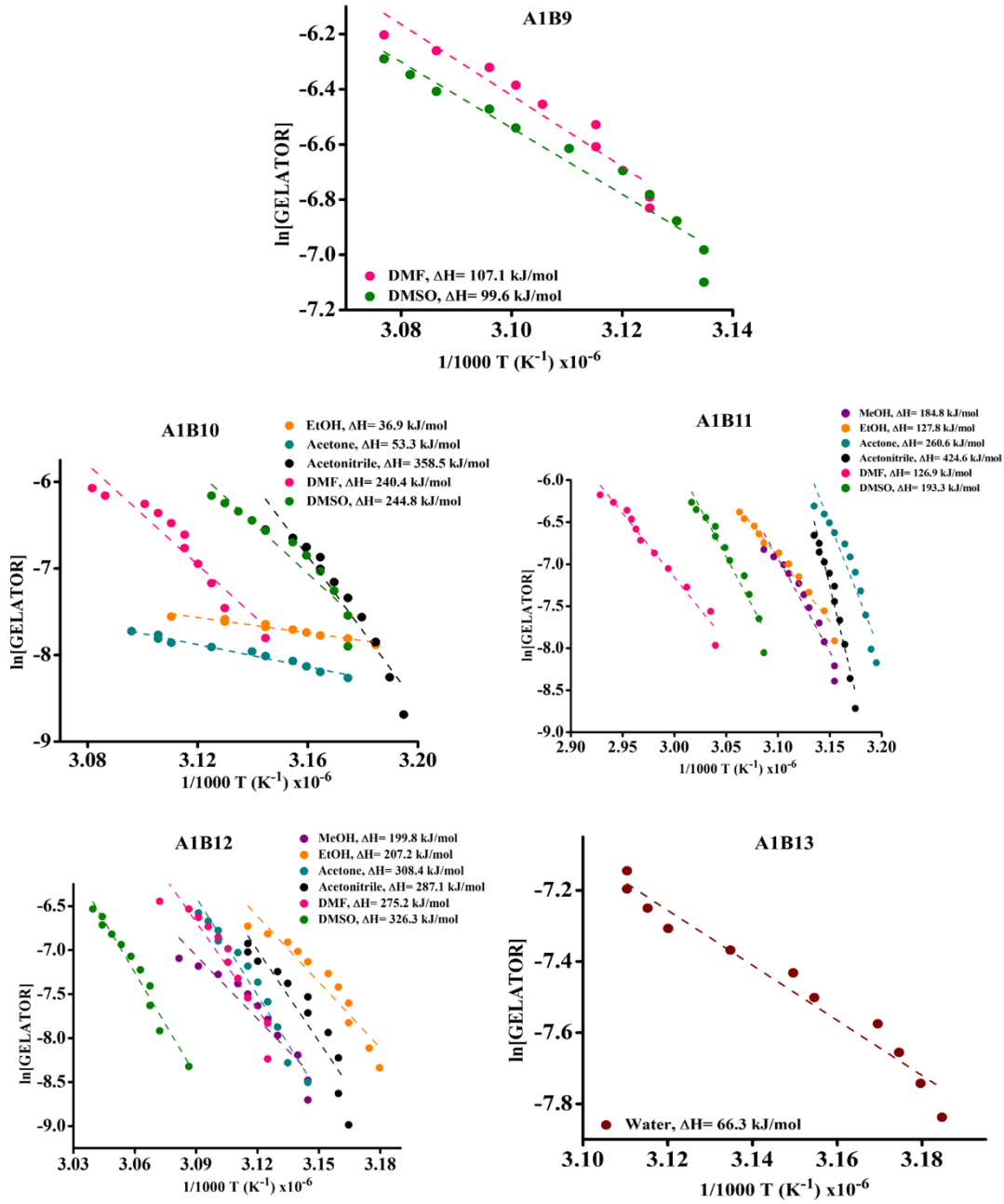

Figure 3.6 Semilog plots between the mole fractions of gelators against 1/1000T (K^{-1}) (II)

A semilog graph of mole fraction of gelator concentration was plotted against 1/1000 T_{gel} (K^{-1}) for every gel which gave a nearly linear relationship according to the Schroeder-van Laar equation- (equation 3.1) (Figures 3.5, 3.6)

$$\mathbf{ln[gelator]} = -\left(\frac{\mathbf{\Delta Hm}}{\boldsymbol{RT_{gel}}}\right) + \mathbf{constant} \qquad \text{- (3.1)}$$

where ΔH_m is the enthalpy of melting and T_{gel} is the transition temperature of gel-to-sol.

ΔH_m values calculated from the plots fell within a range of 12.5-424 kJ/mol. This further confirmed that the gel-to-sol transition can be considered a first order transition as the gel melts into a solution and a known amount of gelator is involved in the transition[28].

3.4.2 Solvent effects on gelation

It has been very well established that the properties of solvents appreciably affect the gel phase and supramolecular assembly of gelator molecules.[29] It is also known that each set of compounds can gel only a limited class of solvents. A variety of attractive and repulsive interactions can operate among the gelator and solvent molecules, and a detailed study of solvent parameters can be useful in providing an understanding of why only certain molecules can gel some specific solvents and others cannot. Solvent parameters have also been employed for in depth study of nanoscale assemblies, where different polymorphs of compounds could be grown from different systems. This phenomenon is not only dependent on solute-solvent interactions at molecular scale, but also on the macroscopic bulk properties of the solvent, like surface tension and viscosity. It is because of this complex interplay between numerous parameters, we cannot fix a single solvent parameter to predict the effect of solvent on the self-assembly process.

On these grounds, we decided to assess the correlation between gelation performance and solvent properties. We divided various solvent parameters (dielectric constant $\boldsymbol{\varepsilon}$, Normalized Dimroth-Reichardt parameter- $\boldsymbol{E_T^N}$, Hildebrand parameter- $\boldsymbol{\delta_0}$[30], Hansen parameters[31,32] and Kamlet-Taft parameters- $\boldsymbol{\alpha}$, $\boldsymbol{\beta}$, $\boldsymbol{\pi^*}$ [33]) into three categories and tried to correlate them with the thermal stability and gelation performance of the gel for salts **A1B10**, **A1B11** and **A1B12.**

Table 3.4 Bulk polarity parameters of solvents screened for gelation trials

Solvents	*Gel/ Sol*	*Bulk Polarity Scales*			
		ε	μ	n_D	*P'*
Methanol	G	32.7	2.87	1.33	5.1
Ethanol	G	25.7	1.66	1.36	5.2
Acetonitrile	G	37.5	3.44	1.34	5.8
Acetone	G	20.7	2.69	1.35	5.1
DMF	G	36.7	3.86	1.43	6.4
DMSO	G	46.7	4.1	1.48	7.2
Water	S	80.1	1.87	1.33	10.2
Isopropyl alcohol	S	19.9	1.66	1.37	3.9
n-butanol	S	17.8	1.66	1.39	3.9
Ethyl Acetate	I	6.02	1.88	1.37	4.4
THF	I	7.58	1.75	1.4	4.2
Diethyl ether	I	4.33	1.15	1.35	2.8
Chloroform	I	4.81	1.15	1.44	4.1
Dichloromethane	I	8.93	1.14	1.42	3.1
n-hexane	I	1.88	0.08	1.37	0
Toluene	I	2.38	0.31	1.49	2.3
Chlorobenzene	I	5.62	1.54	1.52	2.7
Nitrobenzene	I	-	-	1.55	-

Bulk physical polarity scales

This class characterizes the solvents by their bulk properties; these include the dielectric constant- ε, dipole moment- μ, refractive index- η_D and polarity index- ***P'***. The dielectric constant (also called static relative permittivity, ε) is the ratio of amount of electrical energy stored in a material by an applied voltage with respect to that stored in vacuum; the dipole moment- μ arises from non-uniform distribution of atomic charges in a system; the refractive index- η_D corresponds to the velocity of light in a particular solvent as compared to that in vacuum; and the value of polarity index- **P'** gives the degree of solvent-solute interaction.[34]

Although this class considers macroscopic properties of the solvent, utilizing these parameters alone can be insufficient in predicting gelation behavior. If the solvent is considered as a macroscopic continuum, characterized by single physical constant, those parameters may not specifically correlate with the self-assembly process.

The parameters employed for predicting gelation must consider the solvent as a discontinuous phase, consisting of individual, mutually interacting molecules. Various limitations have been proven in this regard, for e.g., the static relative permittivity (dielectric constant) is known to have lower value in the vicinity of a solute than in the bulk, because solvent dipoles in a solvation shell are more constrained.

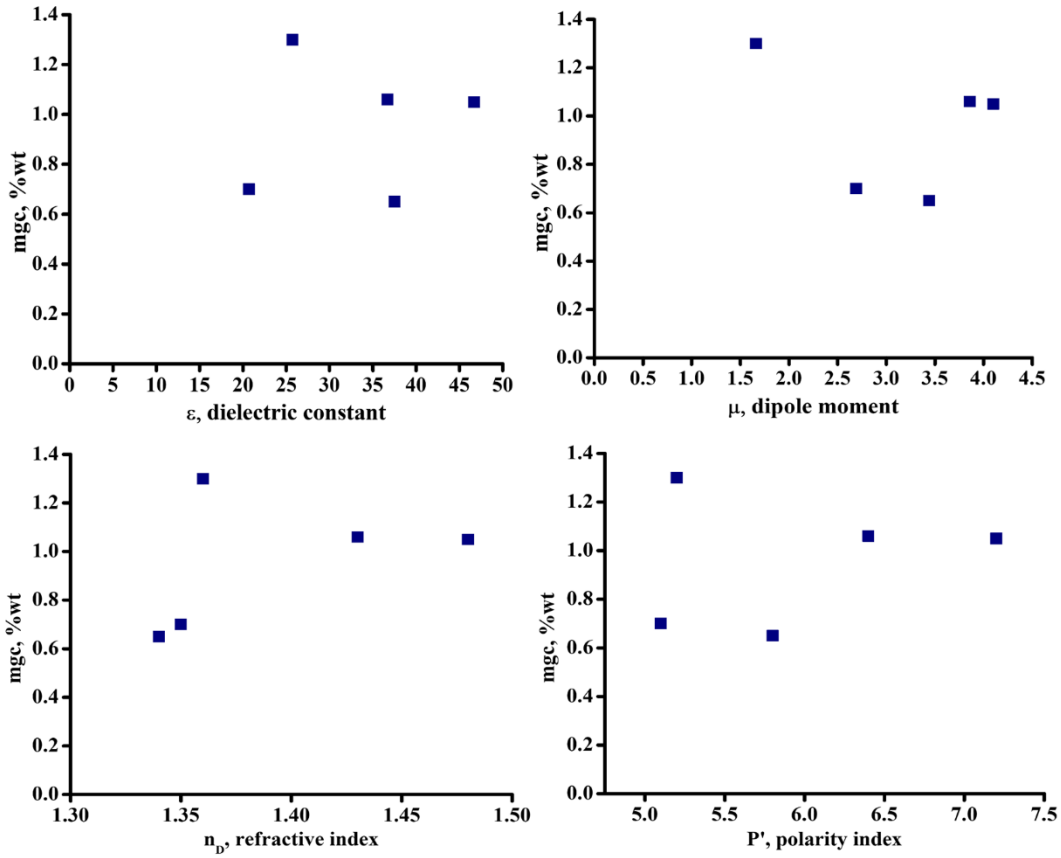

Figure 3.7 Variation of mgc values with dielectric constants, dipole moments, refractive indices and polarity indices of the solvents for salt A1B10

There have been reports where the polarity of the solvents gelled have been associated with the opacity/transparency of the gels formed; more polar solvents tend to form transparent gels in DBS (dibenzylidene sorbitol) based systems.[34] But even though, we cannot derive any insights into why the self-assembly is exhibited in certain solvents and not in others. The refractive index value is used to calculate its molar polarization, and both these parameters are dependent on the polarizability and molar mass of the solvent. So far, no concrete results have been obtained in the literature reports.

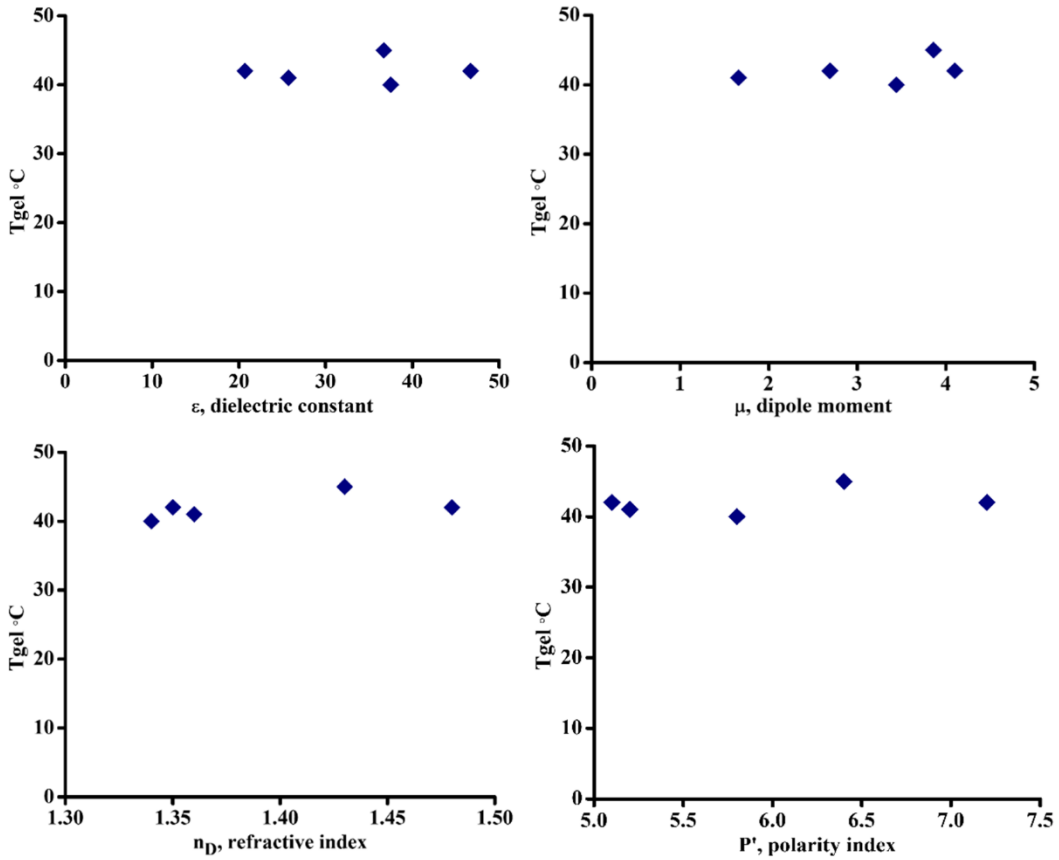

Figure 3.8 Variation of T_{gel} values with dielectric constants, dipole moments, refractive indices and polarity indices of the solvents for salt A1B10

The values of all bulk parameters along with their gelation performance are listed in Table 3.4. A careful examination of parameters for the solvents that gave gelation and the ones that did not, showed that gelation was favored for solvents with a polarity index (***P'***) value greater than 5.

The values of T_{gel} as well as the mgc plotted against all these parameters (Figures 3.7, 3.8, S3.1-S3.4*) gave a slight positive correlation with the T_{gel} values, while the mgc values appeared to be more in a random fashion.

Also, solvents with $\boldsymbol{\varepsilon}$ (dielectric constants) values above 30 favored gelation. This proves that bulk properties of solvents can somehow differentiate between gelation and non-gelation behavior.

Understandably, solvents with very low dielectric constant (low capacity to separate ions in solution) will supposedly form very rigid hydrogen bonded network of

molecules on account of less solubility and very high dielectric constant of solvent (like water) will be detrimental to the charge assisted hydrogen bonded network of molecules, making them too soluble. Therefore, an optimum value of dielectric constant and polarity index is a pre-requisite for gelation, especially in case of organic salts based gelators which primarily rely on the formation of charge assisted assemblies and their H-bonded networks to trigger gelation behavior.

Table 3.5 List of dielectric constants of various solvents employed in gelation trials

Solvent	Dielectric Constant	Solvent	Dielectric Constant
Water	80.1	Dichloromethane	8.93
DMSO	**46.7**	Decanol	8.1
Acetonitrile	**37.5**	Tetrahydrofuran	7.58
DMF	**36.7**	Ethyl Acetate	6.4
Nitrobenzene	**34.82**	Chlorobenzene	5.62
Methanol	**32.7**	Chloroform	4.81
Ethanol	**25.7**	Diethyl ether	4.33
Acetone	**20.7**	Toluene	2.38
iso-propanol	17.9	Chloroform	2.24
n-butanol	10.4	*n*-decane	2.0
tert-butanol	10.3	*n*-heptane	1.92
Octan-2-ol	10.28	*n*-hexane	1.19

An additional plot between the dielectric constants (of all solvents utilized for gelation) and T_{gel} of the subsequent gels formed (Figure 3.9) showed that this class of compounds could gel solvents with dielectric constants in the range of 20-47, with the exception of nitrobenzene (ε=34.82), which coincides with the fact that no gelation was observed in aromatic solvents (Table 3.5).

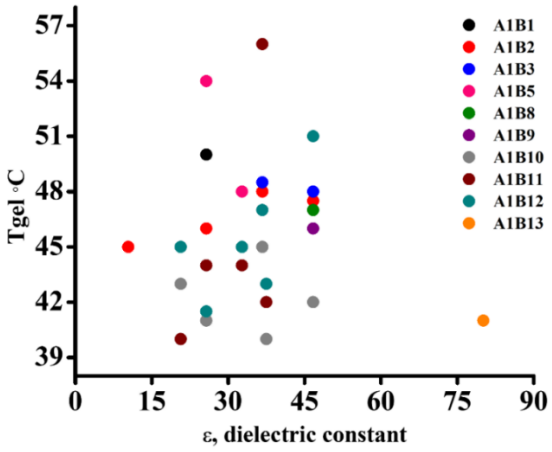

Figure 3.9 Relation between dielectric constants and T_{gel}

Also, it was found that higher alcohols (with lower polarities) were not capable of gelation. Similar was the case with non-polar solvents and chlorinated solvents, where no gelation behavior was observed.

Table 3.6 Solvatochromic parameters of solvents screened for gelation trials

Solvents	*Gel/ Sol*	*Solvatochromic Parameters*			
		E_T^N	α	β	π^*
Methanol	G	0.762	0.93	0.62	0.60
Ethanol	G	0.654	0.83	0.77	0.54
Acetonitrile	G	0.46	0.19	0.31	0.75
Acetone	G	0.355	0.08	0.48	0.71
DMF	G	0.386	0	0.69	0.88
DMSO	G	0.444	0	0.76	1.0
Water	S	1.0	1.17	0.47	1.1
iso-propyl alcohol	S	0.546	0.76	0.84	0.48
n-butanol	S	0.586	0.79	0.88	0.47
Ethyl Acetate	I	0.228	0	0.45	0.55
THF	I	0.207	0	0.55	0.58
Diethyl ether	I	0.117	0	0.47	0.27
Chloroform	I	0.259	0.20	0.10	0.58
Dichloromethane	I	0.309	0.13	0.10	0.82
n-hexane	I	0.009	0	0	-0.4
Toluene	I	0.099	0	0.11	0.54
Chlorobenzene	I	0.188	0	0.07	0.71
Nitrobenzene	I	-	0	0.39	1.01

Solvatochromic Parameters

Solvent polarity can also be measured using solvatochromic dyes. It has been known that a solvent can alter the absorption bands of a dye because of: 1. Dipolar interactions between the solvent and dye, 2. Changes in dipole moment of the dye arising from any optical transition, and 3. the Franck-Condon Principle.[35] Solvatochromic techniques rely on change in the position of UV/vis absorption bands of a solvatochromic dye caused by the solvent in which it is dissolved.[36]

These parameters include the Normalized Dimroth-Reichardt parameter- E_T^N, which is responsible for all possible intermolecular forces between solvent and solute molecules and the Kamlet-Taft parameters, which characterize a solvent with respect to its polarizability- π^*, H-bond donating capacity- α and H-bond accepting capacity- β.[29,34] The α parameter is known to have a correlation with the gelling ability, the magnitude of β affects the stability of the gel and π^* value indicates the influence of fiber–fiber interactions.[37]

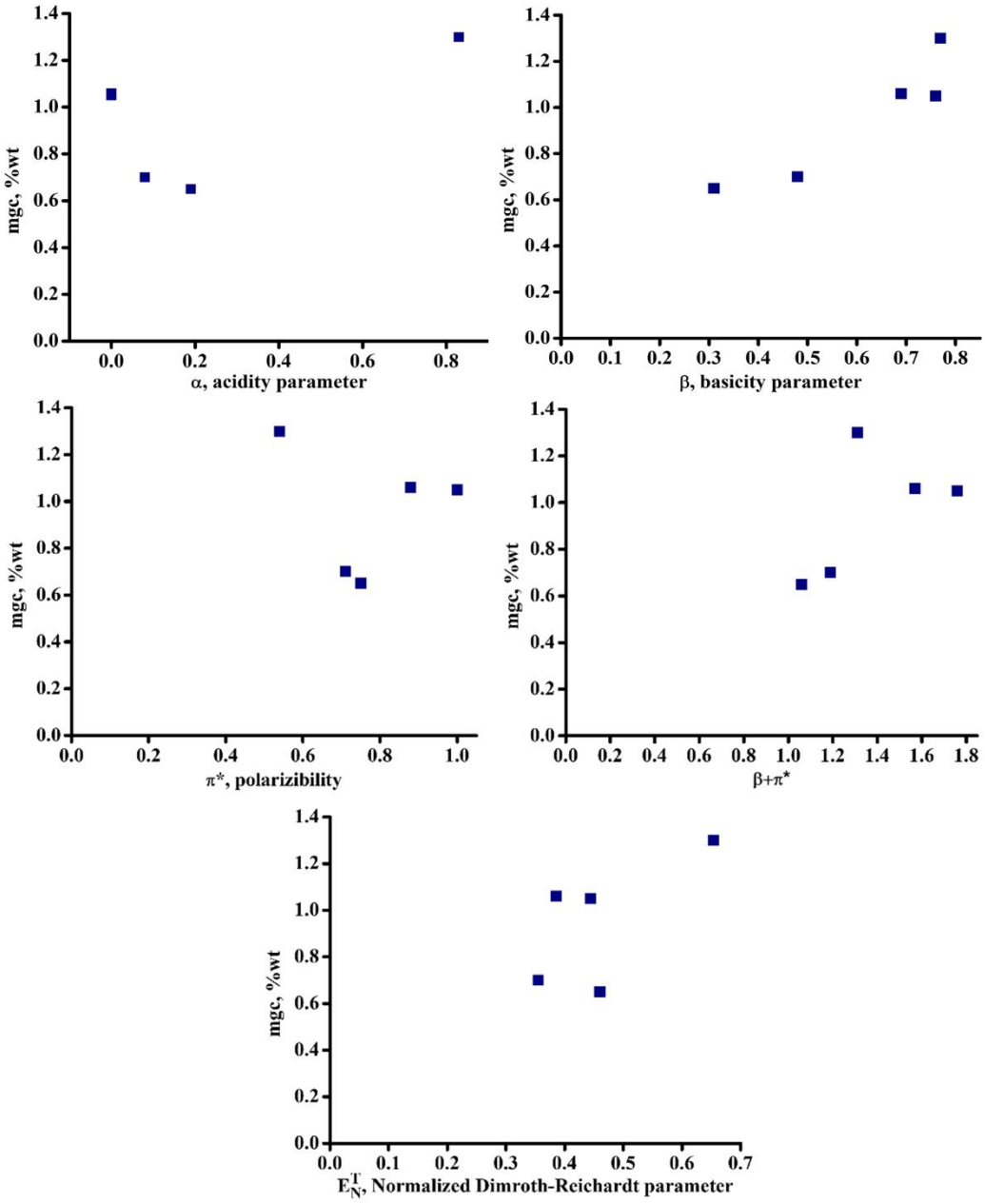

Figure 3.10 Variation of mgc values with acidity and basicity parameters, polarizibilty and Normalized Dimroth-Reichardt parameters of the solvents for salt A1B10

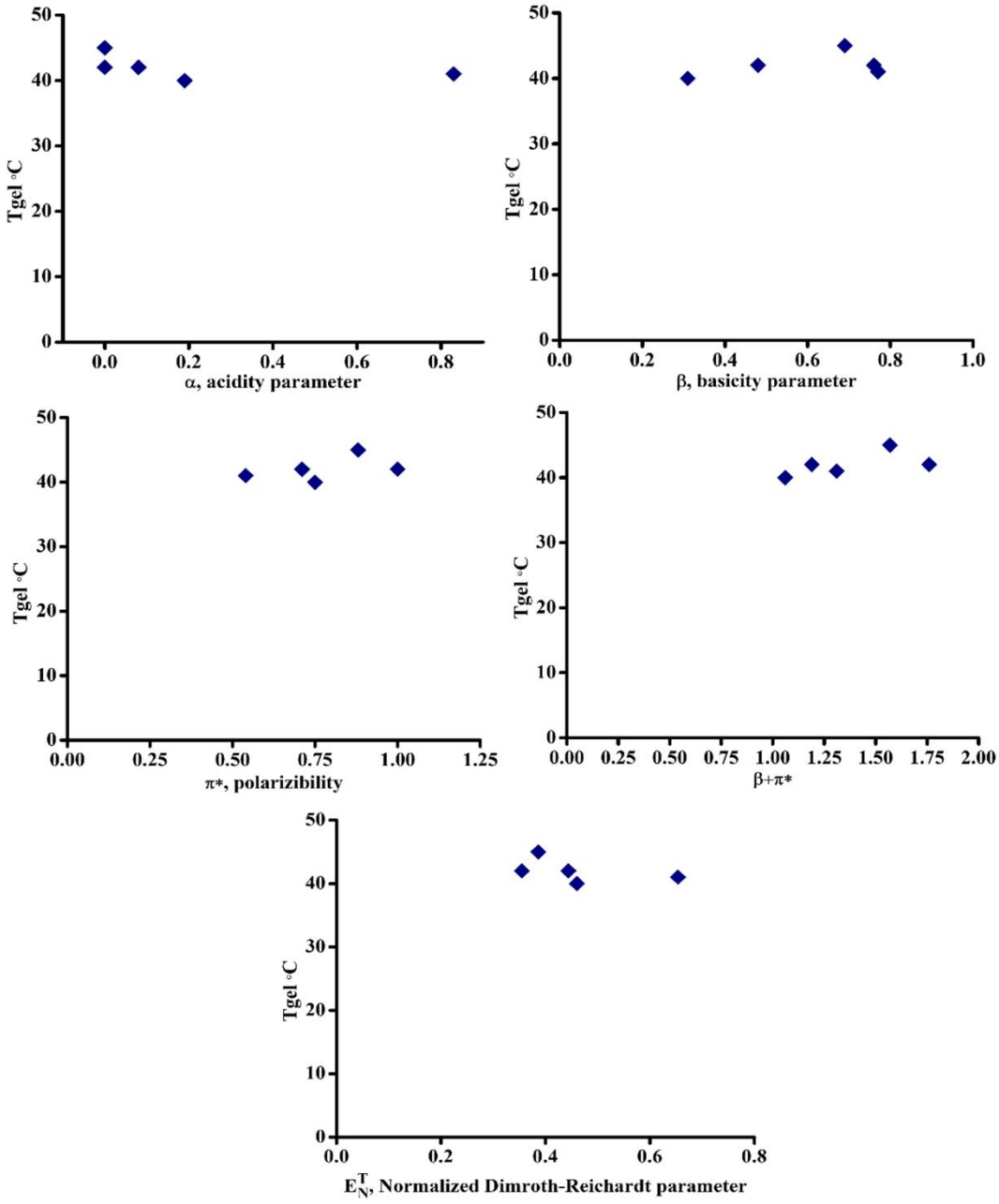

Figure 3.11 Variation of T_{gel} values with acidity and basicity parameters, polarizibilty and Normalized Dimroth-Reichardt parameters of the solvents for salt A1B10

There have been different instances about correlation between the value of $\boldsymbol{\alpha}$ and gel formation. Smith and coworkers have reported that an $\boldsymbol{\alpha}$ value of 0 favored gel formation[1,2,38], whereas Rogers and coworkers illustrated that $\boldsymbol{\alpha}$>0 yielded gelation.[29]

In our study, we found that gelation was favored for both the cases ($\boldsymbol{\alpha}$>0 and $\boldsymbol{\alpha}$=0); Table 3.6. This implies that H-bond donating capacity of the solvents does not control gelation in this series of compounds. The plot of T_{gel} values vs. $\boldsymbol{E_T^N}$, $\boldsymbol{\alpha}$, $\boldsymbol{\beta}$ and $\boldsymbol{\pi^*}$ gave

a slight positive correlation with a few exceptions, whereas the mgc plots were mostly random, as solvents with high polarizability only could be gelled (Figures 3.10, 3.11, S3.5-SS3.8*).

Thermodynamically derived solvent parameters

These parameters rely on the molar Gibbs energy of mixing- ΔG_m, enthalpy- ΔH_m or entropy- $T\Delta S_m$ of either or both the components to define parameters for solvation. These include the Hildebrand parameter, $\boldsymbol{\delta_0}$ and the Hansen solubility parameters, $\boldsymbol{\delta_d}$, $\boldsymbol{\delta_p}$, $\boldsymbol{\delta_h}$, $\boldsymbol{\delta_a}$. The Hildebrand parameter, $\boldsymbol{\delta_0}$ (related to the cohesive energy which combines dispersion forces and polar interactions which determine whether a solvent will promote self-assembly or not[37]) did not give a very relevant correlation with T_{gel} as well as with the mgc values (Figures 3.12, 3.13, S3.9-S3.12*).

Table 3.7 Thermodynamically derived solvent parameters screened for gelation trials

Solvents	*Gel/ Sol*	*Thermodynamically derived Solvent Parameters*				
		$\boldsymbol{\delta_0}$	$\boldsymbol{\delta_d}$	$\boldsymbol{\delta_p}$	$\boldsymbol{\delta_h}$	$\boldsymbol{\delta_a}$
Methanol	G	14.50	7.4	6.0	10.9	12.4
Ethanol	G	12.92	7.73	4.3	9.5	10.45
Acetonitrile	G	11.90	7.5	8.8	3.0	9.30
Acetone	G	9.77	7.58	5.1	3.4	6.13
DMF	G	12.14	8.52	6.7	5.5	8.69
DMSO	G	12.93	9.0	8.0	5.0	9.43
Water	S	23.5	6.0	15.3	16.7	22.8
Isopropyl alcohol	S	-	-	-	-	-
n-butanol	S	11.30	7.81	2.8	7.7	8.20
Ethyl Acetate	I	9.10	7.44	2.6	4.5	5.19
THF	I	9.50	8.2	2.8	3.9	4.8
Diethyl ether	I	7.62	7.05	1.4	2.5	2.88
Chloroform	I	9.30	8.7	1.5	2.8	3.18
Dichloromethane	I	9.90	8.9	3.1	3.0	4.31
n-hexane	I	7.24	7.24	0	0	0
Toluene	I	8.9	8.8	0.7	1.0	1.22
Chlorobenzene	I	9.57	9.28	9.1	1.0	2.33
Nitrobenzene	I	10.62	8.60	6.0	2.0	6.32

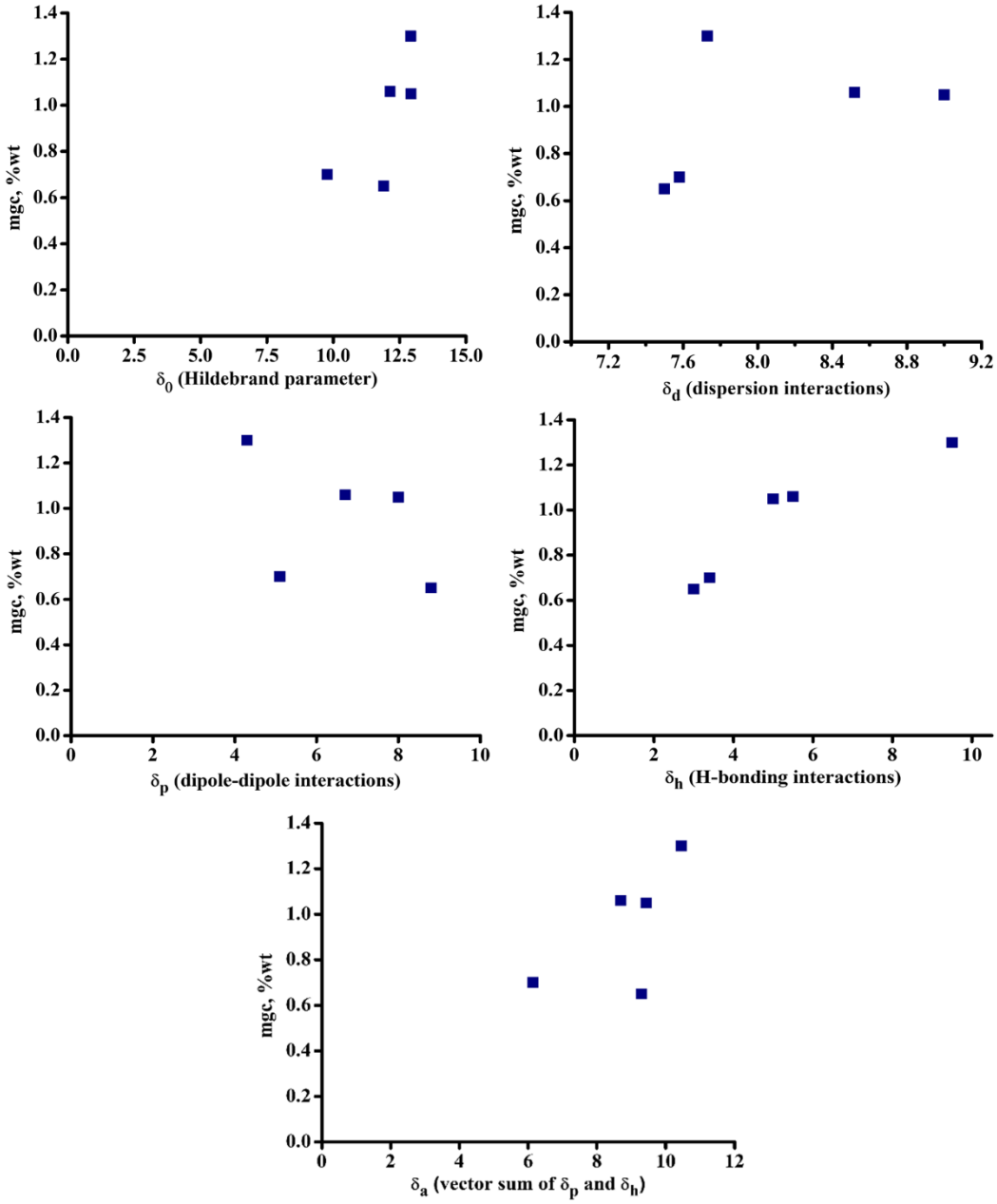

Figure 3.12 Variation of mgc values with thermodynamically derived solvent parameters for salt A1B10

Also, we realized that solvents with high δ_0 values were more likely to exhibit gelation as a result of increased cohesive energy densities, which can substantially affect self-assembly. Previous studies have shown that there is a poor correlation between T_{gel} and δ_0 as this parameter is useful only for low polarity solvents without hydrogen bonding.[29]

The Hansen solubility parameters (HSPs) which categorize the solvent interactions into different types (δ_d = dispersion interactions, δ_p = dipole−dipole interactions, δ_h = H-bonding interactions and δ_a, which is a vector sum of δ_p and δ_h [31,32,34]) provided a slightly positive correlation but remained far from perfect. A slight positive correlation was observed for δ_p (with T_{gel} values), which accounts for interactions due to polar groups on the solvent. We also observed a positive correlation between δ_h and mgc values for all the salts, which indicates the dependence of H-bonding interactions on the gelation behavior. It coincides with a classic literature report where the authors have established that the mgc values scale as a function of the hydrogen bonding HSPs.[39]

Gels would only form in solvents with δ_p values >5 (except for chlorobenzene and nitrobenzene, since aromatic solvents did not support gelation) and δ_a values >8.5, suggesting that permanent dipole-dipole and H-bonding interactions of solvent might be controlling the gel formation in a particular solvent.

From these studies, we can infer that the gelation ability of a solvent (for this series of salts) is primarily controlled by 1. the dielectric constant and polarity index, 2. increased interactions between solvent and solute molecules, 3. a critical combination of H-bond accepting ability (β) and general polarity, π^* and 4. polar cohesive energies (dipole−dipole interactions) and H-bonding interactions.

While a high polarity solvent (like water) would allow the gelator molecules to dissolve, minimizing their ability to form fibers and eventually a gel, a low polarity solvent would be incapable of dissolving such two-component systems. Even though, since we are dealing with charged moieties, they can be best solvated in polar solvents, which might be allowing them to retain their forces of attraction and/or involved in H-bond interactions with the solute molecules, leading to the formation of gel networks.

The presence of varied backbone in amines (alicyclic, aromatic, alicyclic-aromatic, aliphatic) in salts make the solute-solvent interaction study and prediction of gelation behavior of solute extremely sensitive. However, a plot of hydrophobicity of amines vs. T_{gel} values (Figure S3.13*) for each amine was plotted and it displayed a slightly positive correlation for solvents DMSO and acetonitrile, where T_{gel} values increased with increase in hydrophobicity of the amines used, where hydrophobicity of an acid was calculated by the following equation 3.2-

$$Hydrophobicity = \frac{total\ number\ of\ carbon\ atoms}{number\ of\ -COOH\ groups\ present} \quad \text{- (3.2)}$$

Nevertheless, these results may vary with the moieties in consideration and can be very useful in predicating gelation performance in case of low molecular weight organogelators.

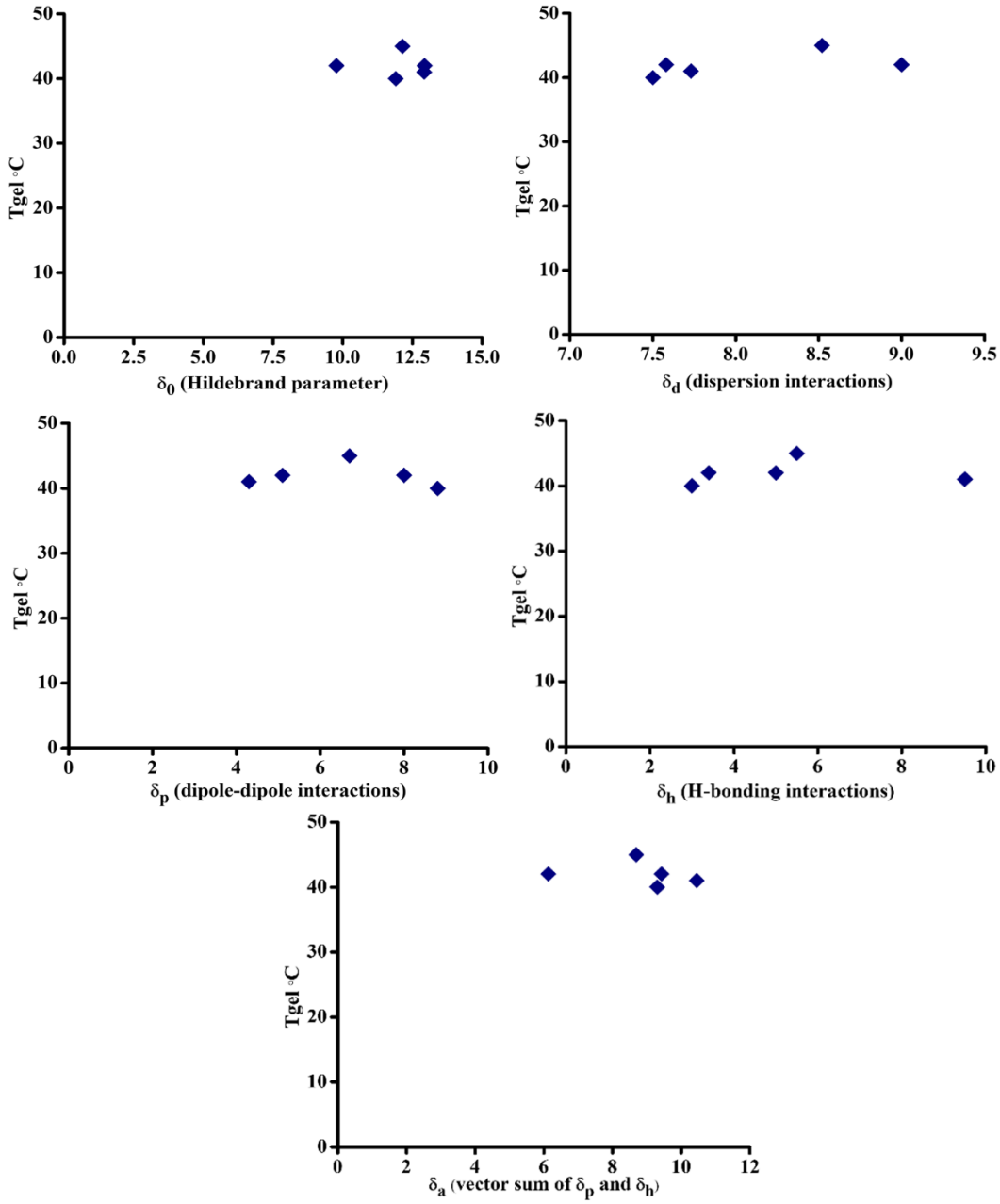

Figure 3.13 Variation of T_{gel} values with thermodynamically derived solvent parameters for salt A1B10

3.4.3 Single crystal X-ray studies

A1B1 ***[ethane-1,2-diaminium pivalate]*** Good quality single crystals of salt **A1B4** were obtained from methanol and ethanol (1:1). **A1B4** crystallizes out in a centrosymmetric, $P2_1/c$ space group of monoclinic system (Figure 3.14). The crystal structure contains one molecule of ethylene diamine (where both the amine groups have converted to primary ammonium cations) and 2 pivalate ions, one on each side of the primary ammonium moiety. Despite many attempts, we could isolate only (2:1) salt. We find the molecules arranged in a 1D assembly, comprising of various types of hetero synthons, as shown. The amine moiety forms a bridge between the zig-zag 1D layers and extends the network in 2 dimensions. We observe a four membered $R_4^2(8)$ type synthon in the 1D layers.

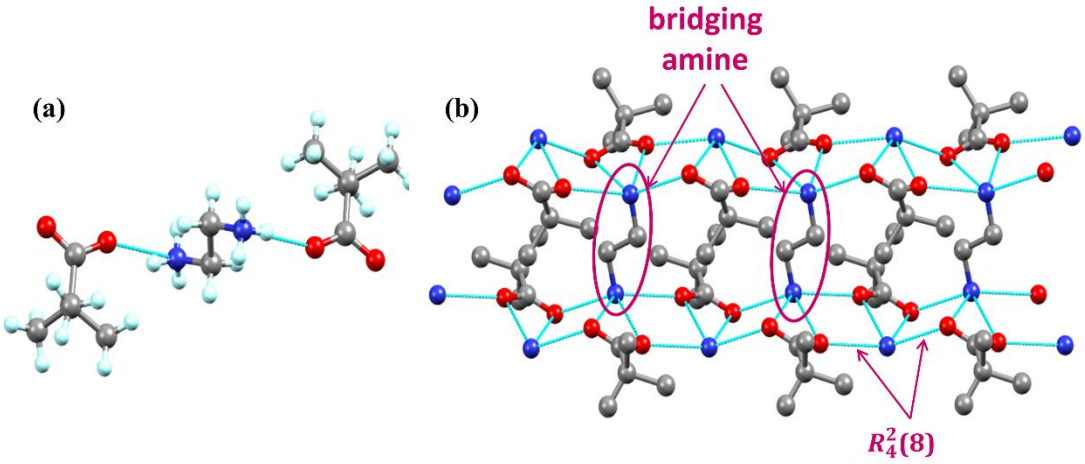

Figure 3.14 (a) asymmetric unit of A1B1, (b) zig-zag 1D layers observed in the structure extending in 2D with the help of bridging amine moieties (Hydrogens are not shown for clarity of image)

A1B7 ***[2-methyl propan-2-aminium pivalate]*** Diffraction quality single crystals of **A1B7** were obtained from a mixture of methanol and acetonitrile.

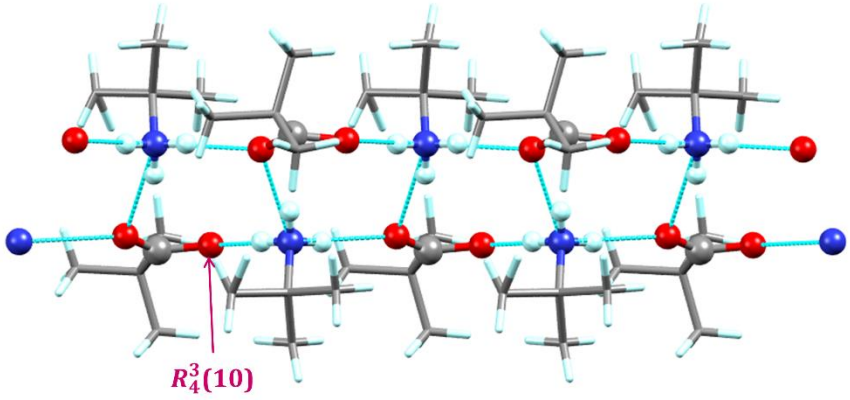

Figure 3.15 One dimensional network of salt A1B7

The salt crystallizes out in an orthorhombic, *Pna2₁* space group, with one molecule each, of pivalate ion and tertiary butyl ammonium cation, present in the asymmetric unit (Figure 3.15). The structure showcases a 6-membered 1D supramolecular synthon, having a graph set type $R_4^3(10)$. The structure also contains various C-H…O type interactions, other than the N-H…O interactions (extending in 1D only!). This salt, despite having the same *tert*-butyl moiety as in pivalic acid as well as a 1D arrangement, fails to gel any solvent.

A1B10 ***[Cyclohexyl aminium pivalate]*** Crystals of **A1B10** were obtained from methanol and the structure was found to crystallize in *P-1* space group of triclinic crystal system. It contains one molecule each, of pivalate ion and cyclohexyl aminium ion in the asymmetric unit (Figure 3.16). The deprotonated carboxylate group and the primary ammonium cation are linked via $COO^-\ldots{}^+H_3N$-R bonds. The supramolecular assembly exhibits the four membered 1D PAM synthon (Synthon 1, Scheme 3.1), having $R_4^2(8)$ type graph set. The structure continues to extend in a 1D pattern along *a* axis even through various short contacts, viz. C-H…O, N-H…C, N-H…O.

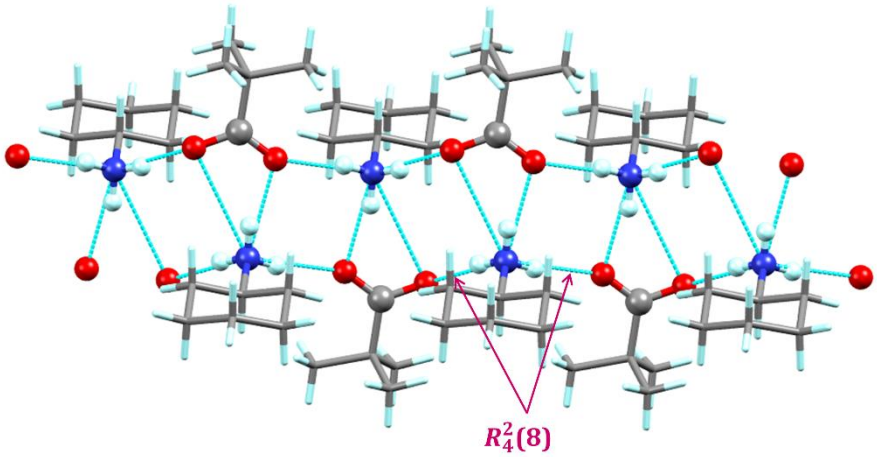

Figure 3.16 Bonding in salt A1B10

A1B11 ***[1-phenylethanaminium pivalate]*** Single crystals of **A1B11** were obtained from ethanol and the structure belongs to orthorhombic, *P2₁2₁2₁* space group (Figure 3.17). The asymmetric unit contains one molecule each of the carboxylate and the primary ammonium cation, which extend to form the familiar four membered 1D

synthon pattern. We also find a variety of other non-covalent interactions like C…H-N, N…H-C, O…H-C, etc. in the crystal structure.

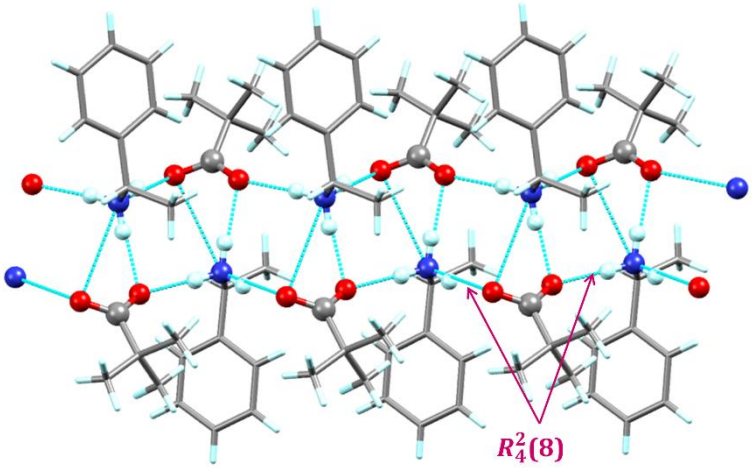

Figure 3.17 1D assembly of salt A1B11

A1B12 ***[1-benzylpiperidin-4-aminium pivalate]*** Crystals of salt **A1B12** were isolated from methanol-ethanol mixture. The structure belongs to $P2_1/n$ space group of monoclinic crystal system. We find a $R_4^3(10)$ type, 6-membered synthon of Type 2 (Scheme 3.1), also exhibiting a 1D zig-zag type arrangement (Figure 3.18), further extending with C-H…N, C-H…O, N-H…C type interactions.

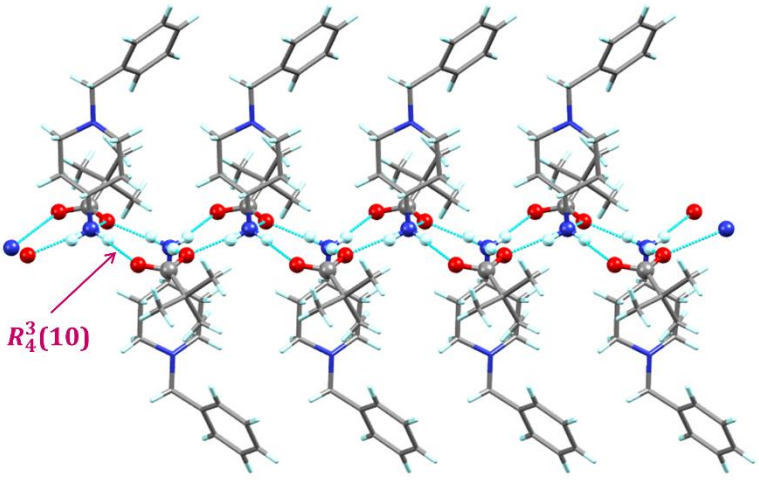

Figure 3.18 One dimensional Hydrogen-bonded network of salt A1B12

3.4.4 Hirshfeld studies

The 2D fingerprint plots of the salts obtained from Hirshfeld studies support the fact that H…H interactions have the most significant contribution in all the structures. They can be found in the middle region (d_i= ~1.2 Å, d_e= ~1.2 Å) of each 2D fingerprint plot.

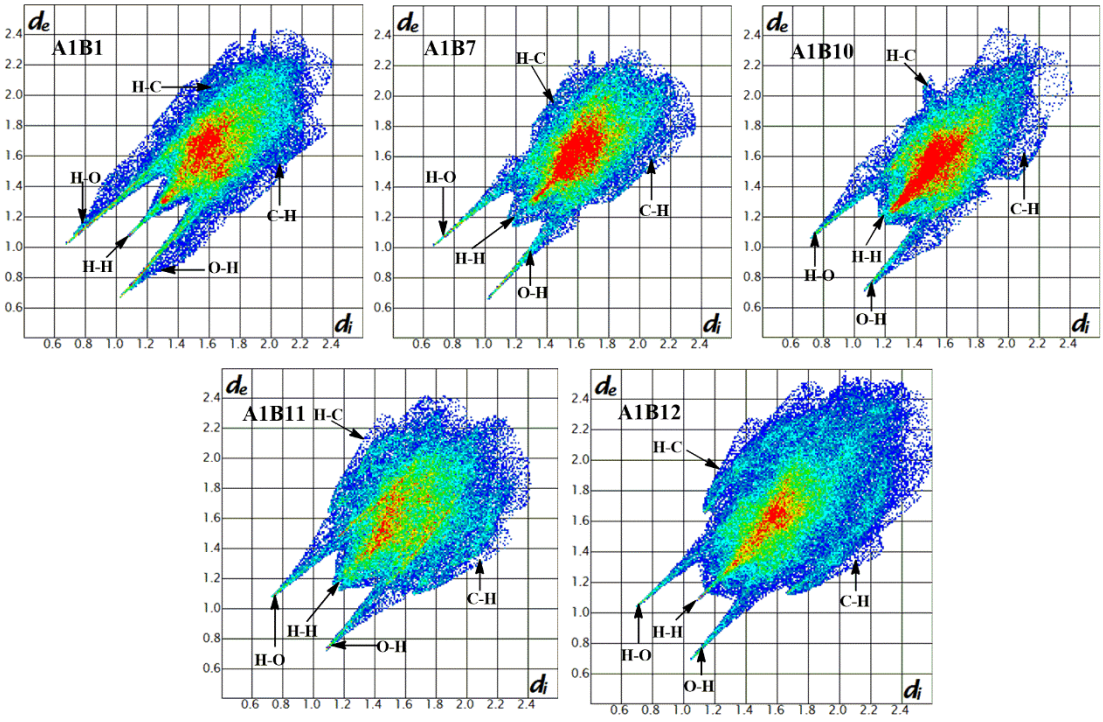

Figure 3.19 Two-Dimensional Hirshfeld fingerprint plots of structures of pivalic acid based salts. The color in the sequence white-blue-green-red is a summary of the frequencies of each combination of distances d_e and d_i across the Hirshfeld surfaces of a molecule (in increasing order), where d_i is internal distance and d_e external distance from the Hirshfeld surface to the nearest molecule.

The O…H interactions appear as two sharp spikes in all the plots having an average contribution of 8.7% (d_i= 0.7 Å, d_e= 1.05 Å). We fail to find any π-π (C…C) interactions in any of the salts. Apart from these, we find C…H (van der Waals') interactions present in all salts (appearing on the outer edges of the 2D plots). One noteworthy point is, all the salts contain negligible amount of C…O and C…N interactions which confirms that the lone pairs of O and N atoms are not involved in lone pair- π interactions (Figure 3.19). The Hirshfeld surface interactions for the salts are summarized in Figure 3.20. 3D Hirshfeld surfaces and ORTEP images for all crystal structures are summarized in Figure S3.14*.

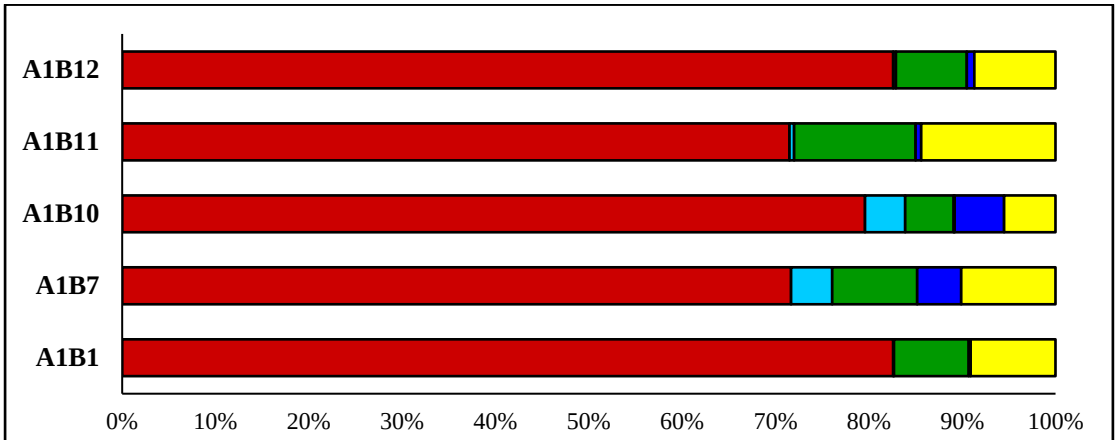

	A1B1	A1B7	A1B10	A1B11	A1B12
H-H	82.6	71.6	79.5	71.5	82.6
H-C	0.1	4.4	4.3	0.5	0.3
H-O	8	9.1	5.2	13	7.6
H-N	0	0	0.1	0	0
C-H	0.2	4.7	5.3	0.6	0.8
C-O	0	0	0	0	0
O-H	9.1	10.1	5.5	14.4	8.7
S-H	0	0	0	0	0
S-O	0	0	0	0	0
S-N	0	0	0	0	0

Figure 3.20 Distribution of contacts on the Hirshfeld surfaces sorted according to the types of contacting atoms in the salts (represented in graphical and tabular form)

3.4.4.1 Hirshfeld energies

We also attempted to calculate intermolecular interaction energies for these salts to get an insight about the %electrostatic and %dispersion contribution in these salts, which, we suspected, might have an impact on the gelation behavior. The energies were calculated for *B3LYP* model for *6-31G* basis set (Table 3.8). We found that the values of %dispersion contribution for all the gelators were higher than those of the non-gelators. Since this dispersion term is mostly connected with the intermolecular interactions and is a stabilizing factor, this result might be relevant to mention here at this point.

Though we could not find a major correlation between the gelation behavior of these salts and their theoretically calculated energies, we opine that understanding the nature, strength and the importance of various intermolecular interactions prevailing in a

crystal structure can always bring us closer to the deceptively complex job of designing of LMOGs.

Table 3.8 Intermolecular interaction energy values for salts and %electrostatic and %dispersion contribution to the total stabilization

Salt	Gel/ Non-gel	E_ele kJ/mol	E_pol kJ/mol	E_rep kJ/mol	E_dis kJ/mol	E_tot kJ/mol	% Electrostatic contribution	% Dispersion contribution
A1B1	Gel	-52.4	-1.8	-15.2	135.2	13.6	-66.9136	166.91
A1B7	Non Gel	-64.7	-2.6	-19.2	171.3	18.8	-64.7115	163.61
A1B10	Gel	-69.8	-2.5	-16.3	177.2	19.6	-68.92	168.92
A1B11	Gel	-58.8	-5.0	-22.2	132.9	-3.1	-92.329	192.32
A1B12	Gel	-74.7	-2.0	-10.5	178.7	20.8	-75.1961	175.19

Where $E_{tot} = k_{ele}E_{ele} + k_{pol}E_{pol} + k_{dis}E_{dis} + k_{rep}E_{rep}$

k_{ele} = 1.019, k_{pol} = 0.651, k_{dis} = 0.901, k_{rep} = 0.811 for **HF/3-21G model**

and E_{ele} = classical electrostatic energy of interaction between monomer charge distributions, E_{pol} = polarization energy, E_{dis} = dispersion energy and E_{rep} = exchange–repulsion energy

Electrostatic contribution to the total stabilization of a particular molecular pair

$= [(E_{ele} + E_{pol}) / (E_{ele} + E_{pol} + E_{disp})] \times 100\%$.

Dispersion contribution to the total stabilization of a particular molecular pair

$= [(E_{disp}) / (E_{ele} + E_{pol} + E_{disp})] \times 100\%$.

3.4.5 Morphology

In order to gain insight into the morphology of these self-assembled systems, POM and SEM studies were carried out on frozen gel samples. Most of the gelators comprised of long crystallites and needle-like fibers which might have immobilized the solvent through various non-covalent interactions (Figures 3.21-3.24). The polarized optical micrographs of the gels show highly birefringent, symmetric bundles of crystalline fibers/needles which organize themselves to more the 3D networks. The SEM images of the gels show a fibrous morphology, which is evident of the formation of self-assembled fibrilar networks (SAFiNs) responsible for gel formation. Interestingly, the fibers in xerogel of **A1B12** were found to have hollow longitudinal spaces (Figure 3.24 (e), (f)). These types of crystalline fibrils were found to be absent in the other gelators.

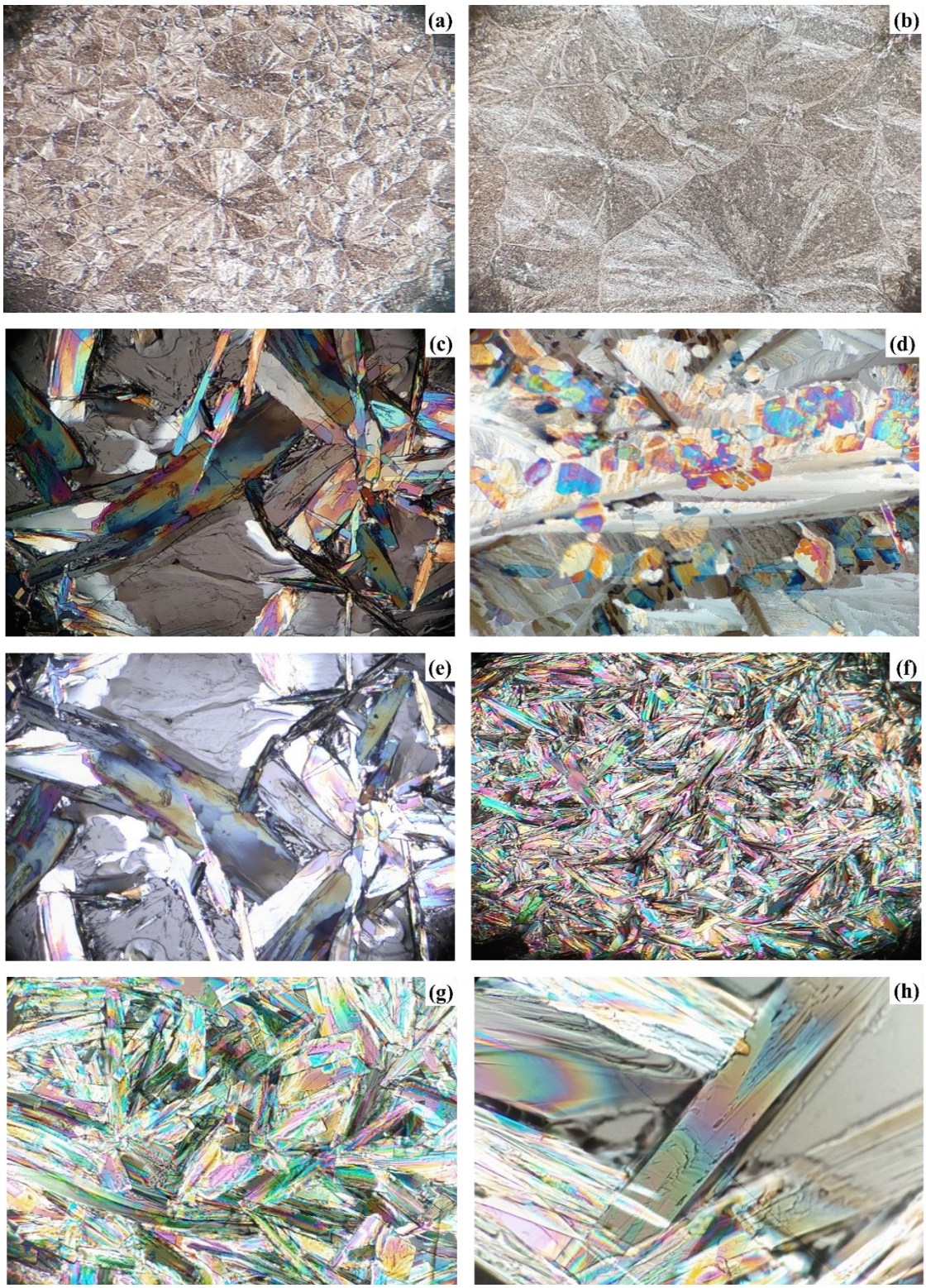

Figure 3.21 POM images of gels (a) A1B1, 4x 45 deg (b) 20x 45 deg (c) A1B2, 10x 45 deg in methanol, (d) A1B3, 10x 45 deg in DMSO, (e) A1B5, 20x 45 deg in methanol, (f) A1B8, 4x 45 deg (g) 20x 45 deg (h) 40x 45 deg in DMSO

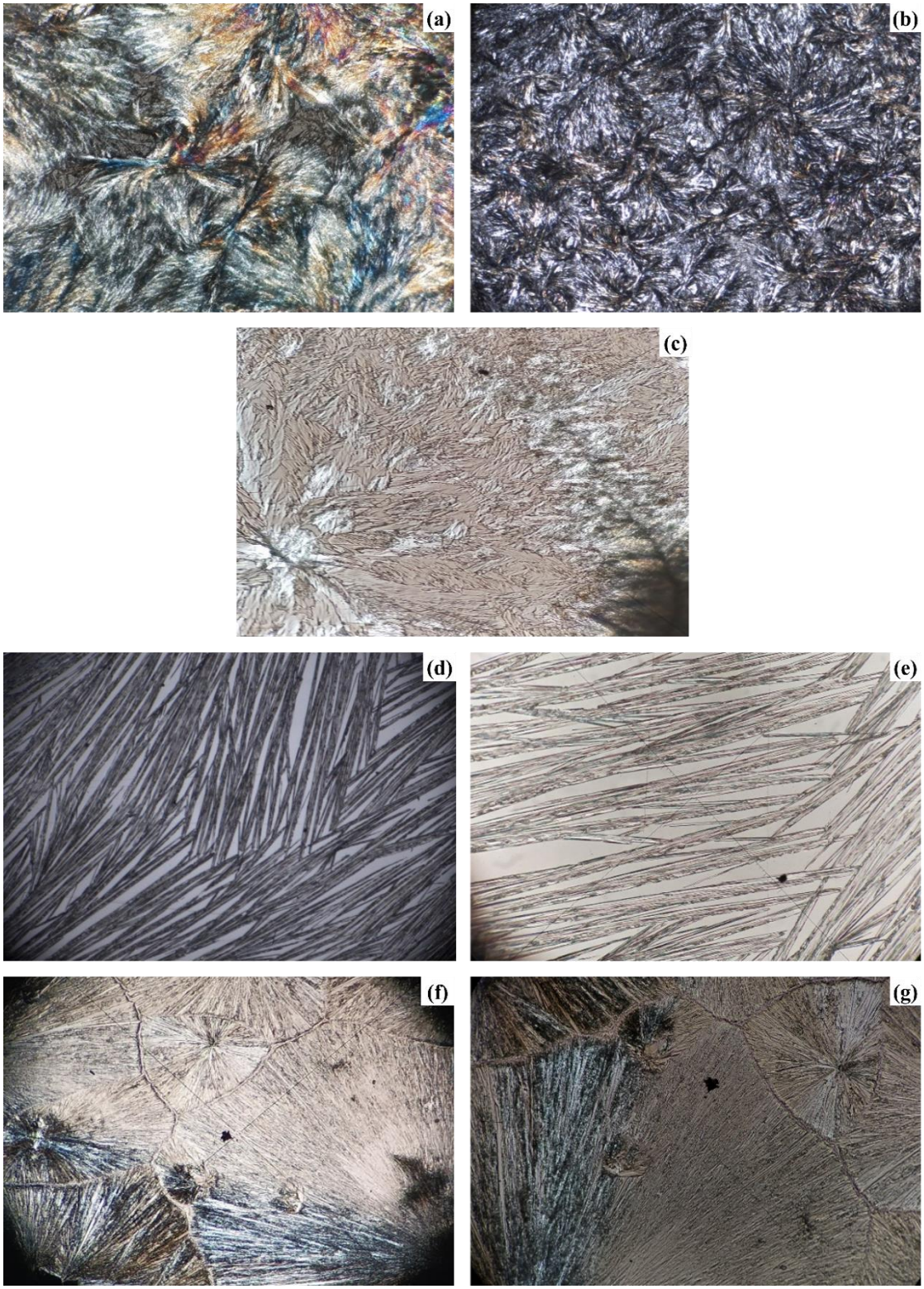

Figure 3.22 POM images of gels (a) A1B9, 4x 45 deg (b) 4x 90 deg in DMSO, (c) A1B10, 10x 45 deg, (d) A1B11, 4x 45 deg (e) 20x 90 deg, (f) 4x 45 deg, (g) A1B12, 10x 45 deg in acetonitrile

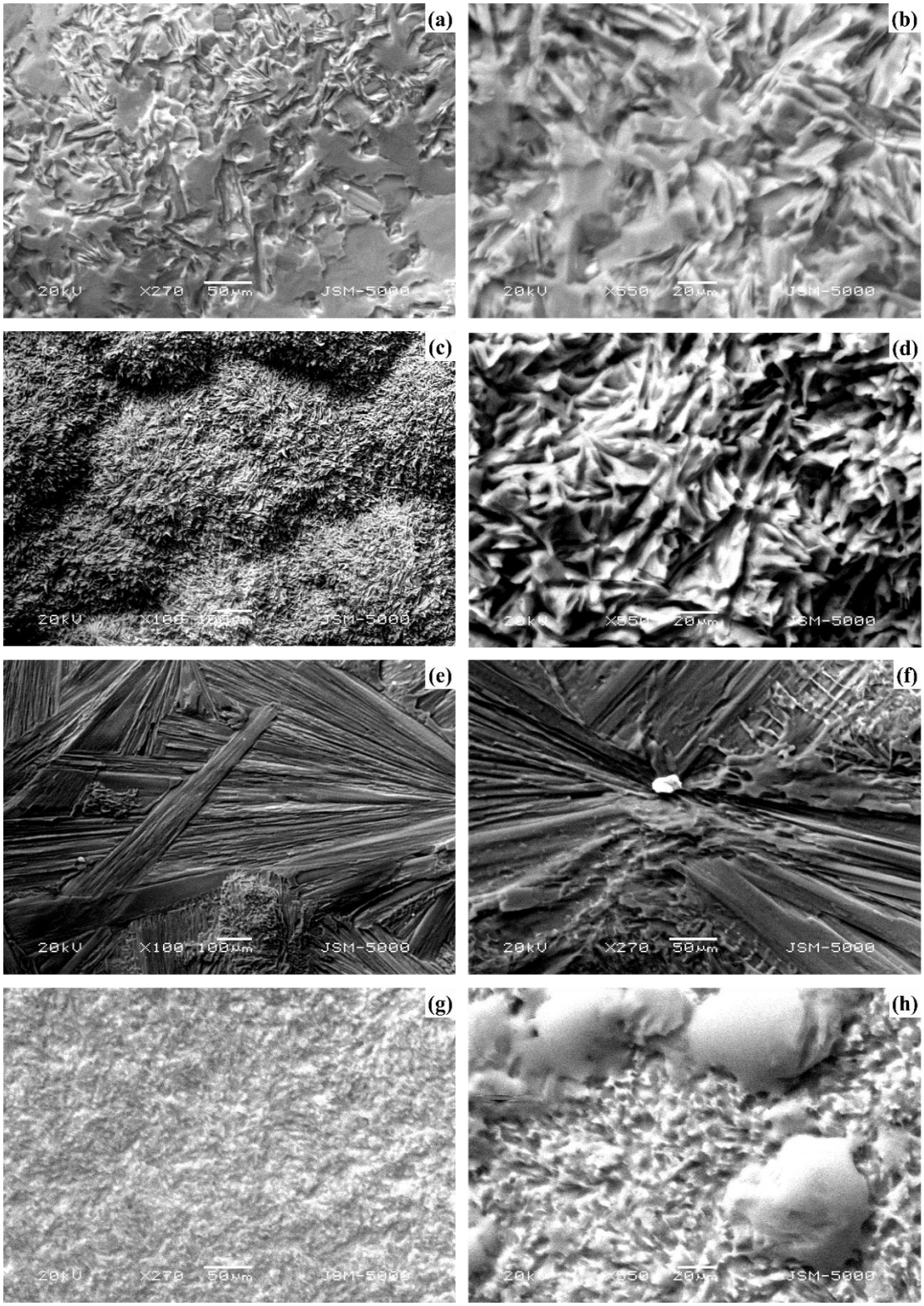

Figure 3.23 SEM images of frozen gels of (a) A1B2, (b) A1B2, (c) A1B3, (d) A1B3, (e) A1B8, (f) A1B8, (g) A1B9, (h) A1B9 in DMSO at different magnifications

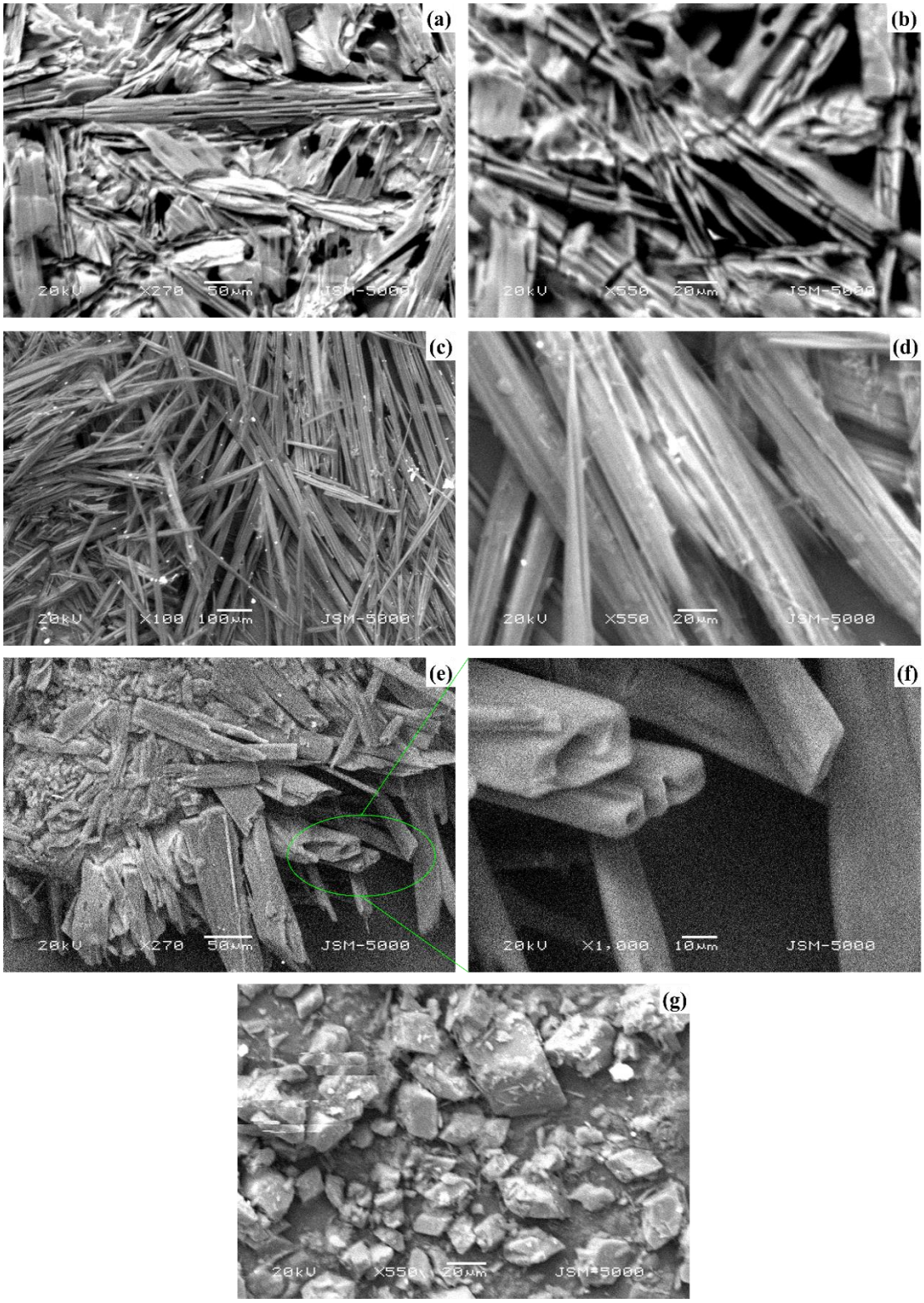

Figure 3.24 SEM images of frozen gels of (a) A1B10, (b) A1B10, (c) A1B11,(d) A1B11, (e) A1B12, (f) A1B12 in acetonitrile solvent and (g) A1B13 in hydrogel, at different magnifications

3.4.6 Rheology

The mechanical strength DMSO gel of **A1B9** was evaluated using rheology (Figure 3.25). The plots of storage modulus, G' and loss modulus, G" remain nearly parallel throughout and the value of G' is more than an order greater than that of G" across the amplitude sweep range. This suggests a static interaction and high degree of elasticity in the gel.

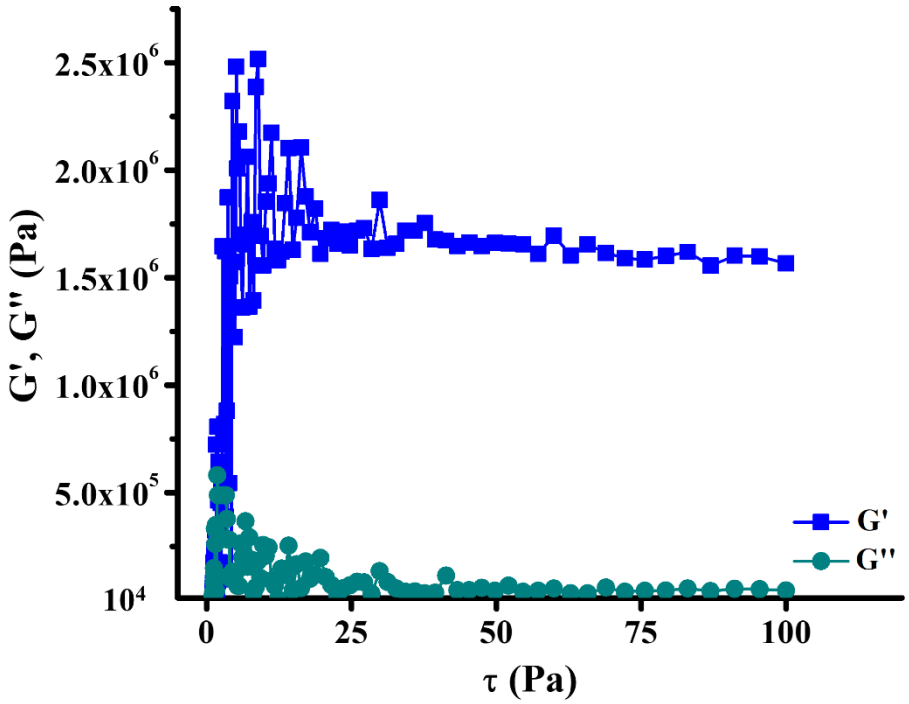

Figure 3.25 Rheological behavior of A1B9 in DMSO gel

3.4.7 Powder X-ray diffraction studies

A detailed powder X-ray diffraction study was carried out to get an insight about the packing of the compounds in gel state. The XRD patterns of salts **A1B10**-**A1B12** in bulk and xerogel (with Acetonitrile as solvent) were compared with the simulated patterns obtained from single crystal studies (Figures 3.26-3.28).

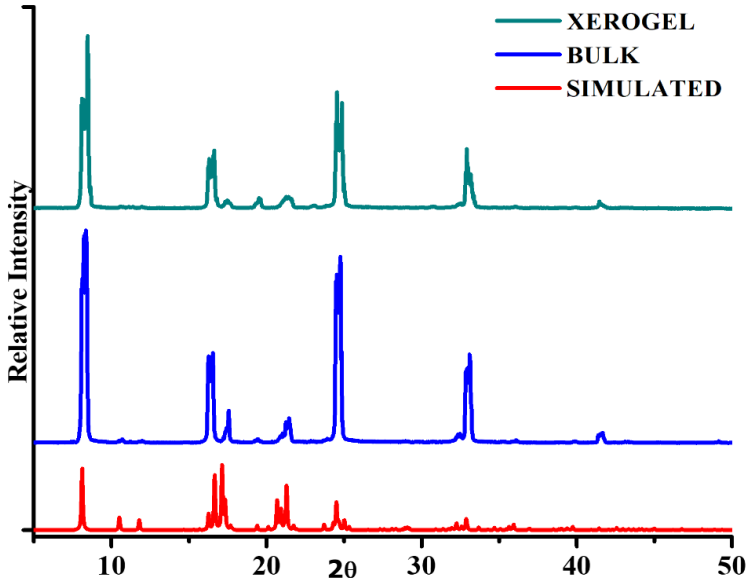

Figure 3.26 Comparison of PXRD patterns for salt A1B10

The patterns of major peaks for **A1B10** were found to be matching with the simulated pattern (Figure 3.26) at 2θ values ~8, 16, 17, 21, 25 and 33.5.

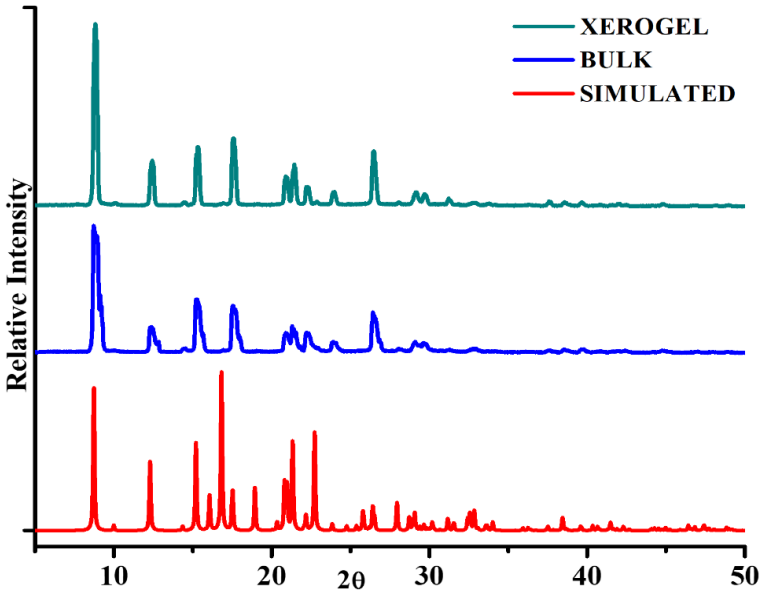

Figure 3.27 Comparison of PXRD patterns for salt A1B11

The major peaks at 2θ values ~8.75, 12.3, 15, 17.5, 21, 22 and 26 in the spectra of **A1B11** were found to be matching with the simulated pattern (Figure 3.27)

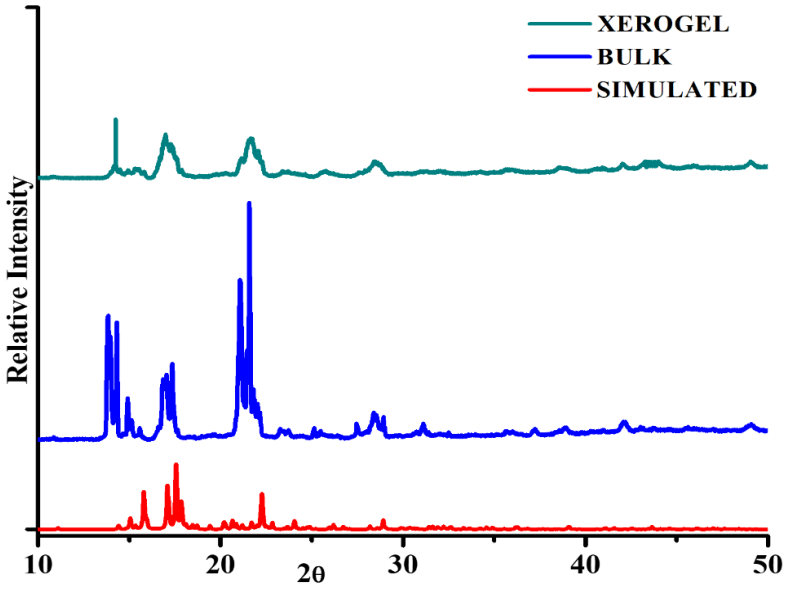

Figure 3.28 Comparison of PXRD patterns for salt A1B12

The peaks at 2θ values ~14, 15, 17, 21, 22 and 28 in **A1B12** were found to be matching with the simulated pattern (Figure 3.28), however the overall patterns remained different from each other, possibly because of minor phase changes.

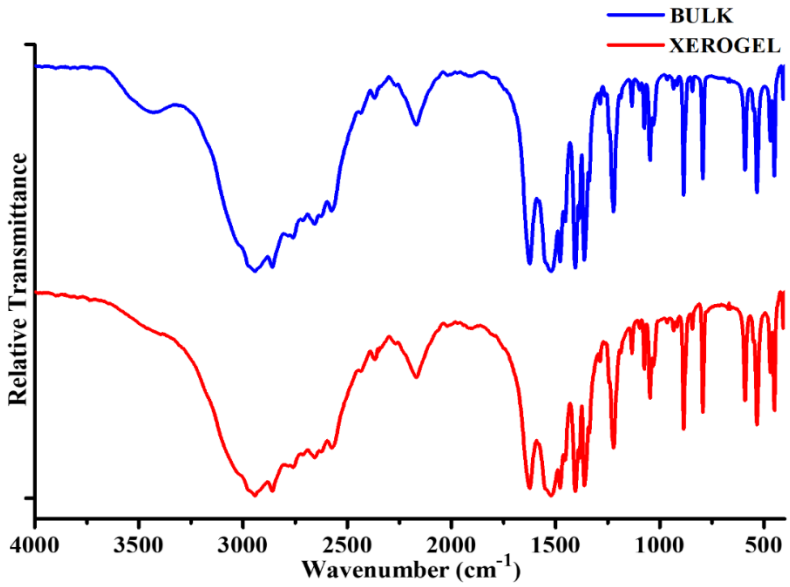

Figure 3.29 Comparative FT-IR patterns in A1B10

3.4.8 Comparative IR studies

Similar comparative IR studies were carried out in bulk and xerogel forms for the same set of salts. (Figures 3.29-3.31)

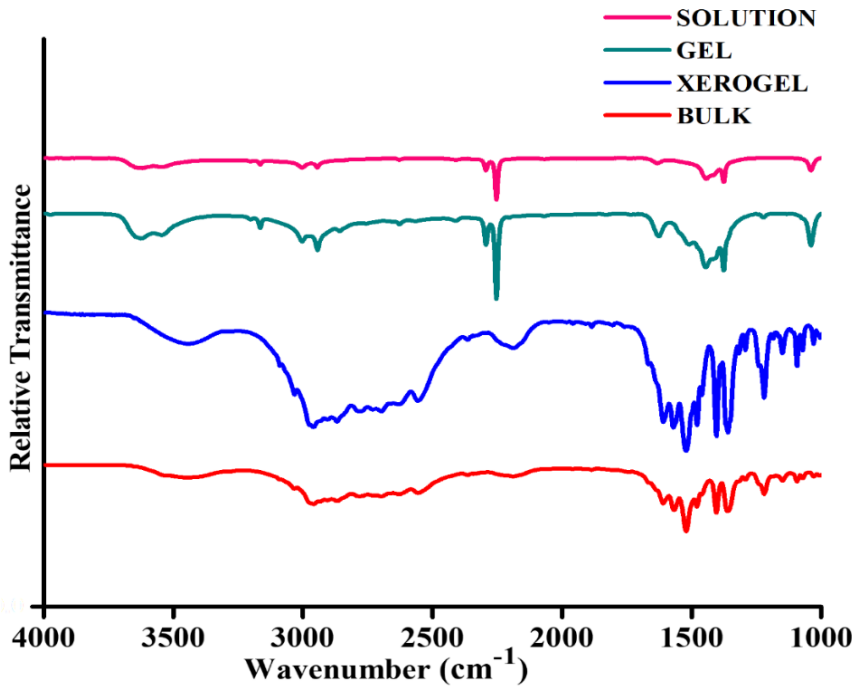

Figure 3.30 Comparative FT-IR patterns in bulk, xerogel, gel and solution phase in A1B11

In case of **A1B11**, we also recorded FT-IR spectrum of the gel phase and solution phase in acetonitrile solvent system. The major peaks were retained in the gel and solution phases with slight shifts, which can be attributed to intermolecular H-bonding.

From these comparative PXRD and FT-IR studies, we can substantiate that the packing in gel phase (xerogel or dried gel) and the crystals grown is similar, which contrasts with the previous literature reports where the packing was found to be substantially different.[40] Although it is believed that the comparison of packing in crystals formed in one solvent (say methanol) with a gel formed in another (acetonitrile, in this case) is not very compelling, even then solving a single crystal of a gelator entity can always bring us closer to understand the underlying mechanism of gelation. Nevertheless, it was found that the basic morphology and internal arrangement remains very similar in both the phases (for this set of compounds), which settles the argument.

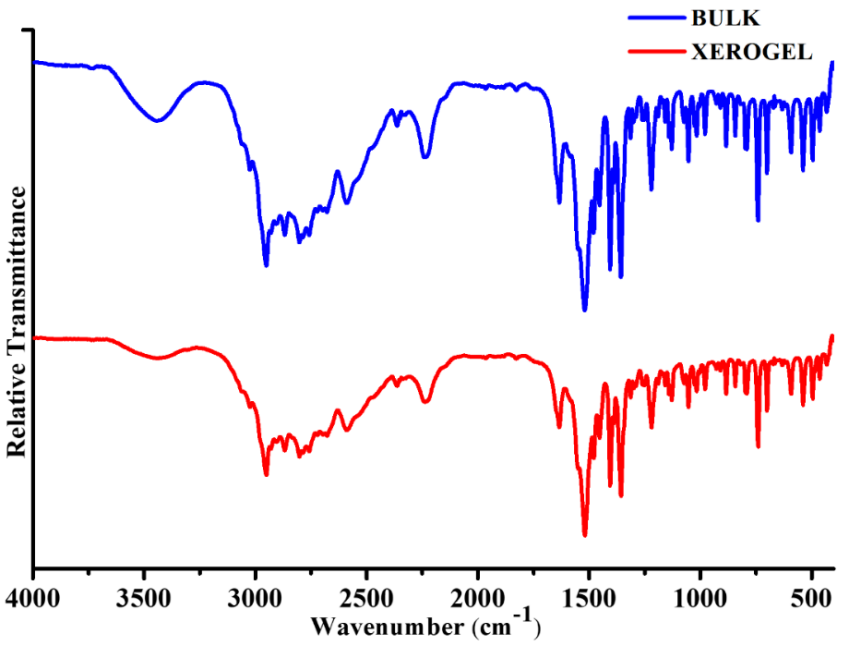

Figure 3.31 Comparative FT-IR patterns in A1B12

3.4.9 Characterization of silver nanoparticles

UV radiation has been known to reduce metal salts to metal nanoparticles in presence of a stabilizer, the gel of salt **A1B12** in acetonitrile was used as a template for synthesis of silver nanoparticles.[41–43] **A1B12** was chosen on account of the hollow tubular architecture of its gel network, which could impact the size and shape of the so formed nanoparticles. The SEM images of Ag nano particles loaded gel (Figure 3.32 (a), (b)) showed formation of small rod like particles of silver.

This gel was extensively dried at RT for 3-4 days and calcined at 200°C for 4 hours in a muffle furnace to remove the organic template. The resultant solid obtained was subjected to FEG-SEM (Figure 3.32 (c), (d)), UV, PXRD and DLS (Figure 3.33) studies. The DLS studies gave a combined effective hydrodynamic diameter of 88 nm.

The DRS spectra of the nanoparticles gave plasma absorption with maxima at 404 nm indicating formation of silver nanoparticles.[44] The PXRD pattern showed distinct diffraction peaks at 38.2, 44.4, 64.5 and 77.5 corresponding to crystalline planes 111, 200, 220 and 311 respectively, which confirm the face centered cubic structure of silver nanoparticles.[45]

The size of the nanoparticles was also obtained from the powder pattern using the Debye-Scherrer equation (equation 3.3),

$$D=k\lambda/\beta\cos\theta \qquad \text{- (3.3)}$$

and was found to be 38 nm.

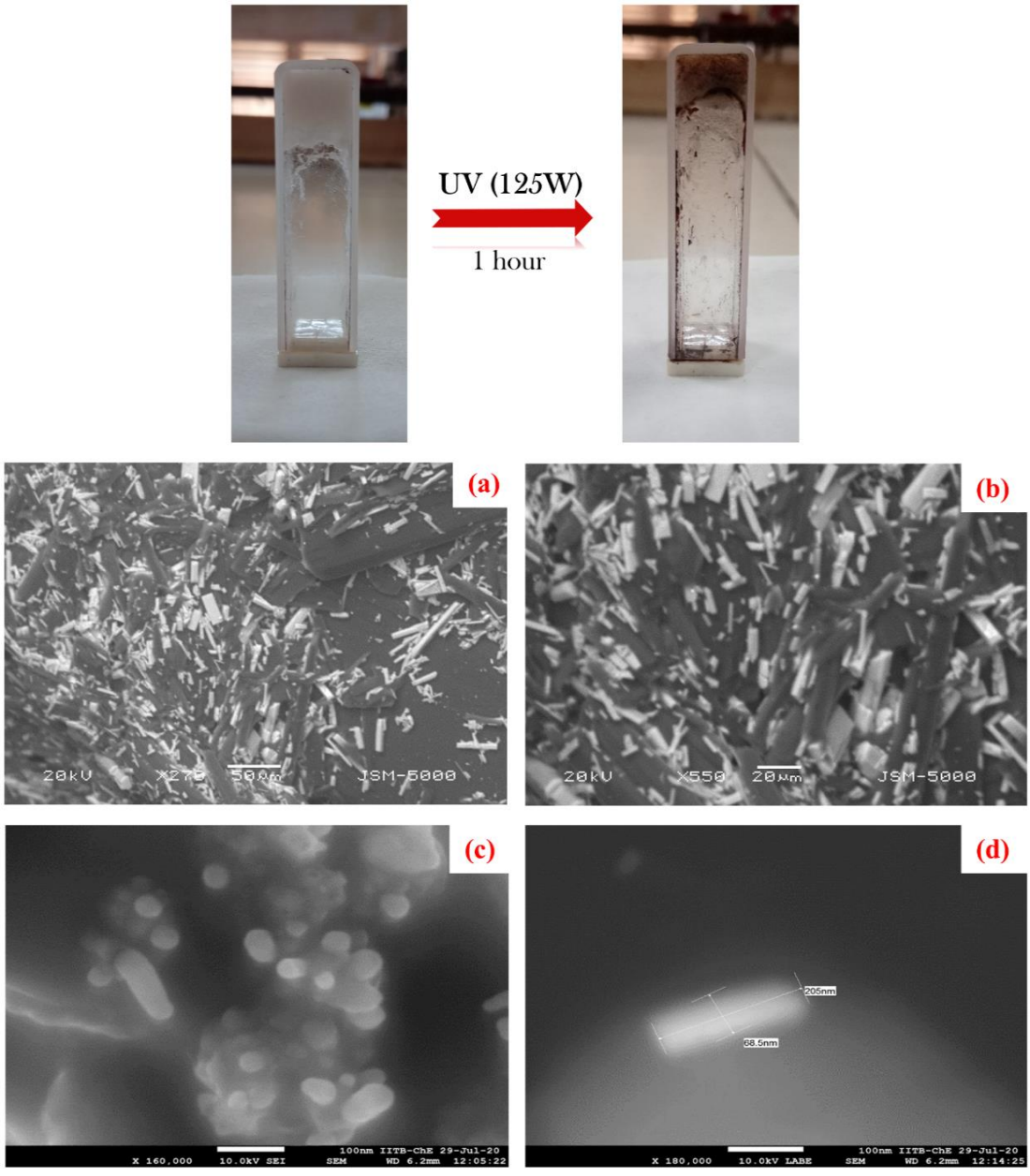

Figure 3.32 Synthesis of Ag nano particles within the gel network, (a), (b) SEM of gel loaded with nano particles; (c), (d) FEG-SEM of isolated nano particles

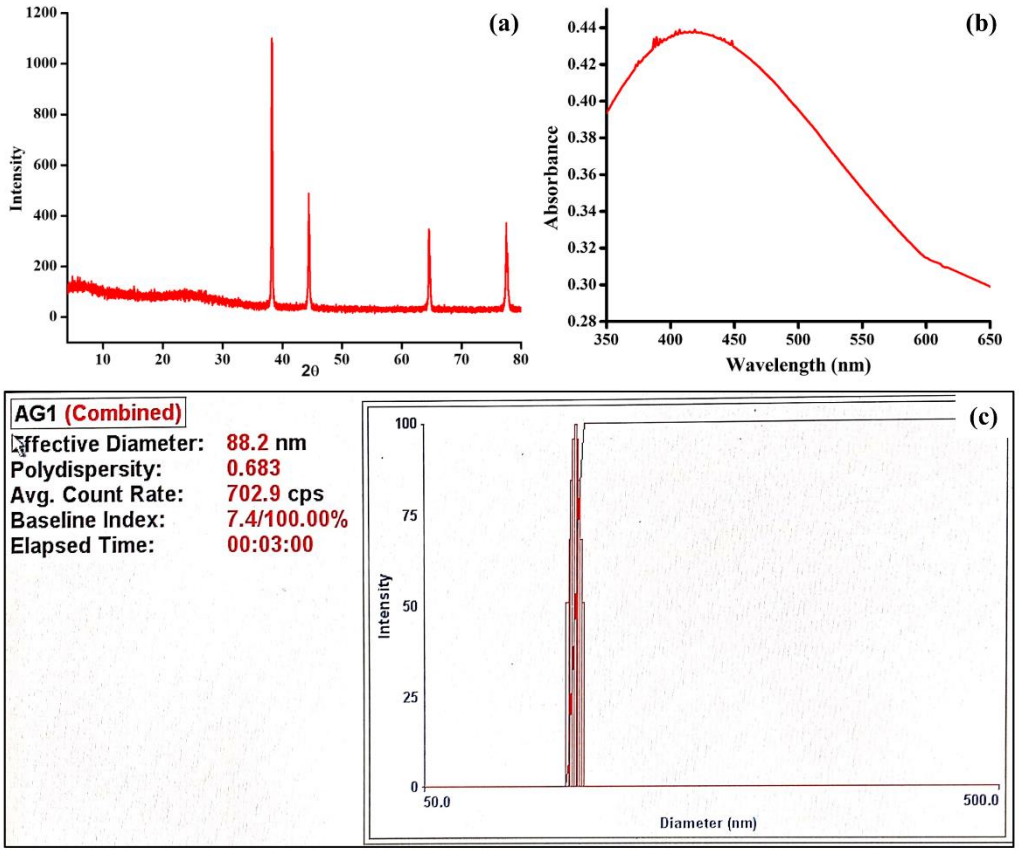

Figure 3.33 (a) DRS (b) PXRD pattern and (c) DLS of calcined Ag nano particles

3.5 CONCLUSIONS

A simple strategy of synthesis of PAM salts of pivalic acid resulted in ten new organogelators. The working hypothesis that 1D H-bonded network supports gelation is well supported by our study. However, the role of the primary amine backbone suggests that aromatic and alicyclic moieties favor gelation over aliphatic backbone. Understandably, supramolecular gelation requires that molecular fibers should assemble into 1D assembly through additional non-covalent interactions such as van der Waals, π…π, C-H…π, etc. along with charge assisted H-bonds, which were inevitably present in the salts (**A1B10-A1B12**). However, other salts showed less gelation properties, in terms of the number of solvents immobilized, due to the presence of a short aliphatic chain. Interestingly, *tert*-butyl amine salt of pivalic acid (**A1B7**) turned out to be a non-gelator despite having 1D H-bond network, which further indicates the critical role of the hydrophobic backbone of amine on gelation behavior. Even though the crystal engineering approach to design a new gelator proved to be fruitful, it could not provide a complete understanding of supramolecular gelation due to lack of information about the role of solvents on gelation behavior.

In the present work, the role of solvent parameters of gelling as well as non-gelling solvents presents some interesting facts such as bulk solvent properties of a solvent (Dielectric constant- $\boldsymbol{\varepsilon}$, and polarity index- ***P'***) may indicate its propensity to gel a solvent. Solvents having dielectric constant in the medium range (20 to 46.7) were found to be capable of undergoing gelation as very high $\boldsymbol{\varepsilon}$ (water) will form well-dissolved gelator molecules and very low $\boldsymbol{\varepsilon}$ values (alkanes) will lead to insoluble gelator molecules. Additionally, the Kamlet-Taft hydrogen bond accepting parameter ($\boldsymbol{\beta}$) and polar cohesive energy parameter ($\boldsymbol{\delta_p}$) displayed a positive correlation with the thermal stability of gel. The mgc values were also found to be positively related to the $\boldsymbol{\delta_h}$ values, the hydrogen bonding HSP.

The unique morphology of xerogel, hollow tubular structures, obtained from acetonitrile gel of salt **A1B12** prompted us to explore it as a template for synthesis of silver nanoparticles. A simple synthetic protocol, UV irradiation of **A1B12** gel in acetonitrile with dissolved silver ions, led to the formation of monodispersed nanoparticles of size 38 nm. This could be a result of electrostatic interactions among

gelator fibers which might be contributing towards the stability of nanoparticles loaded gel. We believe that the holistic method of crystal engineering approach and the study of solvent parameter can lead to the design of new salts based gelators with better understanding of gelation mechanism and applications.

REFERENCES

1. Hirst, A. R. & Smith, D. K. Two-Component Gel-Phase Materials—Highly Tunable Self-Assembling Systems. *Chem. Eur. J.* **11**, 5496–5508 (2005).
2. Edwards, W. & Smith, D. K. Dynamic Evolving Two-Component Supramolecular Gels - Hierarchical Control over Component Selection in Complex Mixtures. *J. Am. Chem. Soc.* **135**, 5911–5920 (2013).
3. Edwards, W. & Smith, D. K. Chiral assembly preferences and directing effects in supramolecular two-component organogels. *Gels* **4**, (2018).
4. Dastidar, P. Supramolecular gelling agents: can they be designed? *Chem. Soc. Rev.* **37**, 2699–2715 (2008).
5. Hanabusa, K., Miki, T., Taguchi, Y., Koyama, T. & Shirai, H. Two-component, small molecule gelling agents. *J. Chem. Soc. Chem. Commun.* 1382–1384 (1993).
6. Yadav, P., Dutta, P. K. & Ballabh, A. Combinatorial library approach to realize 2-aminothiazole-based two-component hydrogelator: A structure - Property correlation. *Cryst. Growth Des.* **14**, 5966–5975 (2014).
7. Jung, J. H., Ono, Y. & Shinkai, S. Organogels of azacrown-appended cholesterol derivatives can be stabilized by host-guest interactions. *Tetrahedron Lett.* **40**, 8395–8399 (1999).
8. Willemen, H. M., Vermonden, T., Marcelis, A. T. M. & Sudho, E. J. R. Alkyl Derivatives of Cholic Acid as Organogelators : One-Component and Two-Component Gels. *Langmuir* **18**, 7102–7106 (2002).
9. Jung, J. H., Lee, S. J., Rim, J. A., Lee, H., Bae, T. S., Lee, S. S. & Shinkai, S. Stabilization of crown-based organogelators by charge-transfer interaction. *Chem. Mater.* **17**, 459–462 (2005).
10. Maitra, U., Kumar, P. V., Chandra, N., D'Souza, L. J., Prasanna, M. D. & Raju, A. R. First donor-acceptor interaction promoted gelation of organic fluids. *Chem. Commun.* 595–596 (1999).
11. Ballabh, A., Trivedi, D. R. & Dastidar, P. Structural studies of a new low molecular mass organic gelator for organic liquids based on simple salt. *Chem. Mater.* **15**, 2136–2140 (2003).
12. Trivedi, D. R., Ballabh, A., Dastidar, P. & Ganguly, B. Structure-property correlation of a new family of organogelators based on organic salts and their selective gelation of oil from oil/water mixtures. *Chem. - A Eur. J.* **10**, 5311–5322 (2004).
13. Ballabh, A., Trivedi, D. R. & Dastidar, P. New series of organogelators derived from a combinatorial library of primary ammonium monocarboxylate salts. *Chem. Mater.* **18**, 3795–3800 (2006).
14. Sangeetha, N. M. & Maitra, U. Supramolecular gels : Functions and uses. *Chem. Soc. Rev.* **34**, 821–836 (2005).
15. Raeburn, J., Cardoso, A. Z. & Adams, D. J. The importance of the self-assembly process to control mechanical properties of low molecular weight hydrogels. *Chem. Soc. Rev.* **42**, 5143–5156 (2013).
16. Yu, G., Yan, X., Han, C. & Huang, F. Characterization of supramolecular gels. *Chem. Soc. Rev.* **42**, 6697–6722 (2013).
17. Dastidar, P. Designing supramolecular gelators: Challenges, frustrations, and hopes. *Gels* **5**, (2019).
18. Yadav, P. & Ballabh, A. N-(thiazol-2-yl)benzamide derivatives as a new series of supramolecular gelators: Role of methyl functionality and S···O interaction. *J. Solid State*

Chem. **281**, 121027 (2020).
19. Mikhailova, T. B., Pakhmutova, E. V., Malkov, A. E., Golovaneva, I. F., Sidorov, A. A., Fomina, I. G., Aleksandrov, G. G., Ikorskii, V. N., Novotortsev, V. M., Eremenko, I. L. & Moiseev, I. I. CCDC 243972: Experimental Crystal Structure Determination. (2004) doi:https://doi.org/10.5517/cc85w2c.
20. Etter, M. C. Encoding and Decoding Hydrogen-Bond Patterns of Organic Compounds. *Acc. Chem. Res.* **23**, 120–126 (1990).
21. McKinnon, J. J., Mitchell, A. S. & Spackman, M. A. Hirshfeld surfaces: A new tool for visualising and exploring molecular crystals. *Chem. Eur. J.* **4**, 2136–2141 (1998).
22. Dolomanov, O. V., Bourhis, L. J., Gildea, R. J., Howard, J. A. K. & Puschmann, H. OLEX2: A complete structure solution, refinement and analysis program. *J. Appl. Crystallogr.* **42**, 339–341 (2009).
23. Sheldrick, G. M. A short history of SHELX. *Acta Crystallogr. Sect. A Found. Crystallogr.* **64**, 112–122 (2008).
24. Spackman, M. A. & Byrom, P. G. A novel definition of a molecule in a crystal. *Chem. Phys. Lett.* **267**, 215–220 (1997).
25. Spackman, M. A. & Mckinnon, J. J. Fingerprinting intermolecular interactions in molecular crystals. *CrystEngComm* **4**, 378–392 (2002).
26. McKinnon, J. J., Jayatilaka, D. & Spackman, M. A. Towards quantitative analysis of intermolecular interactions with Hirshfeld surfaces. *Chem. Commun.* 3814–3816 (2007).
27. Spackman, M. A. & Jayatilaka, D. Hirshfeld surface analysis. *CrystEngComm* **11**, 19–32 (2009).
28. Das, U. K., Trivedi, D. R., Adarsh, N. N. & Dastidar, P. Supramolecular Synthons in Noncovalent Synthesis of a Class of Gelators Derived from Simple Organic Salts : Instant Gelation of Organic Fluids at Room Temperature via in Situ Synthesis of the Gelators. *J. Org. Chem.* **74**, 7111–7121 (2009).
29. Lan, Y., Corradini, M. G., Weiss, R. G., Raghavan, S. R. & Rogers, M. A. To gel or not to gel: correlating molecular gelation with solvent parameters. *Chem. Soc. Rev.* **44**, 6035–6058 (2015).
30. Hildebrand, J. H. & Scott, R. L. *The Solubility of Nonelectrolytes*. (Dover Publications, Reinhold, NY, 1959).
31. Hansen, C. M. *Hansen Solubility Parameters in Practice – Complete with software, data, and examples*. (www.hansen-solubility.com, 2015).
32. Hansen, C. M. The Three Dimensional Solubility Parameter - Key to Paint Component Affinities I. - Solvents, Plasticizers, Polymers, and Resins. *J. Paint Techn.* **39**, 104–117 (1967).
33. Kamlet, M. J., Abboud, J.-L. M., Abraham, M. H. & Taft, R. W. Linear Solvation Energy Relationships. 23. A Comprehensive Collection of the Solvatochromic Parameters,. *J. Org. Chem.* 2877–2887 (1983).
34. Lan, Y., Corradini, M. G., Liu, X., May, T. E., Borondics, F., Weiss, R. G. & Rogers, M. A. Comparing and correlating solubility parameters governing the self-assembly of molecular gels using 1,3:2,4-dibenzylidene sorbitol as the gelator. *Langmuir* **30**, 14128–14142 (2014).
35. Bayliss, N. S. & McRae, E. G. Solvent effects in the spectra of acetone, crotonaldehyde, nitromethane and nitrobenzene. *J. Phys. Chem.* **58**, 1006–1011 (1954).
36. Reichardt, C. *Solvents and Solvent Effects in Chemisry*. (Weinheim, Germany, 1988).
37. Barton, A. F. M. Solubility Parameters. *Chem. Rev.* **75**, 731–753 (1975).
38. Edwards, W., Lagadec, C. A. & Smith, D. K. Solvent–gelator interactions—using

empirical solvent parameters to better understand the self-assembly of gel-phase materials understand the self-assembly of gel-phase materials. *Soft Matter* **7**, 110–117 (2011).

39. Gao, J., Wu, S. & Rogers, M. A. Harnessing Hansen solubility parameters to predict organogel formation. *J. Mater. Chem.* **22**, 12651–12658 (2012).
40. Draper, E. R. & Adams, D. J. Low-Molecular-Weight Gels: The State of the Art. *Chem* **3**, 390–410 (2017).
41. Torigoe, K. & Esumi, K. Formation of Nonspherical Palladium Nanocrystals in SDS/Poly(acrylamide) Gel. *Langmuir* **11**, 4199–4201 (1995).
42. Gundiah, G., Mukhopadhyay, S., Tumkurkar, U. G., Govindaraj, A., Maitra, U. & Rao, C. N. R. Hydrogel route to nanotubes of metal oxides and sulfates. *J. Mater. Chem.* **13**, 2118–2122 (2003).
43. Bommel, K. J. C. Van, Friggeri, A. & Shinkai, S. Organic Templates for the Generation of Inorganic Materials. *Angew. Chem. Int. Ed.* **42**, 980–999 (2003).
44. Mock, J. J., Barbic, M., Smith, D. R., Schultz, D. A. & Schultz, S. Shape effects in plasmon resonance of individual colloidal silver nanoparticles. *J. Chem. Phys.* **116**, 6755–6759 (2002).
45. Mantion, A., Guex, A. G., Foelske, A., Mirolo, L., Fromm, K. M., Painsi, M. & Taubert, A. Silver nanoparticle engineering via oligovaline organogels. *Soft Matter* **4**, 606–617 (2008).

*SUPPLEMENTARY DATA

Crystallographic Data

Table S3.1 Crystallographic Data and Structure refinement parameters

	A1B1	A1B7	A1B10	A1B11	A1B12
Empirical formula	$C_{12}H_{28}N_2O_4$	$C_9H_{21}NO_2$	$C_{11}H_{23}NO_2$	$C_{13}H_{21}NO_2$	$C_{17}H_{28}N_2O_2$
Formula weight	264.36	175.27	201.30	223.31	292.41
Temperature/ K	293	293	293	293	293
Crystal system	monoclinic	orthorhombic	Triclinic	orthorhombic	monoclinic
Space group	$P2_1/c$	$Pna2_1$	$P\text{-}1$	$P2_12_12_1$	$P2_1/n$
a/Å	12.1933(8)	19.0329(18)	6.7121(9)	6.1662(8)	15.9520(18)
b/Å	6.7837(4)	9.4763(8)	8.6129(12)	12.3330(13)	6.2958(5)
c/Å	20.0399(15)	6.5281(8)	11.1663(13)	17.6898(15)	18.2802(17)
α/°	90	90	102.644(11)	90	90
β/°	92.215(7)	90	91.314(11)	90	92.460(9)
γ/°	90	90	91.346(12)	90	90
Volume/Å^3	1656.38(19)	1177.4(2)	629.44(14)	1345.3(2)	1834.2(3)
Z	4	4	2	4	4
ρ_{calc}g/cm^3	1.060	0.989	1.062	1.103	1.059
μ/mm^{-1}	0.078	0.068	0.072	0.074	0.069
F(000)	584.0	392.0	224.0	488.0	640.0
Crystal size/mm^3	0.7 × 0.4 × 0.2	0.4 × 0.3 × 0.1	0.8 × 0.4 × 0.1	0.5 × 0.3 × 0.1	0.9 × 0.8 × 0.14
Index ranges	$-15 \le h \le 15$, $-8 \le k \le 8$, $-24 \le l \le 25$	$-23 \le h \le 23$, $-11 \le k \le 11$, $-8 \le l \le 8$	$-8 \le h \le 8$, $-11 \le k \le 10$, $-15 \le l \le 12$	$-7 \le h \le 7$, $-15 \le k \le 15$, $-20 \le l \le 22$	$-19 \le h \le 19$, $-7 \le k \le 7$, $-22 \le l \le 22$
Reflections collected	15561	6481	4846	8139	18715
Independent reflections	3092 [R_{int} = 0.0402, R_{sigma} = 0.0285]	2235 [R_{int} = 0.0801, R_{sigma} = 0.1069]	2844 [R_{int} = 0.0176, R_{sigma} = 0.0361]	2736 [R_{int} = 0.0987, R_{sigma} = 0.1338]	3725 [R_{int} = 0.0553, R_{sigma} = 0.0418]
Data/restraints/parameters	3092/0/171	2235/1/135	2844/0/131	2736/0/150	3725/0/194
Goodness-of-fit on F^2	1.391	0.958	1.619	0.928	1.356
Final R indexes [I>=2σ (I)]	R_1 = 0.0979, wR_2 = 0.2219	R_1 = 0.0816, wR_2 = 0.1861	R_1 = 0.0911, wR_2 = 0.2593	R_1 = 0.0968, wR_2 = 0.2546	R_1 = 0.0880, wR_2 = 0.2348
Final R indexes [all data]	R_1 = 0.1442, wR_2 = 0.2556	R_1 = 0.1944, wR_2 = 0.2583	R_1 = 0.1251, wR_2 = 0.2858	R_1 = 0.2039, wR_2 = 0.3447	R_1 = 0.1253, wR_2 = 0.2606
Largest diff. peak/hole / e Å^{-3}	0.42/-0.24	0.32/-0.15	0.68/-0.24	0.33/-0.20	0.40/-0.21
Flack Parameter	-	-2.1(10)	-	3.1(10)	-
CCDC Number	1861605	1989691	1858950	1989687	1858607

H-bonds for salts 1A-1K

Table S3.2 Hydrogen bond parameters for salts

D	H	A	d(D-H) /Å	d(H-A) /Å	d(D-A)/Å	D-H-A /°	Symmetry operation for A
A1B1							
N1	H1A	O3	0.89	1.87	2.753(3)	170.4	+X, +Y, +Z
N1	H1B	O4	0.89	2.58	3.315(3)	140.5	-X, 1/2+Y, 1/2-Z
N1	H1B	O3	0.89	1.91	2.767(3)	161.3	-X, 1/2+Y, 1/2-Z
N1	H1C	O4	0.89	1.83	2.696(3)	163.2	+X,1+Y,+Z
N2	H2A	O1	0.89	2.46	3.154(3)	135.7	-X,2-Y,-Z
N2	H2A	O2	0.89	1.91	2.786(3)	166.3	-X,2-Y,-Z
N2	H2B	O2	0.89	1.90	2.725(3)	154.0	+X, +Y, +Z
N2	H2C	O1	0.89	1.82	2.698(3)	168.2	+X,-1+Y,+Z
C6	H6B	O4	0.97	2.54	3.377(3)	144.9	-X, 1/2+Y, 1/2-Z
A1B7							
N1	H1A	O2	0.89	1.92	2.793(8)	166.8	1-X, 1-Y, -1/2+Z
N1	H1B	O2	0.89	1.95	2.803(7)	160.6	+X, +Y, +Z
N1	H1C	O1	0.89	1.80	2.684(7)	170.6	1-X,1-Y,1/2+Z
A1B10							
N1	H1A	O2	0.89	1.95	2.811(3)	162.7	1-X, 1-Y, -Z
N1	H1B	O1	0.89	1.85	2.728(3)	169.5	+X, +Y, +Z
N1	H1C	O2	0.89	1.90	2.773(3)	166.3	-1+X, +Y, +Z
A1B11							
N1	H1A	O1	0.89	1.93	2.789(9)	160.6	1+X, +Y, +Z
N1	H1B	O2	0.89	1.82	2.713(9)	177.7	+X, +Y, +Z
N1	H1C	O2	0.89	1.93	2.812(8)	172.0	1/2+X, -1/2-Y, -1-Z
A1B12							
N1	H1A	O2	0.89	1.90	2.786(3)	170.8	3/2-X, -1/2+Y, 1/2-Z
N1	H1B	O2	0.89	1.86	2.732(3)	167.0	+X,-1+Y,+Z
N1	H1C	O1	0.89	1.82	2.701(3)	170.4	+X, +Y, +Z

Solvent Parameter Plots

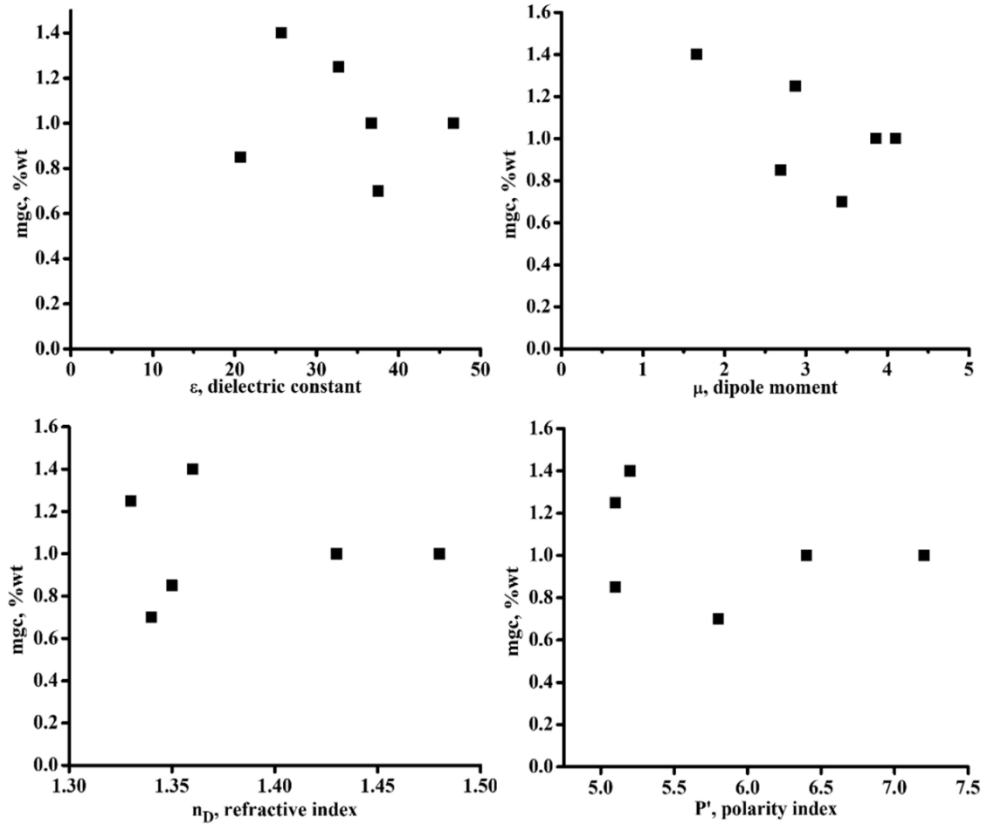

Figure S3.1 Variation of mgc values with dielectric constants, dipole moments, refractive indices and polarity indices of the solvents for salt A1B11

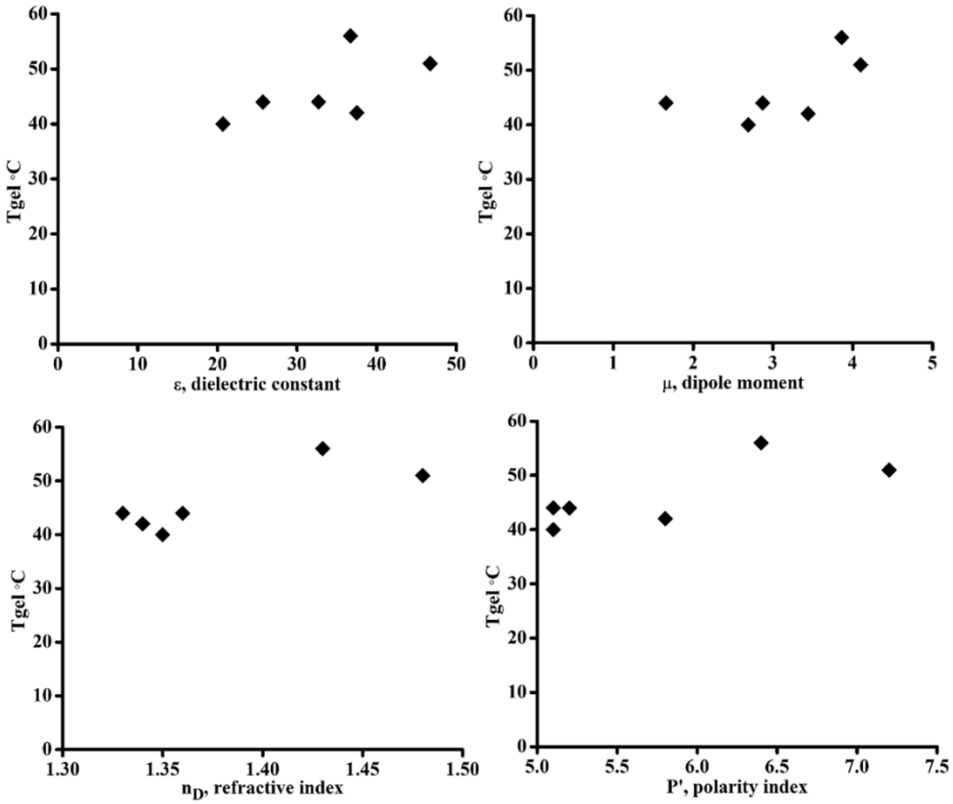

Figure S3.2 Variation of T_{gel} values with dielectric constants, dipole moments, refractive indices and polarity indices of the solvents for salt A1B11

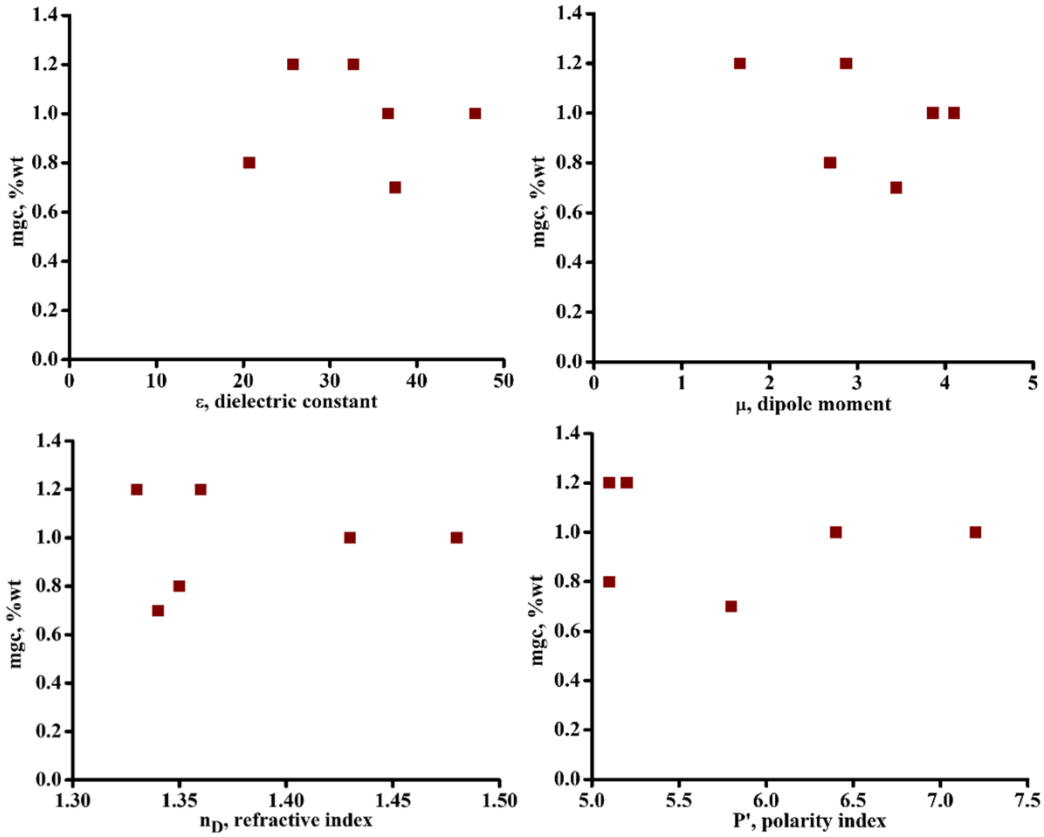

Figure S3.3 Variation of mgc values with dielectric constants, dipole moments, refractive indices and polarity indices of the solvents for salt A1B12

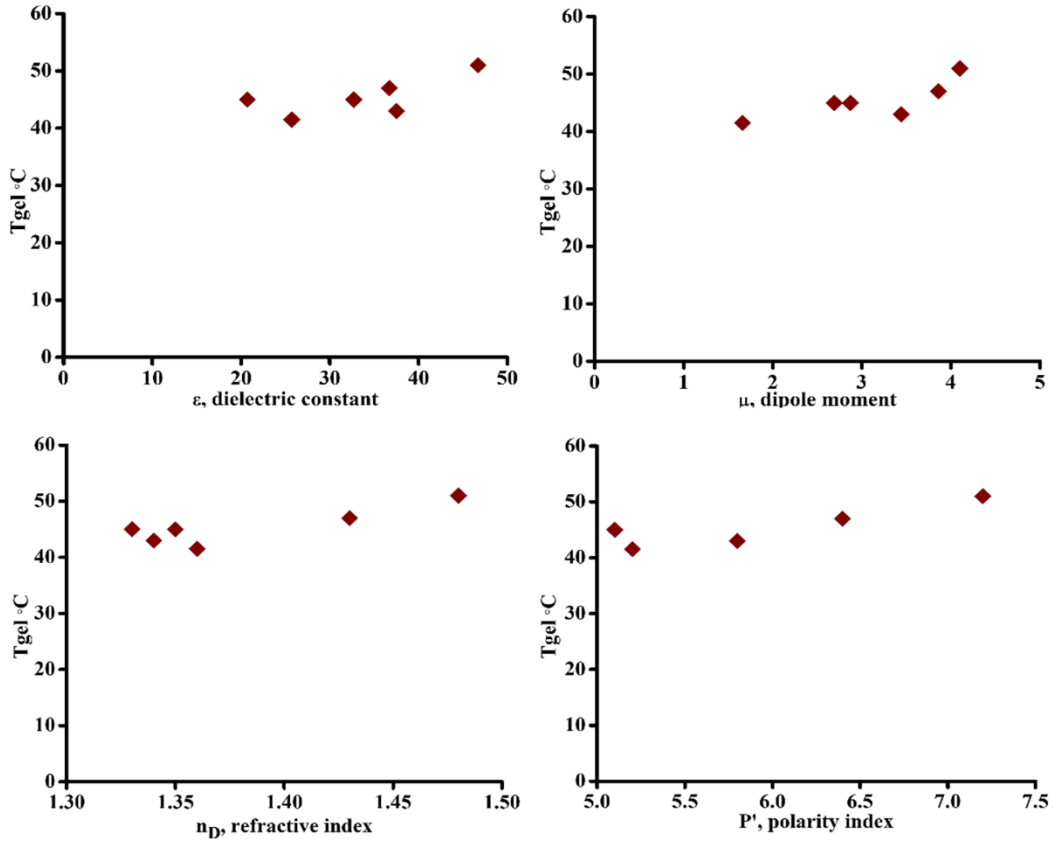

Figure S3.4 Variation of T_{gel} values with dielectric constants, dipole moments, refractive indices and polarity indices of the solvents for salt A1B12

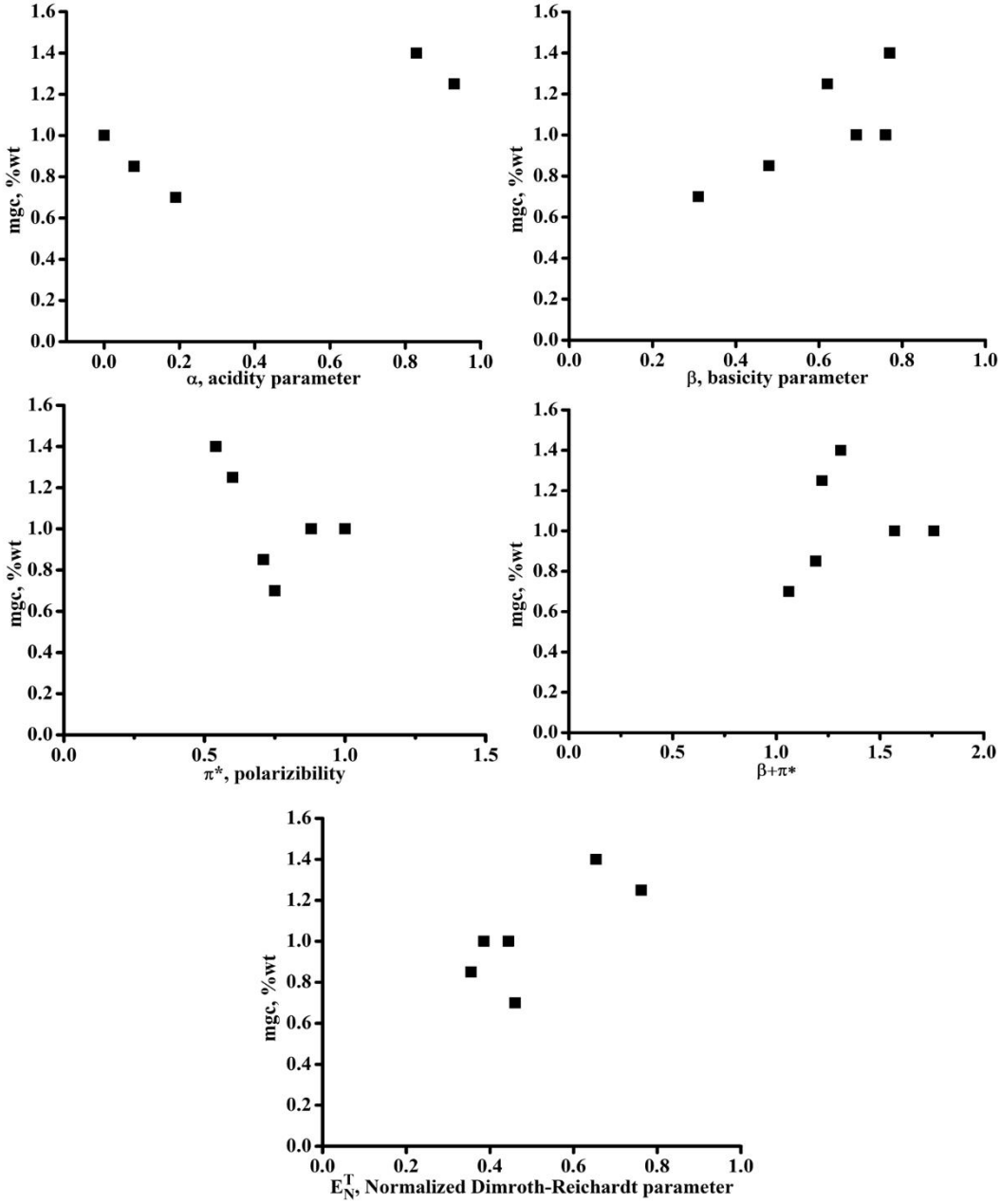

Figure S3.5 Variation of mgc values with acidity and basicity parameters, polarizibilty and Normalized Dimroth-Reichardt parameters of the solvents for salt A1B11

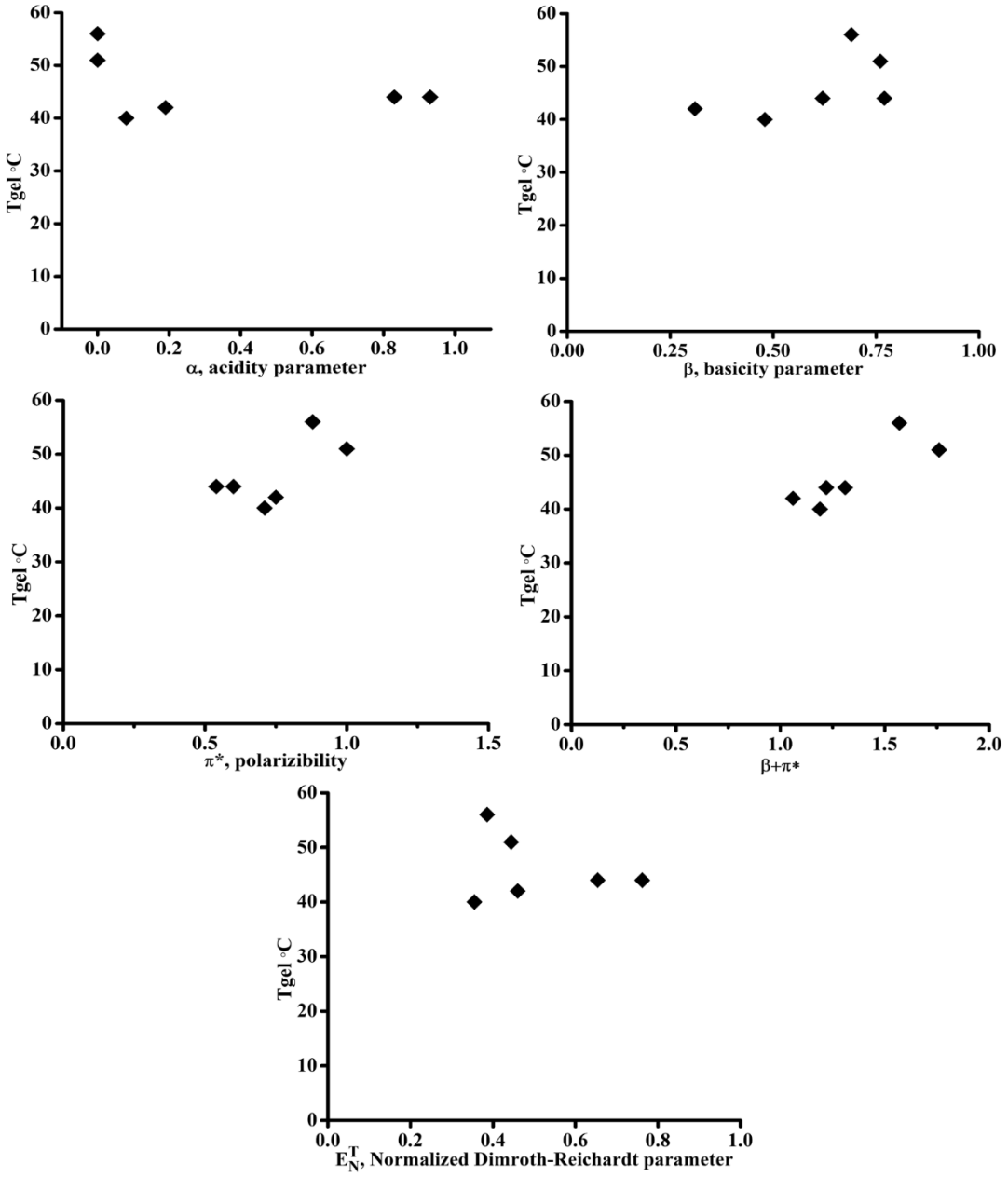

Figure S3.6 Variation of T_{gel} values with acidity and basicity parameters, polarizibilty and Normalized Dimroth-Reichardt parameters of the solvents for salt A1B11

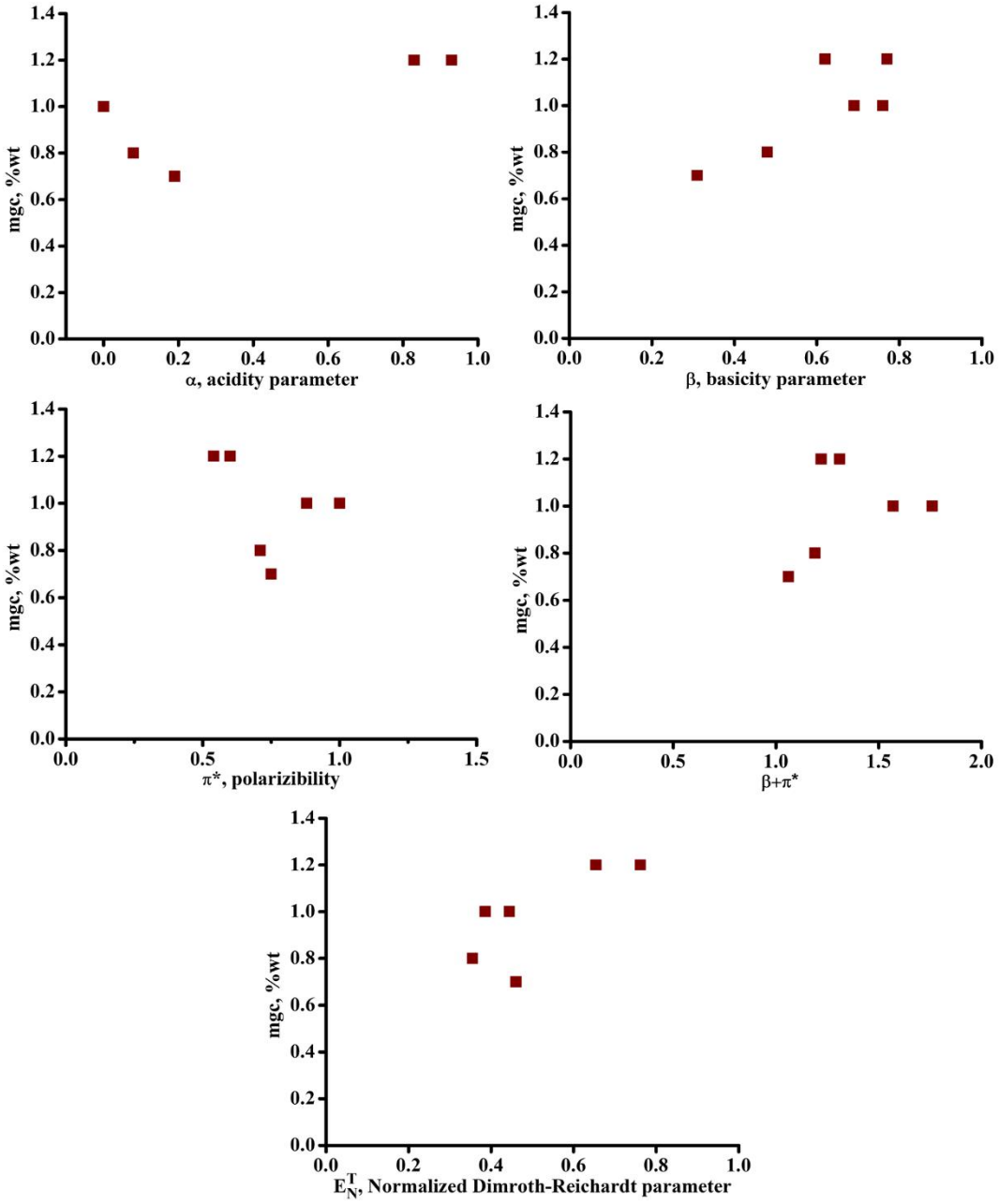

Figure S3.7 Variation of mgc values with acidity and basicity parameters, polarizibilty and Normalized Dimroth-Reichardt parameters of the solvents for salt A1B12

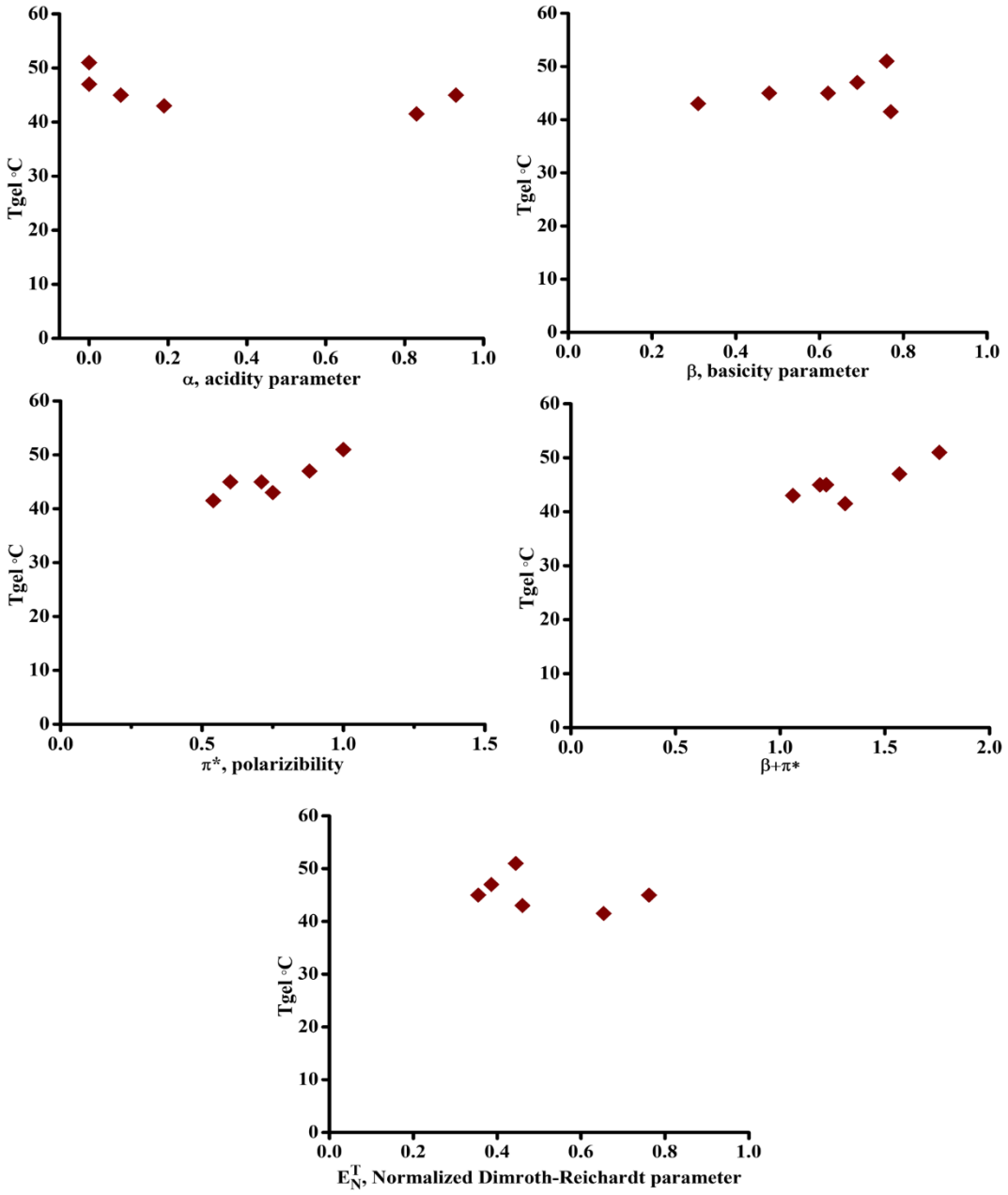

Figure S3.8 Variation of T_{gel} values with acidity and basicity parameters, polarizibilty and Normalized Dimroth-Reichardt parameters of the solvents for salt A1B12

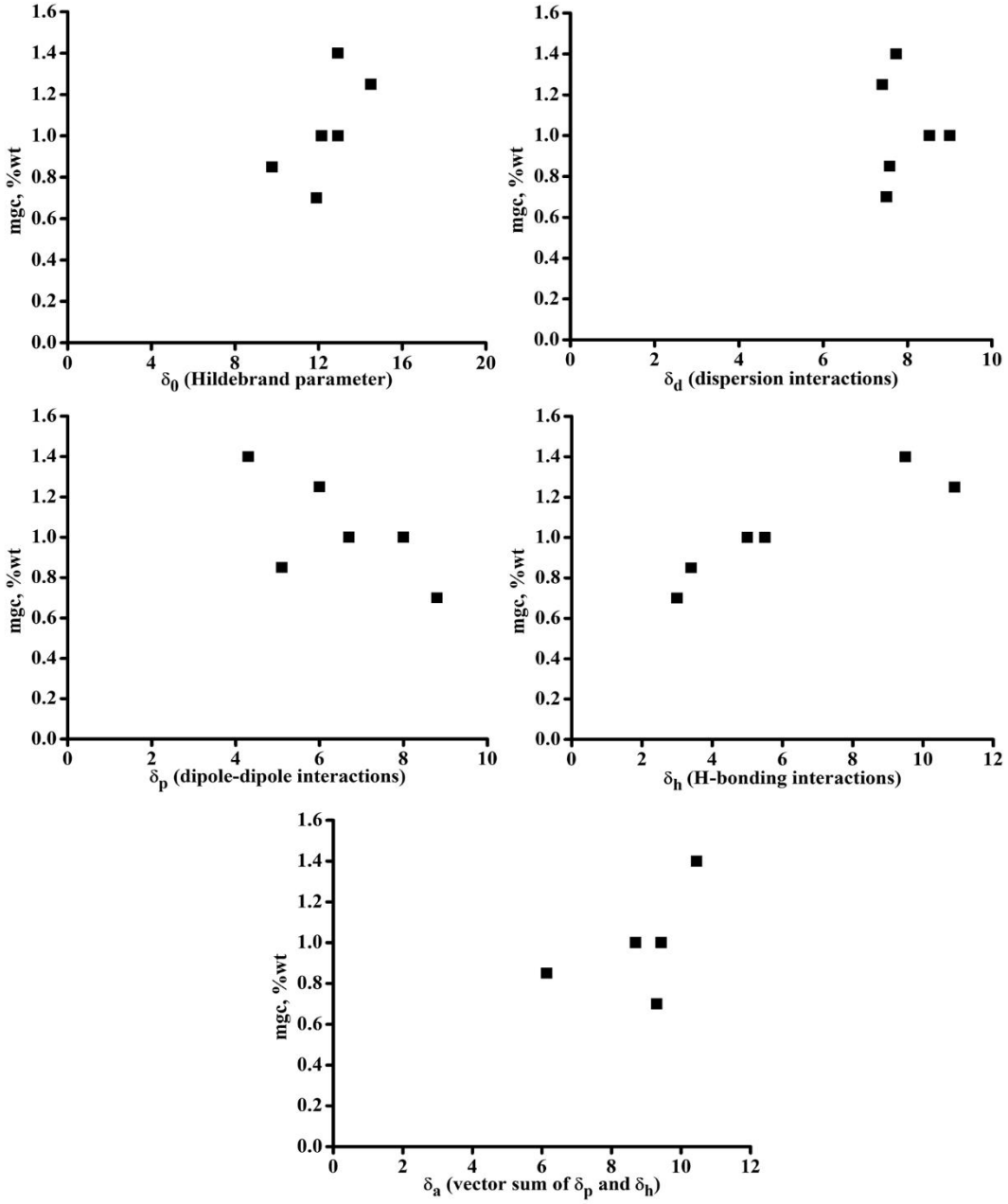

Figure S3.9 Variation of mgc values with thermodynamically derived solvent parameters for salt A1B11

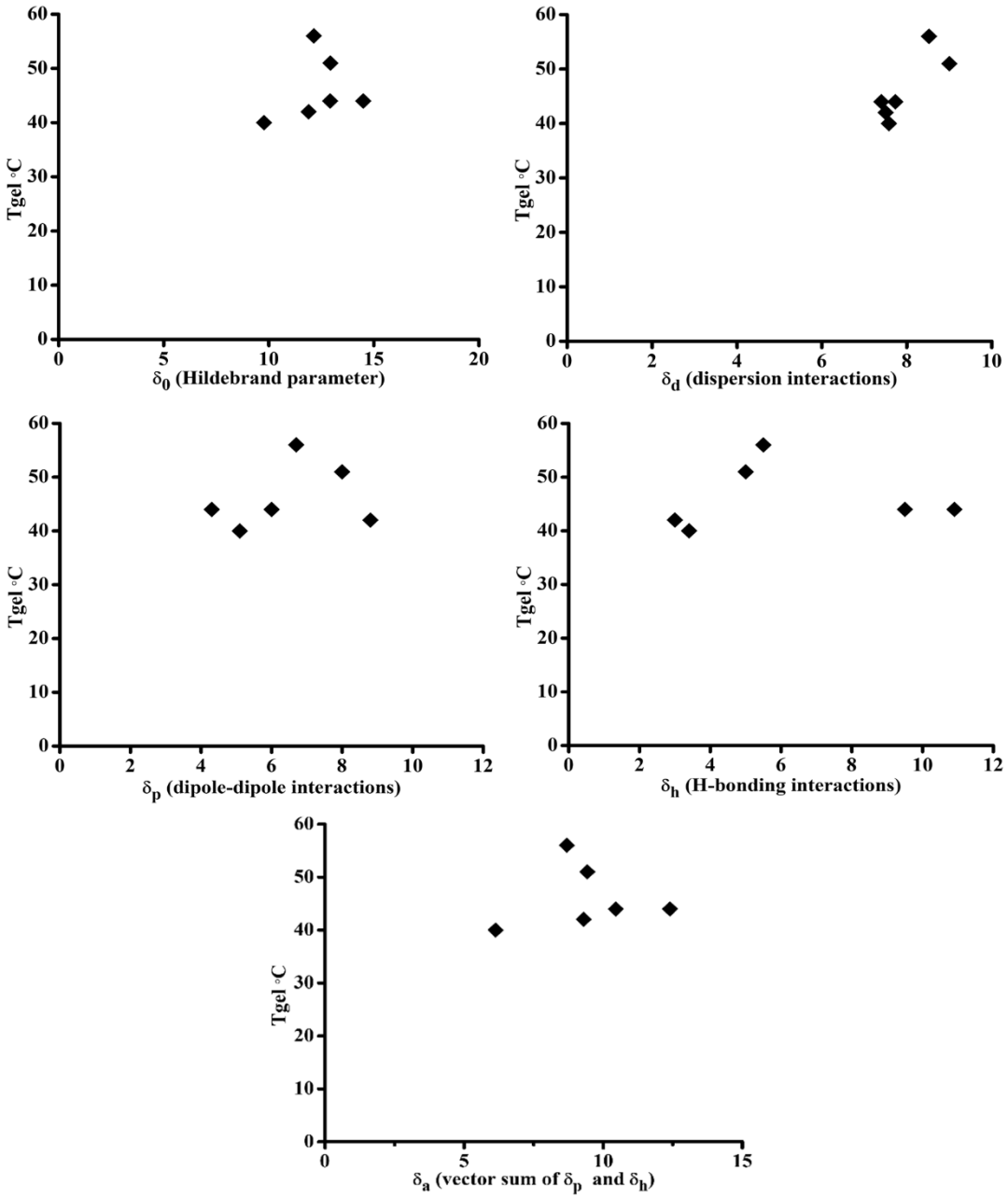

Figure S3.10 Variation of T_{gel} values with thermodynamically derived solvent parameters for salt A1B11

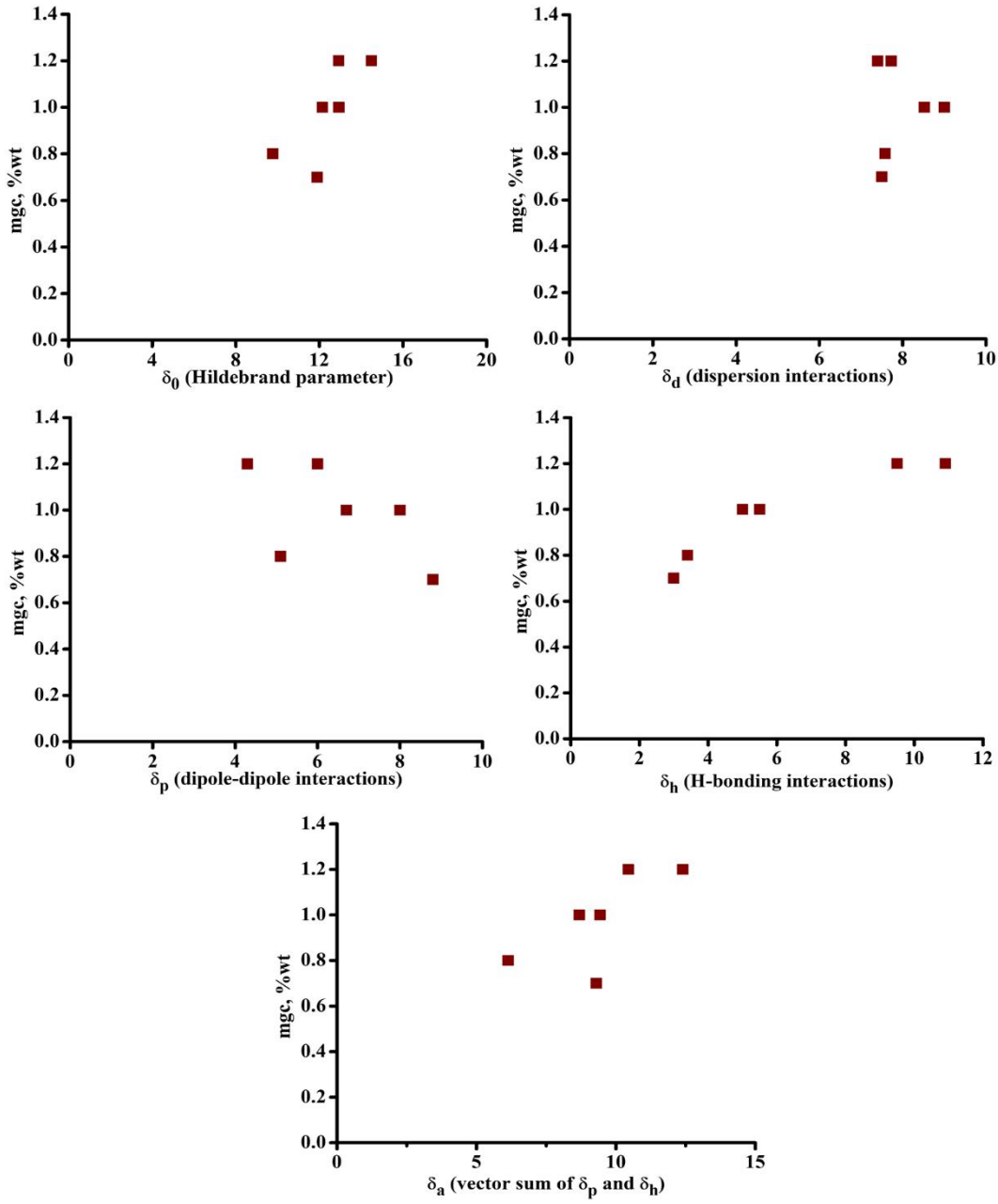

Figure S3.11 Variation of mgc values with thermodynamically derived solvent parameters for salt A1B12

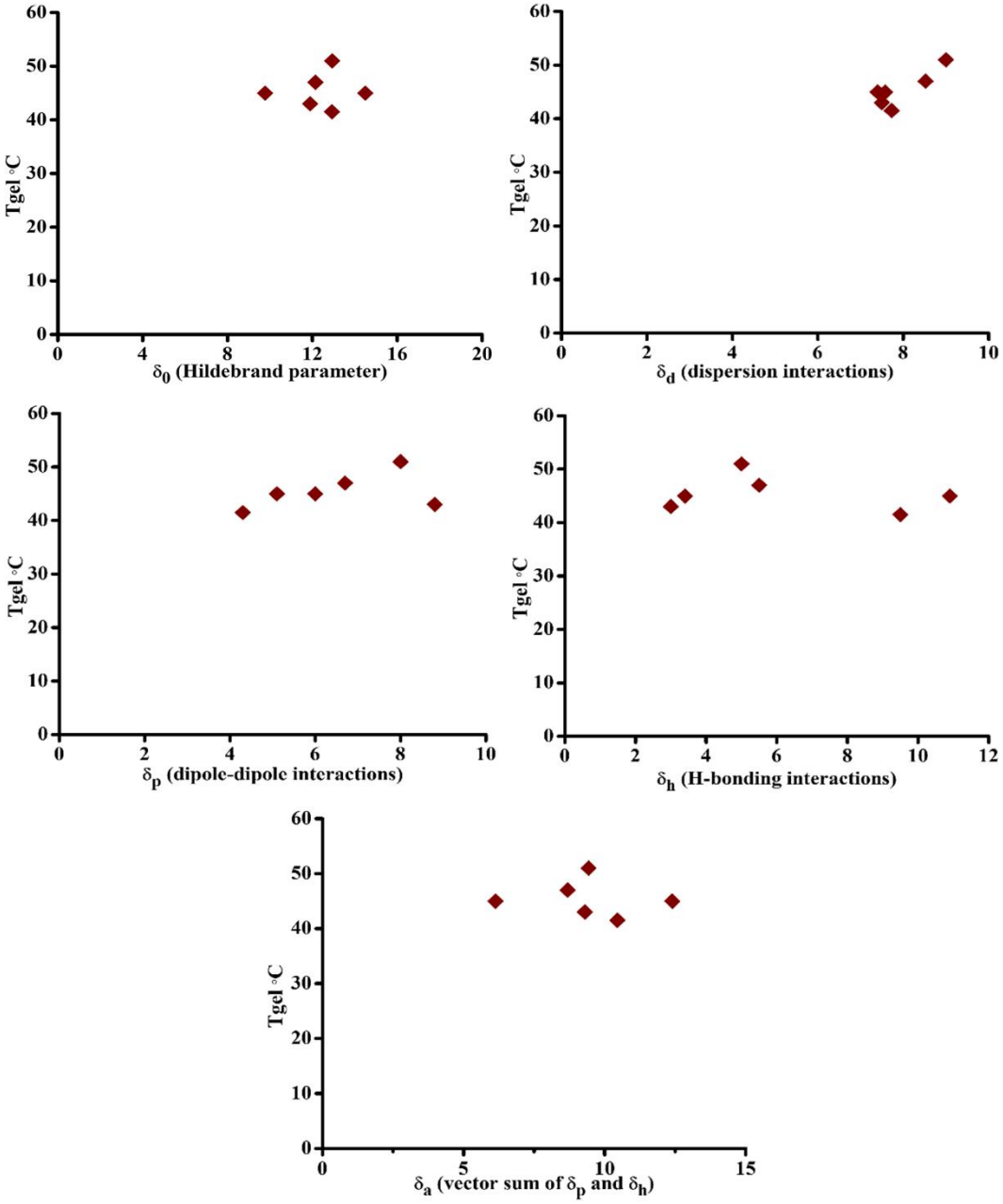

Figure S3.12 Variation of T_{gel} values with thermodynamically derived solvent parameters for salt A1B12

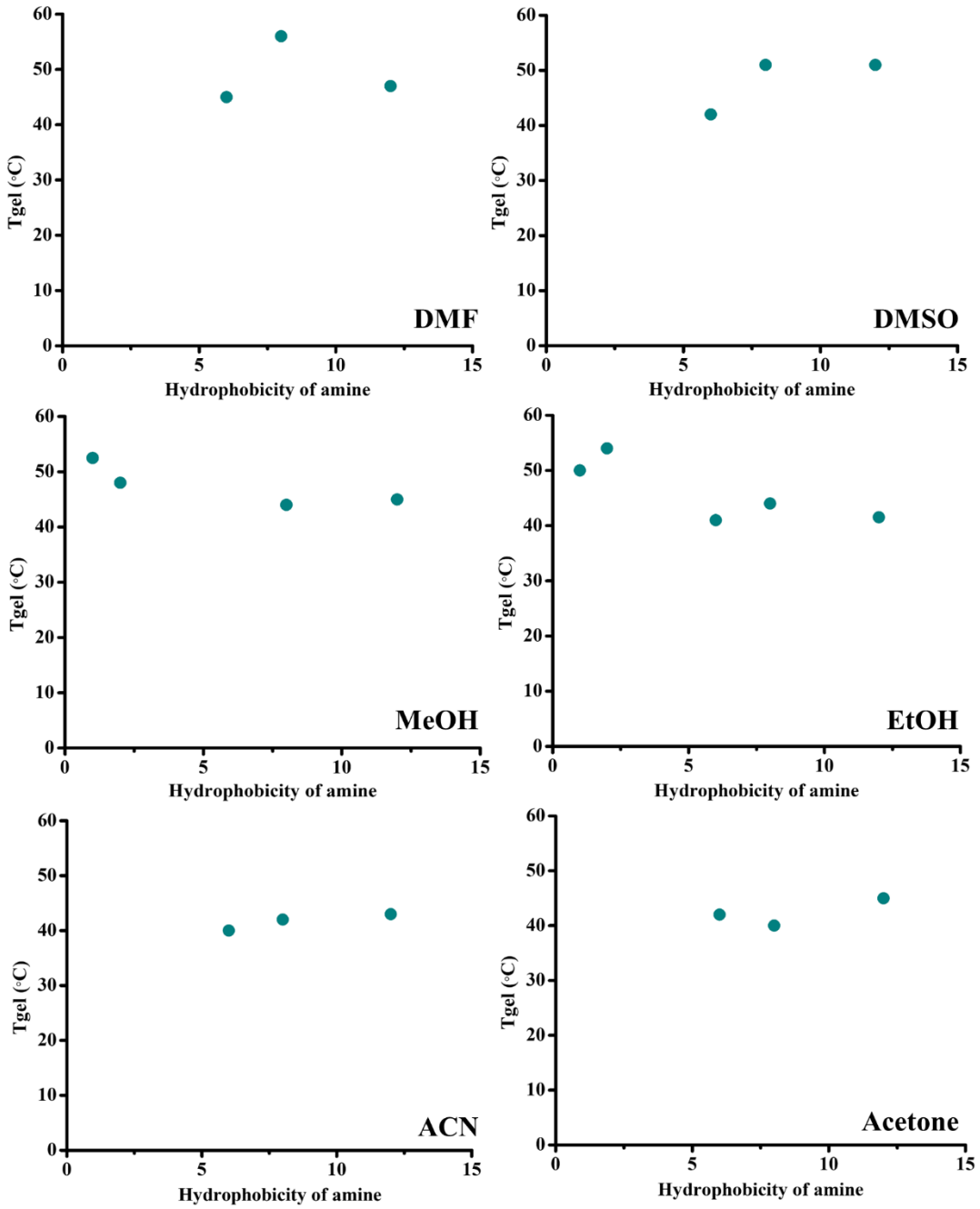

Figure S3.13 Variation of T_{gel} values with hydrophobicity of amines used

3D Hirshfeld surfaces and ORTEP images

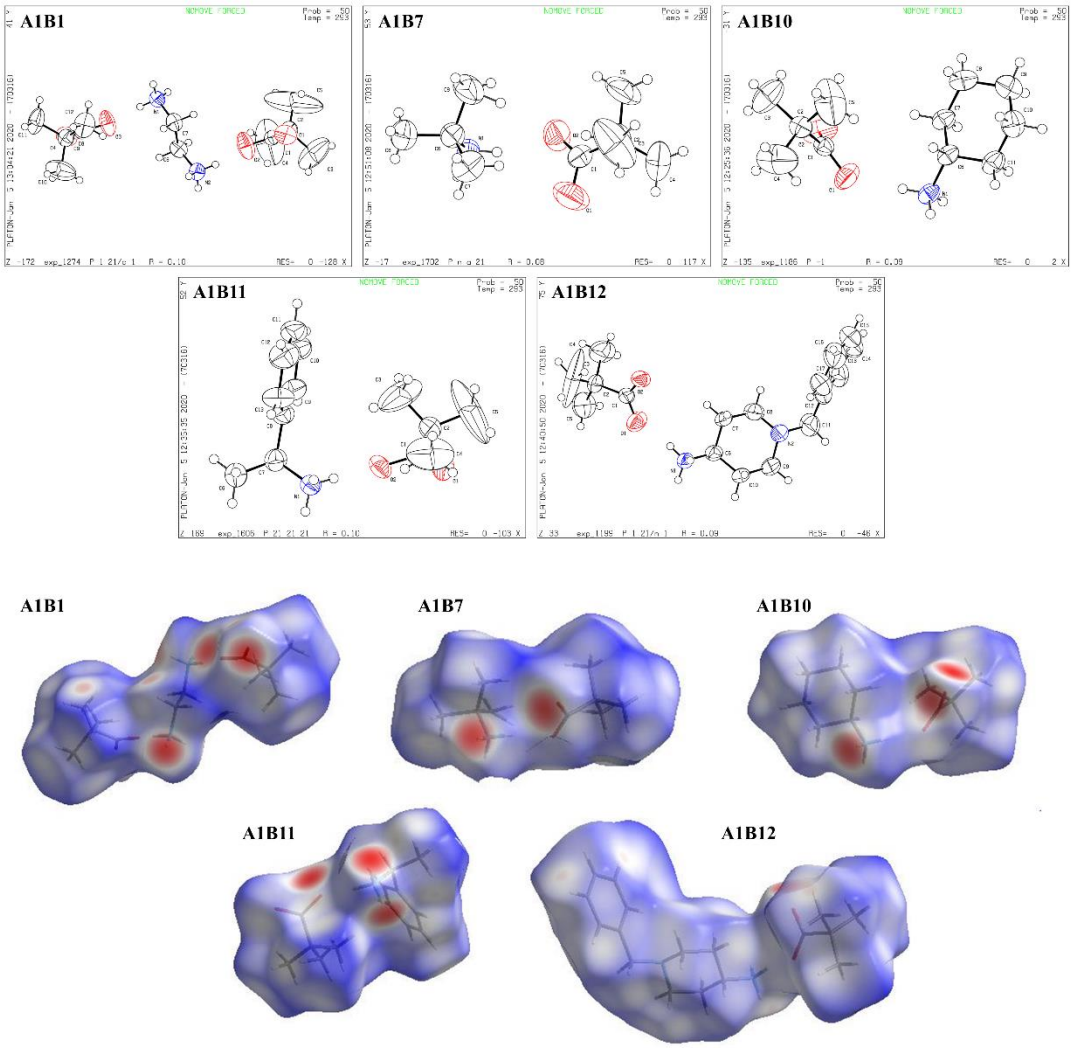

Figure S3.14 ORTEP and 3D Hirshfeld surfaces of all single crystal structures

Spectral Data – NMR and FT-IR

A1B1

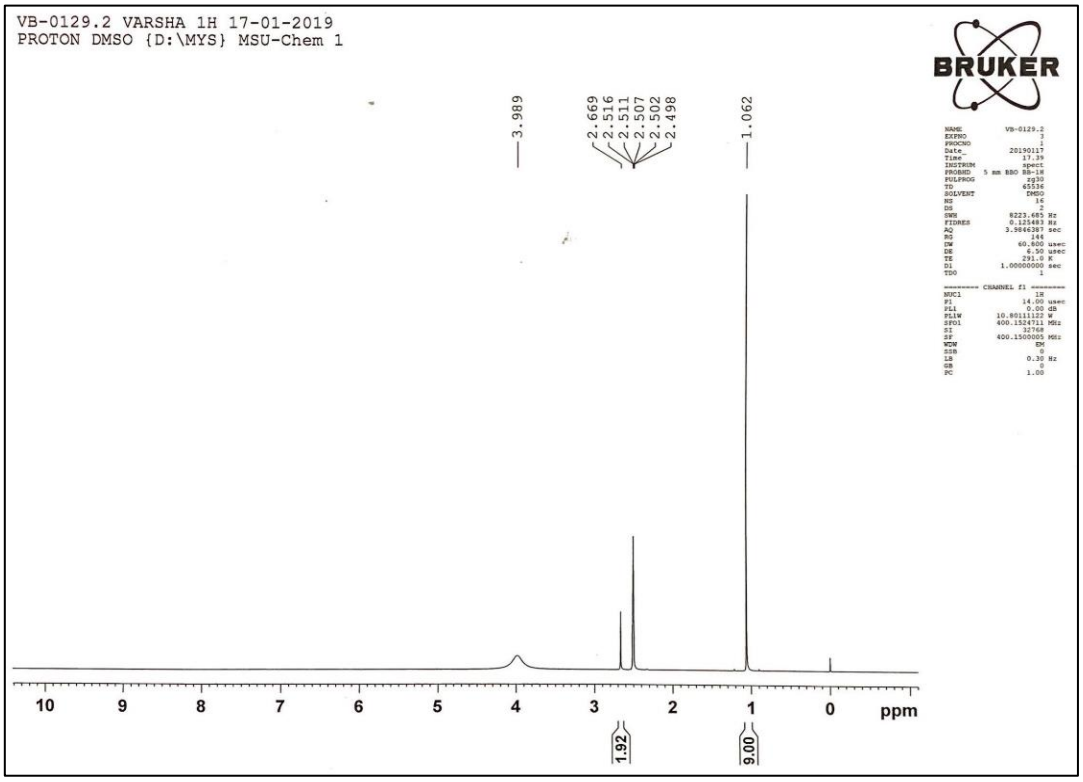

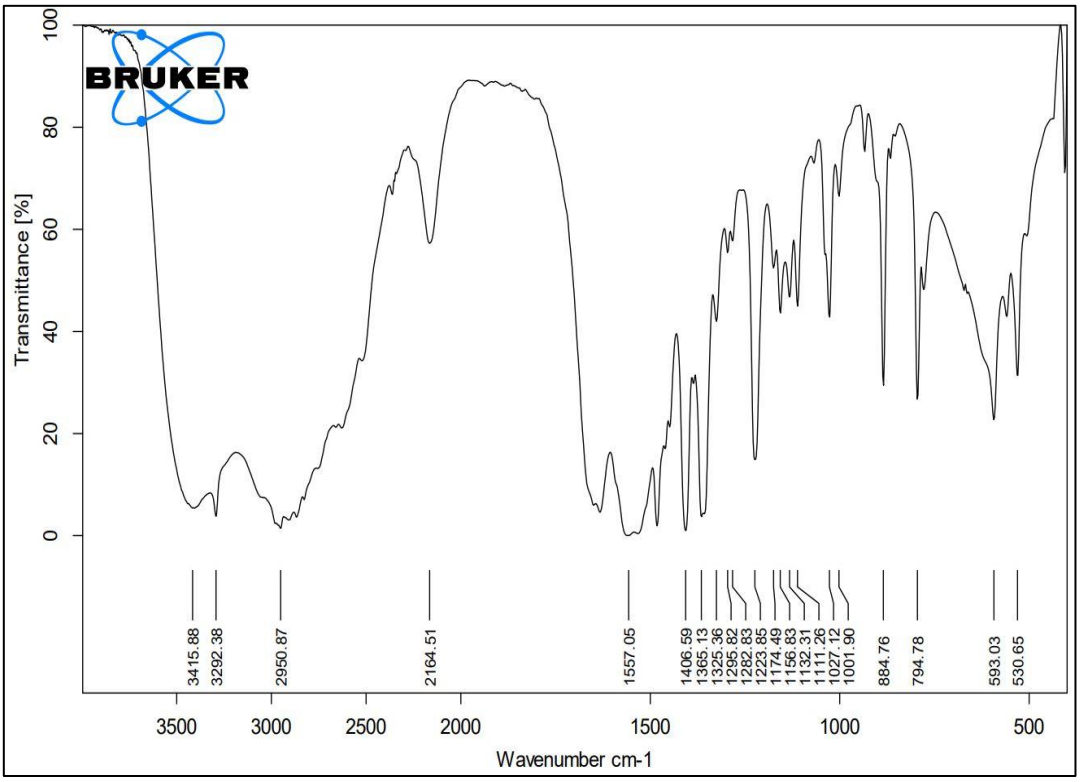

A1B2

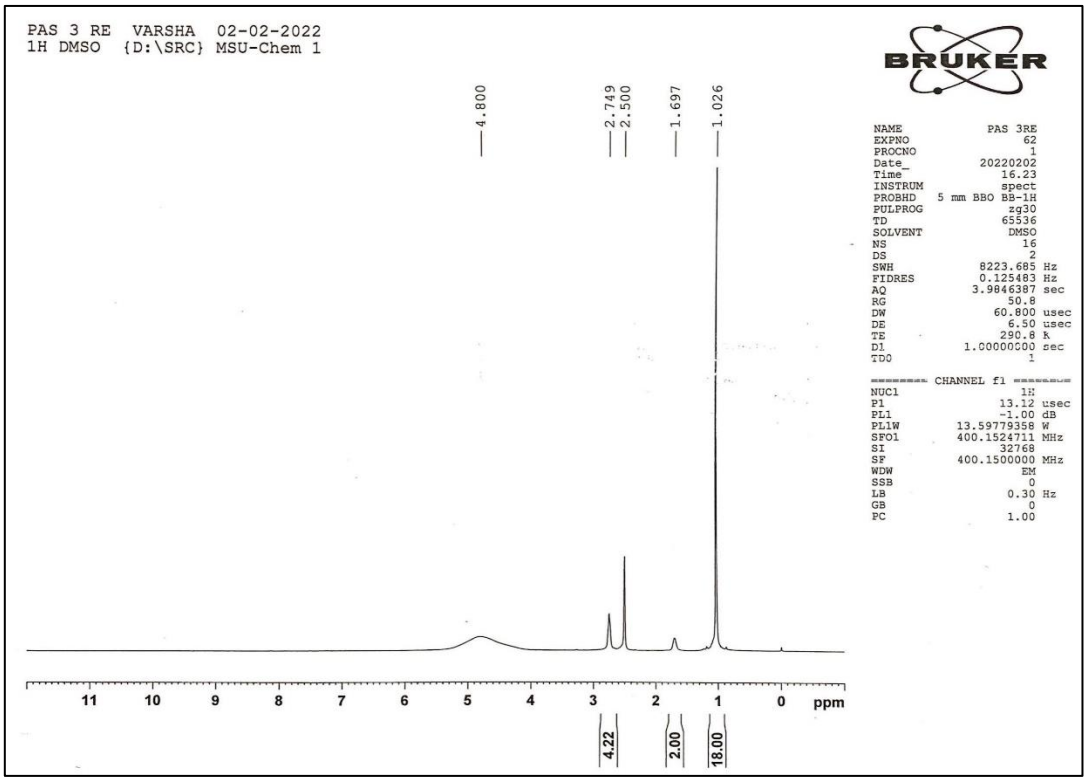
PAS 3 RE VARSHA 02-02-2022
1H DMSO {D:\SRC} MSU-Chem 1
BRUKER
4.800
2.749
2.500
1.697
1.026
NAME PAS 3RE
EXPNO 62
PROCNO 1
Date_ 20220202
Time 16.23
INSTRUM spect
PROBHD 5 mm BBO BB-1H
PULPROG zg30
TD 65536
SOLVENT DMSO
NS 16
DS 2
SWH 8223.685 Hz
FIDRES 0.125483 Hz
AQ 3.9846387 sec
RG 50.8
DW 60.800 usec
DE 6.50 usec
TE 290.8 k
D1 1.00000000 sec
TD0 1
CHANNEL f1
NUC1 1H
P1 13.12 usec
PL1 -1.00 dB
PL1W 13.59779358 W
SFO1 400.1524711 MHz
SI 32768
SF 400.1500000 MHz
WDW EM
SSB 0
LB 0.30 Hz
GB 0
PC 1.00
11 10 9 8 7 6 5 4 3 2 1 0 ppm
4.22
2.00
18.00

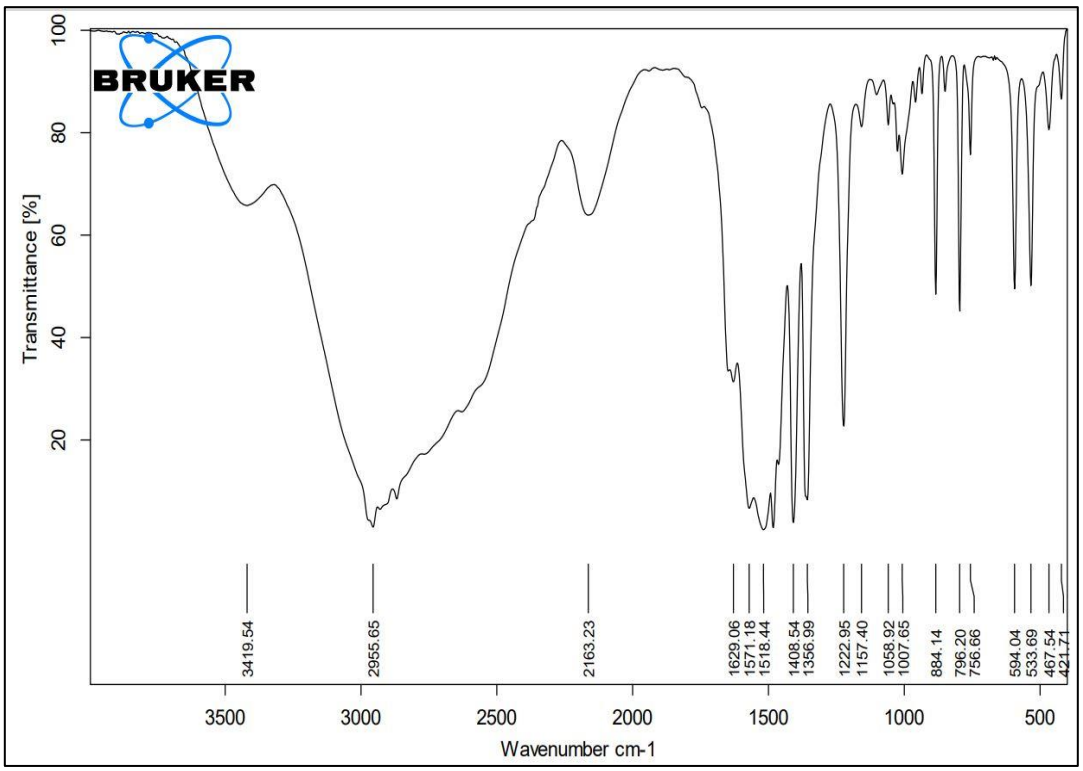
BRUKER
Transmittance [%]
100
80
60
40
20
3419.54
2955.65
2163.23
1629.06
1571.18
1518.44
1408.54
1356.99
1222.95
1157.40
1058.92
1007.65
884.14
796.20
756.66
594.04
533.69
467.54
421.71
3500
3000
2500
2000
1500
1000
500
Wavenumber cm-1

A1B3

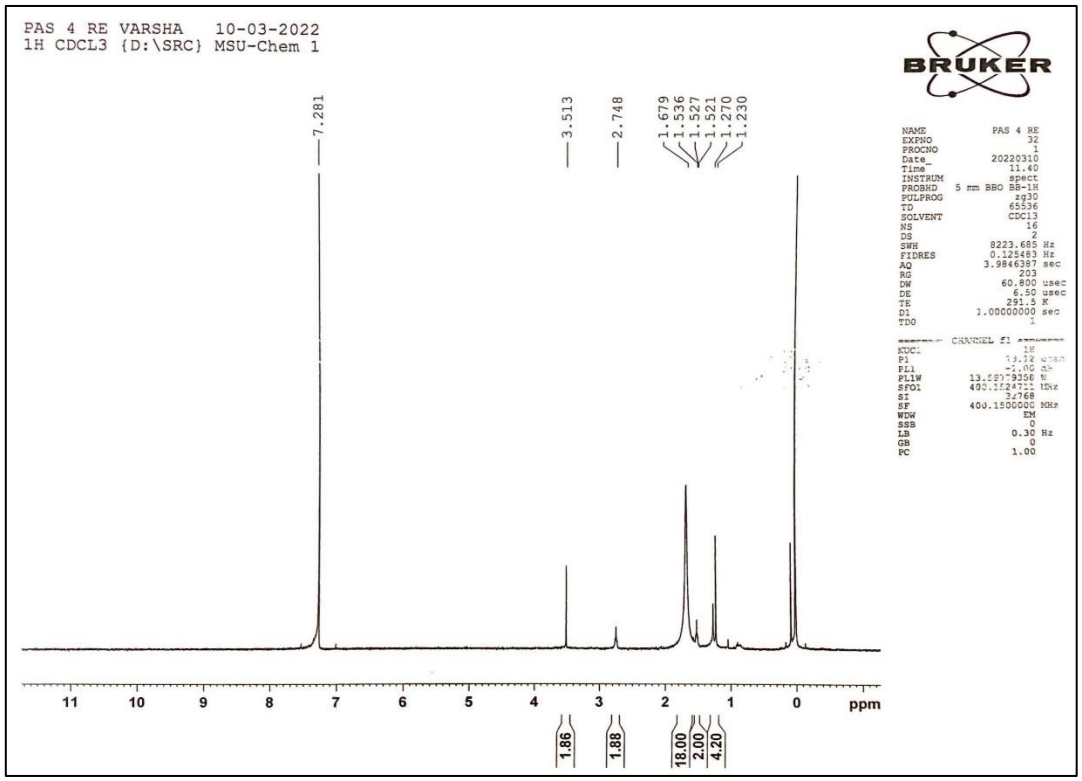
PAS 4 RE VARSHA 10-03-2022
1H CDCL3 {D:\SRC} MSU-Chem 1
BRUKER
7.281
3.513
2.748
1.679
1.536
1.527
1.521
1.270
1.230
11 10 9 8 7 6 5 4 3 2 1 0 ppm
1.86
1.88
18.00
2.00
4.20

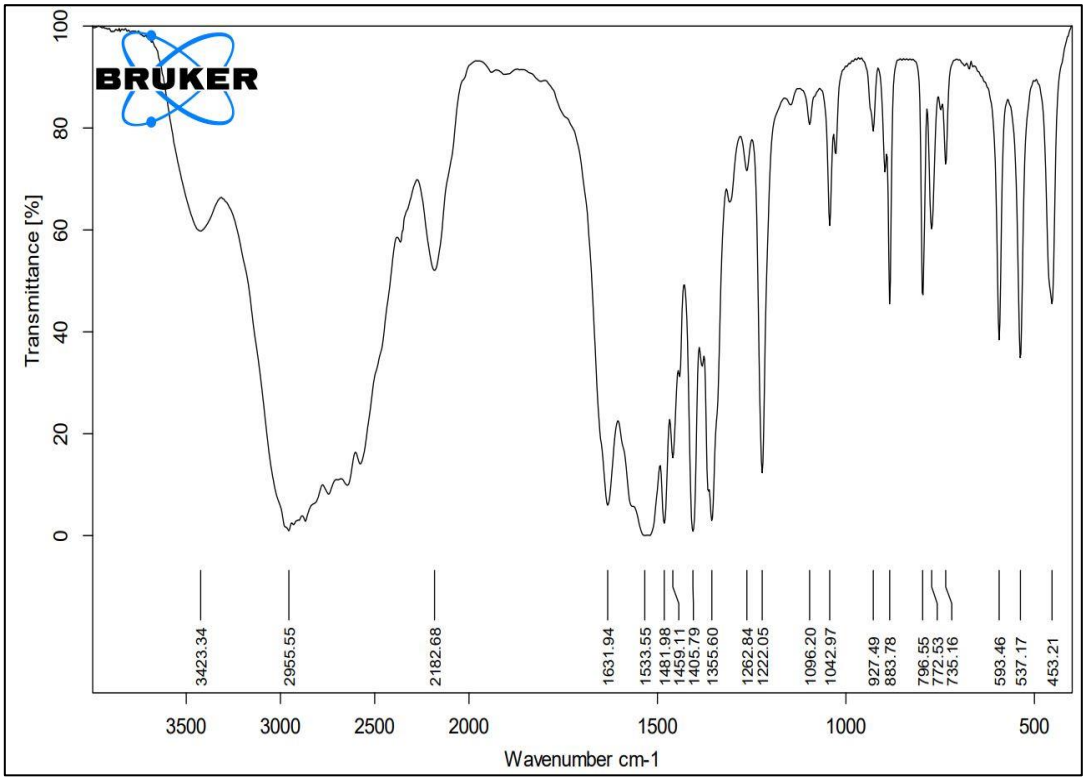
BRUKER
Transmittance [%]
100
80
60
40
20
0
3423.34
2955.55
2182.68
1631.94
1533.55
1481.98
1459.11
1405.79
1355.60
1262.84
1222.05
1096.20
1042.97
927.49
883.78
796.55
772.53
735.16
593.46
537.17
453.21
3500 3000 2500 2000 1500 1000 500
Wavenumber cm-1

A1B4

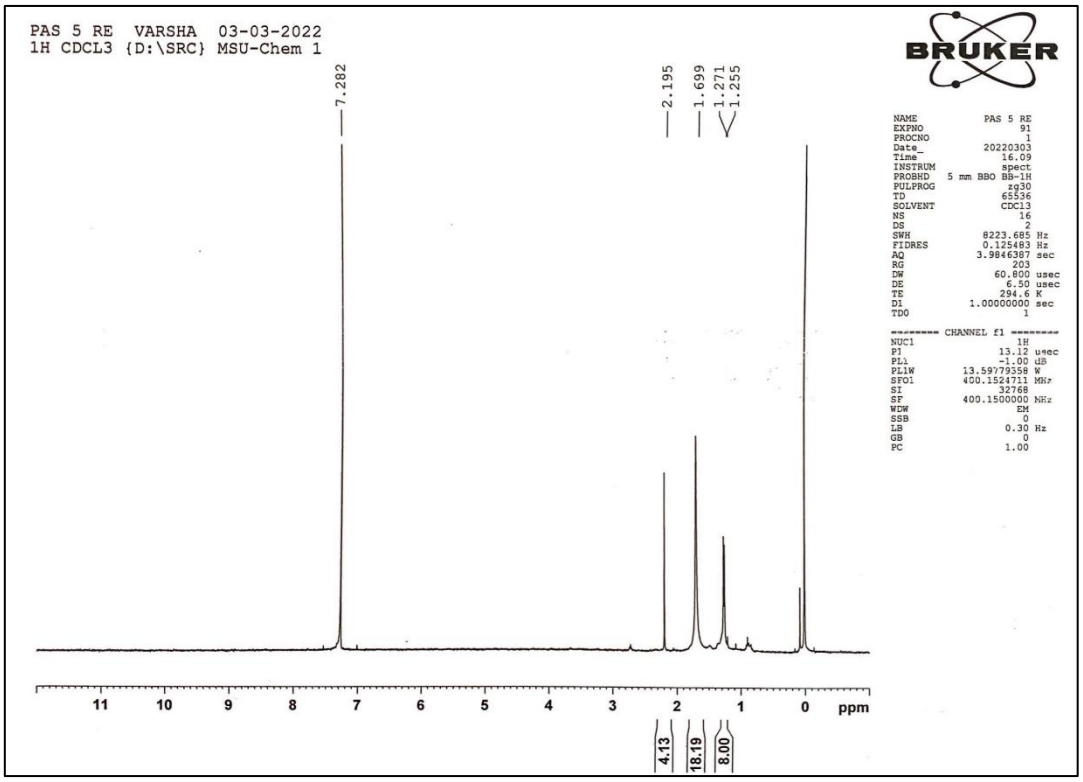
PAS 5 RE VARSHA 03-03-2022
1H CDCL3 {D:\SRC} MSU-Chem 1
BRUKER
7.282
2.195
1.699
1.271
1.255
11 10 9 8 7 6 5 4 3 2 1 0 ppm
4.13
18.19
8.00
NAME PAS 5 RE
EXPNO 91
PROCNO 1
Date_ 20220303
Time_ 16.09
INSTRUM spect
PROBHD 5 mm BBO BB-1H
PULPROG zg30
TD 65536
SOLVENT CDCl3
NS 16
DS 2
SWH 8223.685 Hz
FIDRES 0.125483 Hz
AQ 3.9846387 sec
RG 203
DW 60.800 usec
DE 6.50 usec
TE 294.6 K
D1 1.00000000 sec
TD0 1
CHANNEL f1
NUC1 1H
P1 13.12 usec
PL1 -1.00 dB
PL1W 13.59779358 W
SFO1 400.1524711 MHz
SI 32768
SF 400.1500000 MHz
WDW EM
SSB 0
LB 0.30 Hz
GB 0
PC 1.00

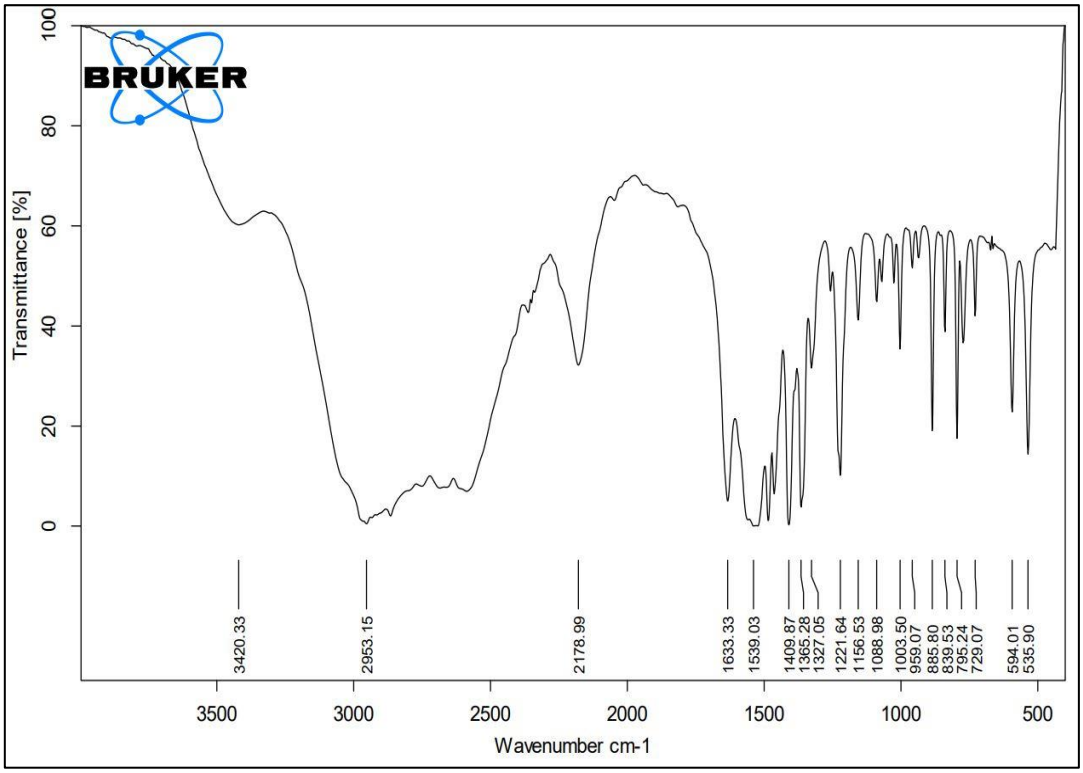
BRUKER
Transmittance [%]
0 20 40 60 80 100
3420.33
2953.15
2178.99
1633.33
1539.03
1409.87
1365.28
1327.05
1221.64
1156.53
1088.98
1003.50
959.07
885.80
839.53
795.24
729.07
594.01
535.90
3500 3000 2500 2000 1500 1000 500
Wavenumber cm-1

A1B5

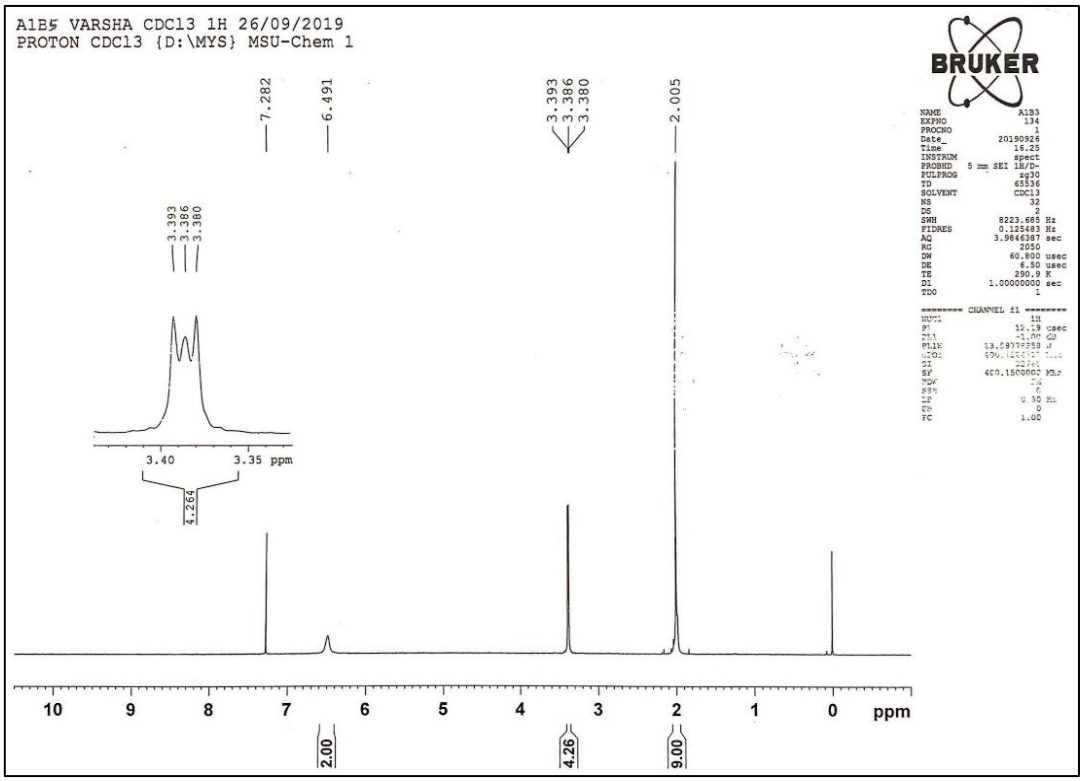
A1B5 VARSHA CDCl3 1H 26/09/2019
PROTON CDCl3 {D:\MYS} MSU-Chem 1
BRUKER
7.282
6.491
3.393
3.386
3.380
2.005
3.40
3.35 ppm
4.264
10
9
8
7
6
5
4
3
2
1
0
ppm
2.00
4.26
9.00

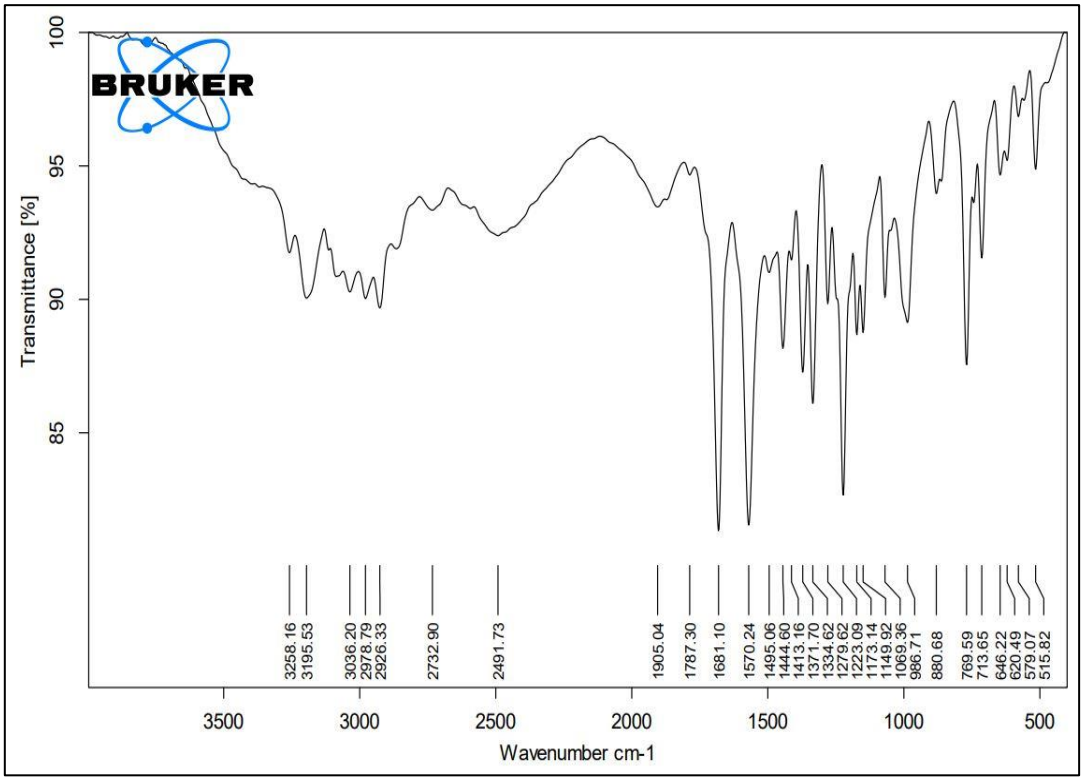
BRUKER
Transmittance [%]
100
95
90
85
3258.16
3195.53
3036.20
2978.79
2926.33
2732.90
2491.73
1905.04
1787.30
1681.10
1570.24
1495.06
1444.60
1413.16
1371.70
1334.62
1279.62
1223.09
1173.14
1149.92
1069.36
986.71
880.68
769.59
713.65
646.22
620.49
579.07
515.82
3500
3000
2500
2000
1500
1000
500
Wavenumber cm-1

A1B6

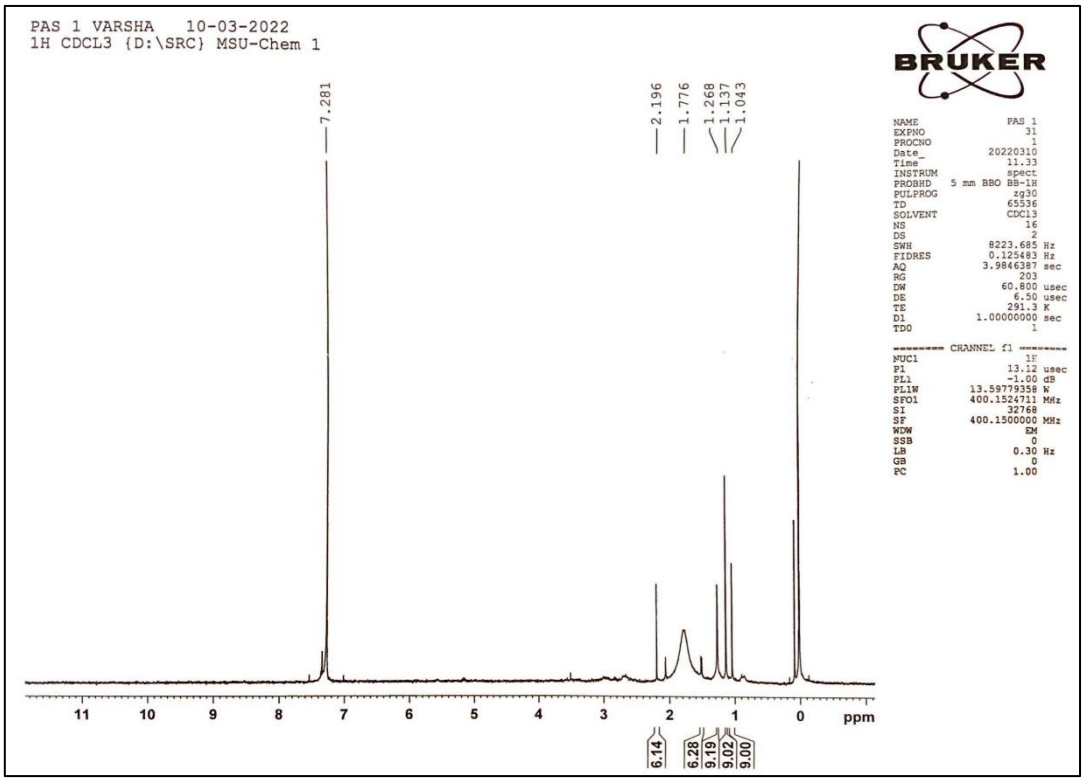
PAS 1 VARSHA 10-03-2022
1H CDCL3 {D:\SRC} MSU-Chem 1
BRUKER
7.281
2.196
1.776
1.268
1.137
1.043
11
10
9
8
7
6
5
4
3
2
1
0
ppm
6.14
6.28
9.19
9.02
9.00
NAME PAS 1
EXPNO 31
PROCNO 1
Date_ 20220310
Time 11.33
INSTRUM spect
PROBHD 5 mm BBO BB-1H
PULPROG zg30
TD 65536
SOLVENT CDCl3
NS 16
DS 2
SWH 8223.685 Hz
FIDRES 0.125483 Hz
AQ 3.9846387 sec
RG 203
DW 60.800 usec
DE 6.50 usec
TE 291.3 K
D1 1.00000000 sec
TD0 1
CHANNEL f1
NUC1 1H
P1 13.12 usec
PL1 -1.00 dB
PL1W 13.59779358 W
SFO1 400.1524711 MHz
SI 32768
SF 400.1500000 MHz
WDW EM
SSB 0
LB 0.30 Hz
GB 0
PC 1.00

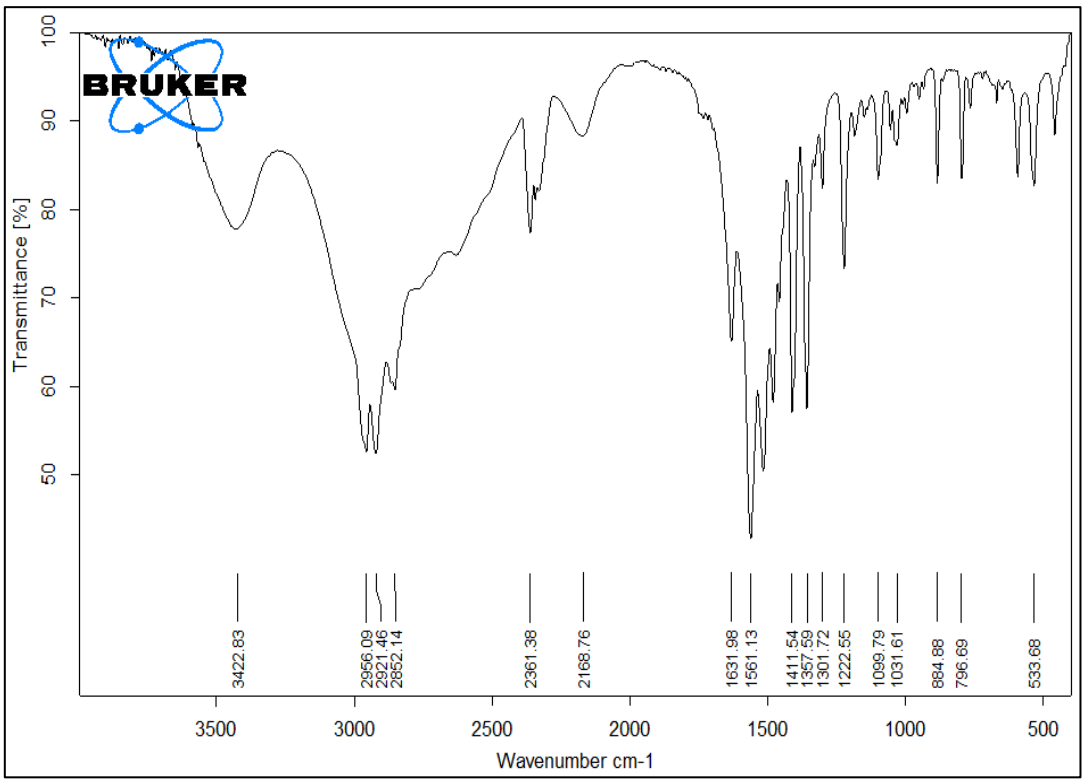
BRUKER
Transmittance [%]
100
90
80
70
60
50
3422.83
2956.09
2921.46
2852.14
2361.38
2168.76
1631.98
1561.13
1411.54
1357.59
1301.72
1222.55
1099.79
1031.61
884.88
796.69
533.68
3500
3000
2500
2000
1500
1000
500
Wavenumber cm-1

A1B7

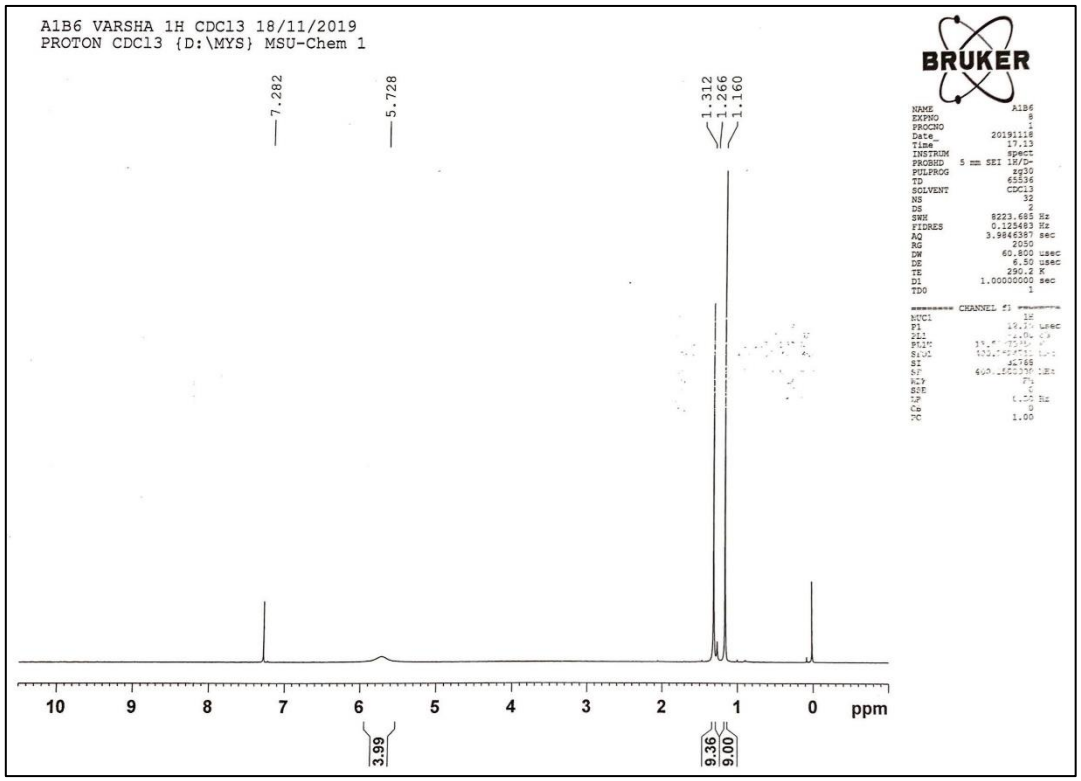
A1B6 VARSHA 1H CDCl3 18/11/2019
PROTON CDCl3 {D:\MYS} MSU-Chem 1
BRUKER
7.282
5.728
1.312
1.266
1.160
10
9
8
7
6
5
4
3
2
1
0
ppm
3.99
9.36
9.00

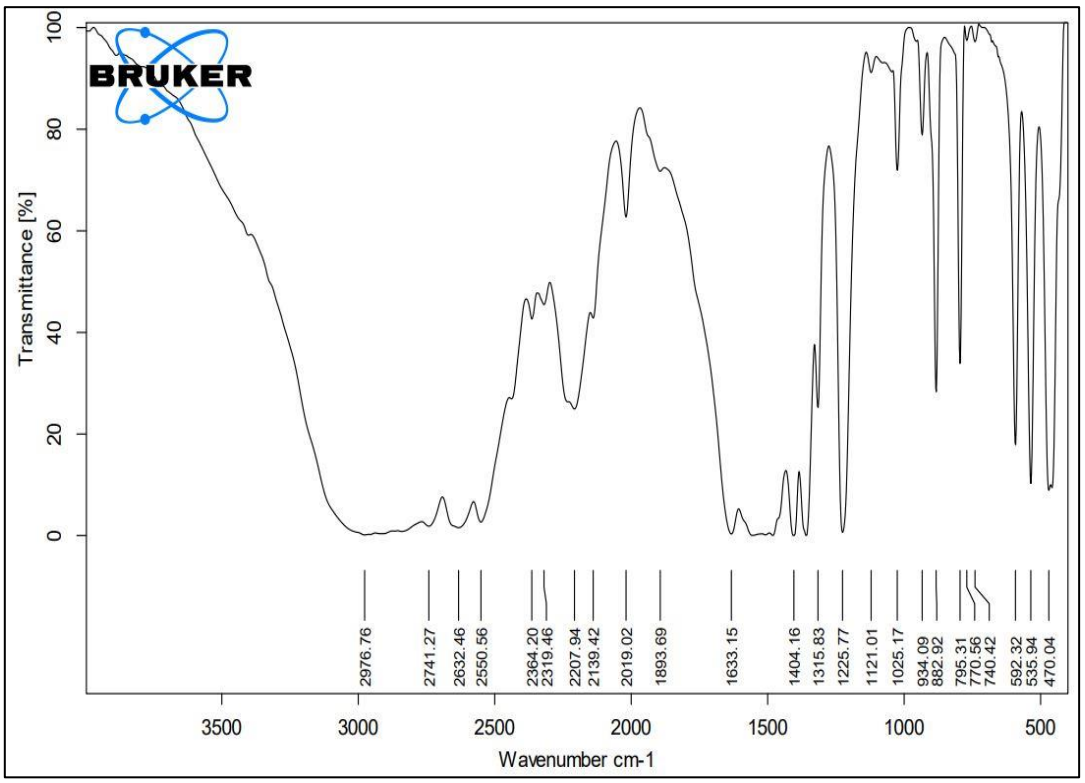
BRUKER
Transmittance [%]
100
80
60
40
20
0
2976.76
2741.27
2632.46
2550.56
2364.20
2319.46
2207.94
2139.42
2019.02
1893.69
1633.15
1404.16
1315.83
1225.77
1121.01
1025.17
934.09
882.92
795.31
770.56
740.42
592.32
535.94
470.04
3500
3000
2500
2000
1500
1000
500
Wavenumber cm-1

A1B8

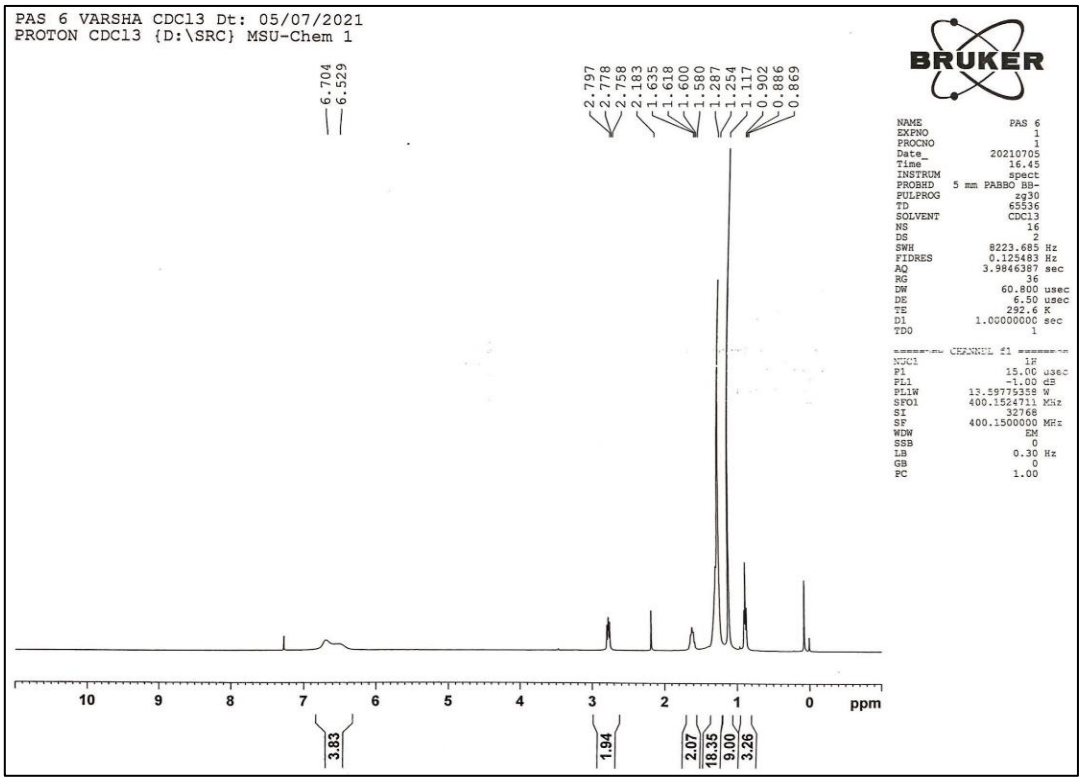
PAS 6 VARSHA CDCl3 Dt: 05/07/2021
PROTON CDCl3 {D:\SRC} MSU-Chem 1
6.704
6.529
2.797
2.778
2.758
2.183
1.635
1.618
1.600
1.580
1.287
1.254
1.117
0.902
0.886
0.869
BRUKER
NAME PAS 6
EXPNO 1
PROCNO 1
Date_ 20210705
Time 16.45
INSTRUM spect
PROBHD 5 mm PABBO BB-
PULPROG zg30
TD 65536
SOLVENT CDCl3
NS 16
DS 2
SWH 8223.685 Hz
FIDRES 0.125483 Hz
AQ 3.9846387 sec
RG 36
DW 60.800 usec
DE 6.50 usec
TE 292.6 K
D1 1.00000000 sec
TD0 1
CHANNEL f1
NUC1 1H
P1 15.00 usec
PL1 -1.00 dB
PL1W 13.59775358 W
SFO1 400.1524711 MHz
SI 32768
SF 400.1500000 MHz
WDW EM
SSB 0
LB 0.30 Hz
GB 0
PC 1.00
10 9 8 7 6 5 4 3 2 1 0 ppm
3.83
1.94
2.07
18.35
9.00
3.26

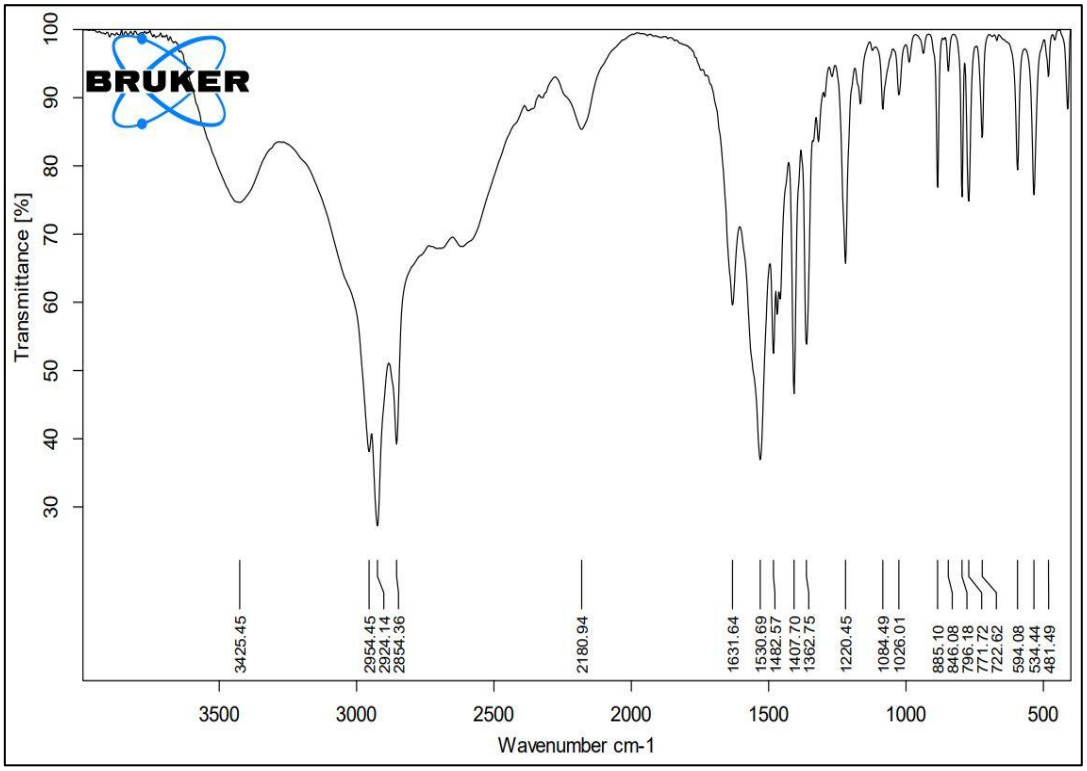
BRUKER
Transmittance [%]
100
90
80
70
60
50
40
30
3425.45
2954.45
2924.14
2854.36
2180.94
1631.64
1530.69
1482.57
1407.70
1362.75
1220.45
1084.49
1026.01
885.10
846.08
796.18
771.72
722.62
594.08
534.44
481.49
3500
3000
2500
2000
1500
1000
500
Wavenumber cm-1

A1B9

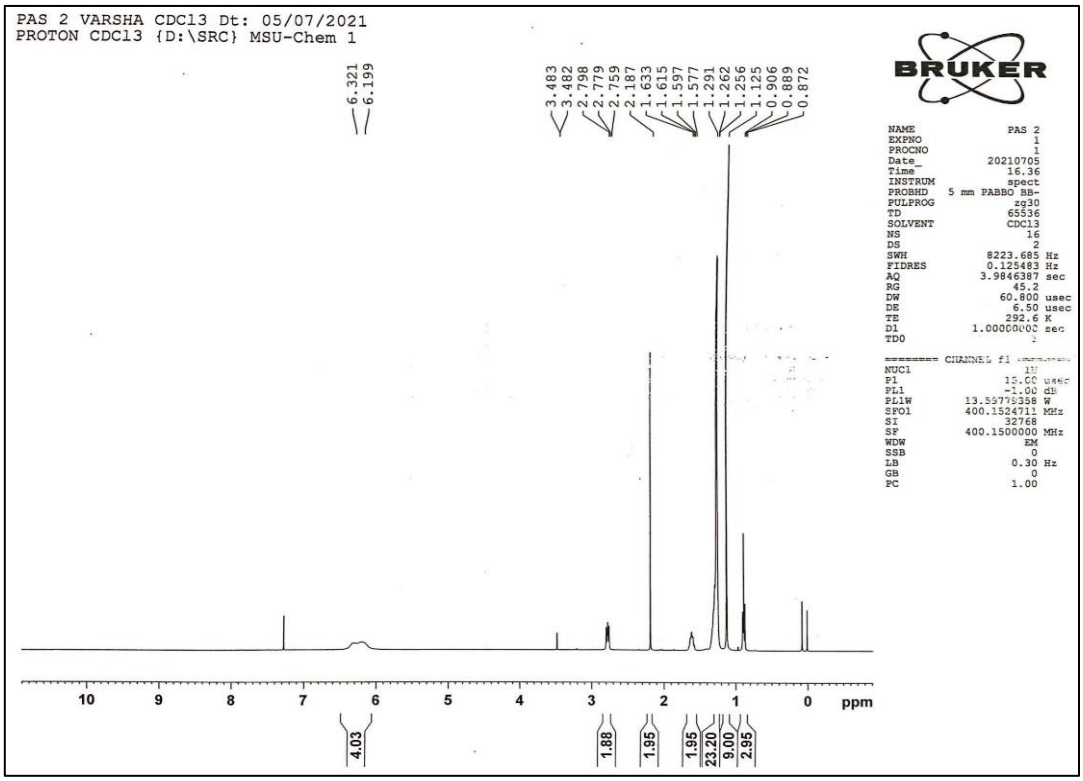
PAS 2 VARSHA CDCl3 Dt: 05/07/2021
PROTON CDCl3 {D:\SRC} MSU-Chem 1
6.321
6.199
3.483
3.482
2.798
2.779
2.759
2.187
1.633
1.615
1.597
1.577
1.291
1.262
1.256
1.125
0.906
0.889
0.872
BRUKER
NAME PAS 2
EXPNO 1
PROCNO 1
Date_ 20210705
Time_ 16.36
INSTRUM spect
PROBHD 5 mm PABBO BB-
PULPROG zg30
TD 65536
SOLVENT CDCl3
NS 16
DS 2
SWH 8223.685 Hz
FIDRES 0.125483 Hz
AQ 3.9846387 sec
RG 45.2
DW 60.800 usec
DE 6.50 usec
TE 292.6 K
D1 1.00000000 sec
TD0 1
NUC1 1H
P1 15.00 usec
PL1 -1.00 dB
PLW 13.55776398 W
SFO1 400.1524711 MHz
SI 32768
SF 400.1500000 MHz
WDW EM
SSB 0
LB 0.30 Hz
GB 0
PC 1.00
10 9 8 7 6 5 4 3 2 1 0 ppm
4.03
1.88
1.95
1.95
23.20
9.00
2.95

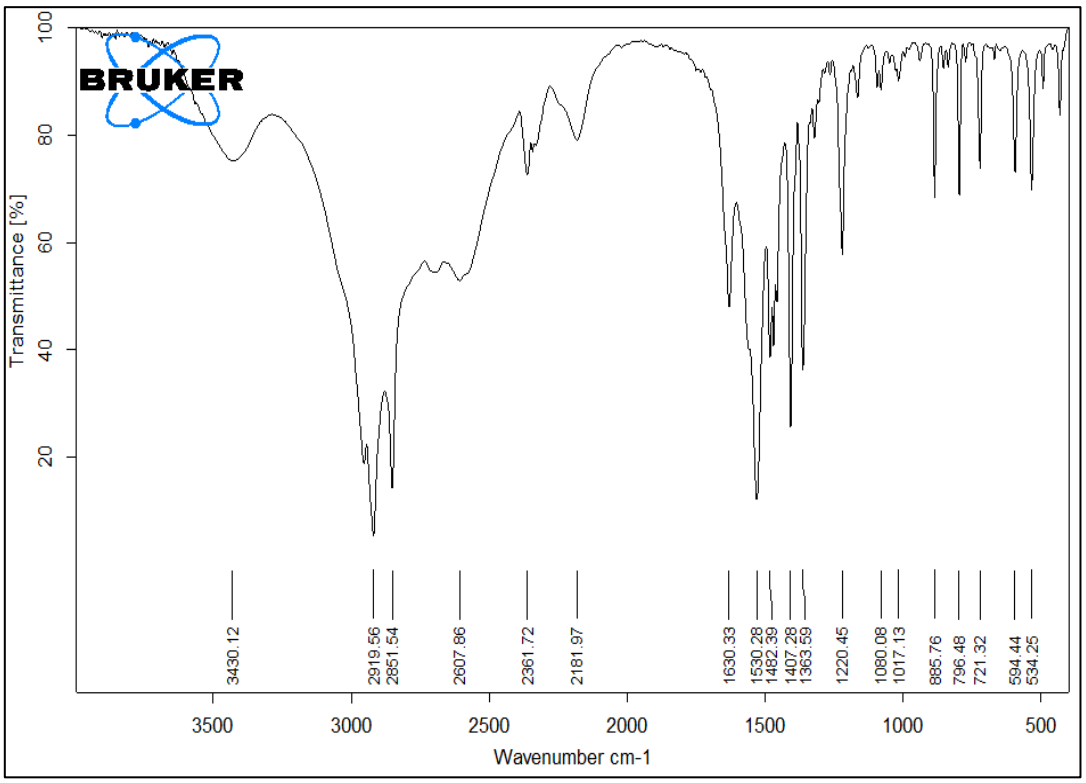
BRUKER
Transmittance [%]
100
80
60
40
20
3430.12
2919.56
2851.54
2607.86
2361.72
2181.97
1630.33
1530.28
1482.39
1407.28
1363.59
1220.45
1080.08
1017.13
885.76
796.48
721.32
594.44
534.25
3500
3000
2500
2000
1500
1000
500
Wavenumber cm-1

A1B10

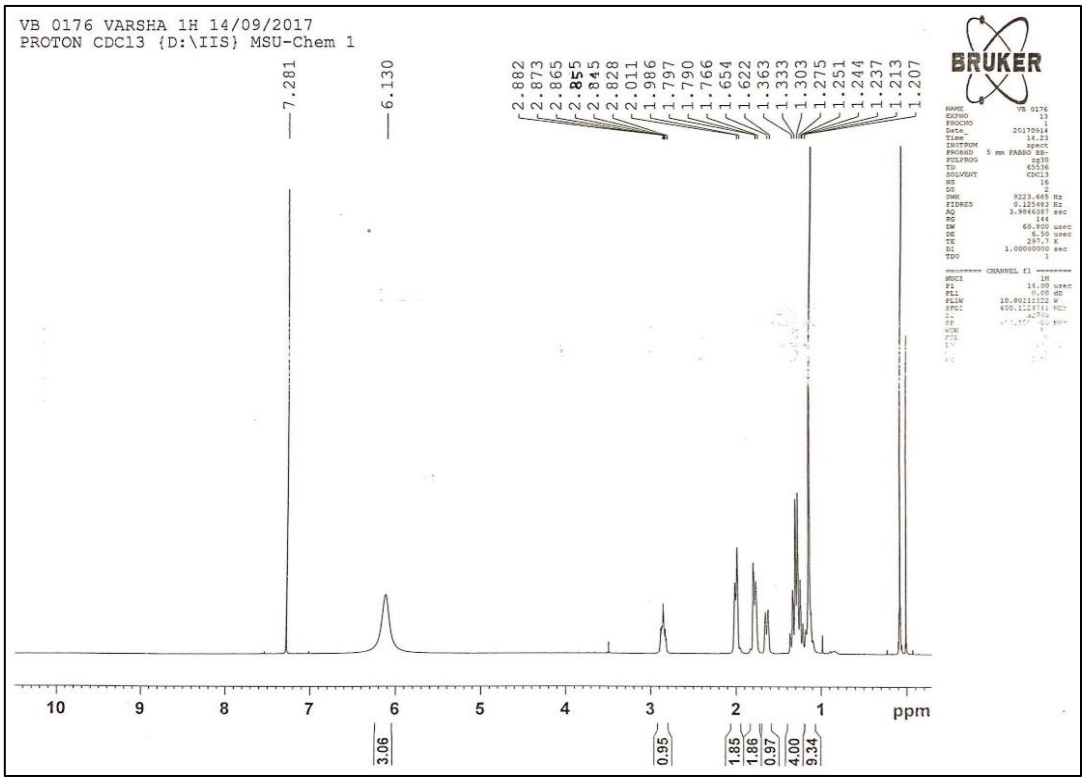
VB 0176 VARSHA 1H 14/09/2017
PROTON CDCl3 {D:\IIS} MSU-Chem 1
BRUKER
7.281
6.130
2.882
2.873
2.865
2.855
2.845
2.828
2.011
1.986
1.797
1.790
1.766
1.654
1.622
1.363
1.333
1.303
1.275
1.251
1.244
1.237
1.213
1.207
10
9
8
7
6
5
4
3
2
1
ppm
3.06
0.95
1.85
1.86
0.97
4.00
9.34

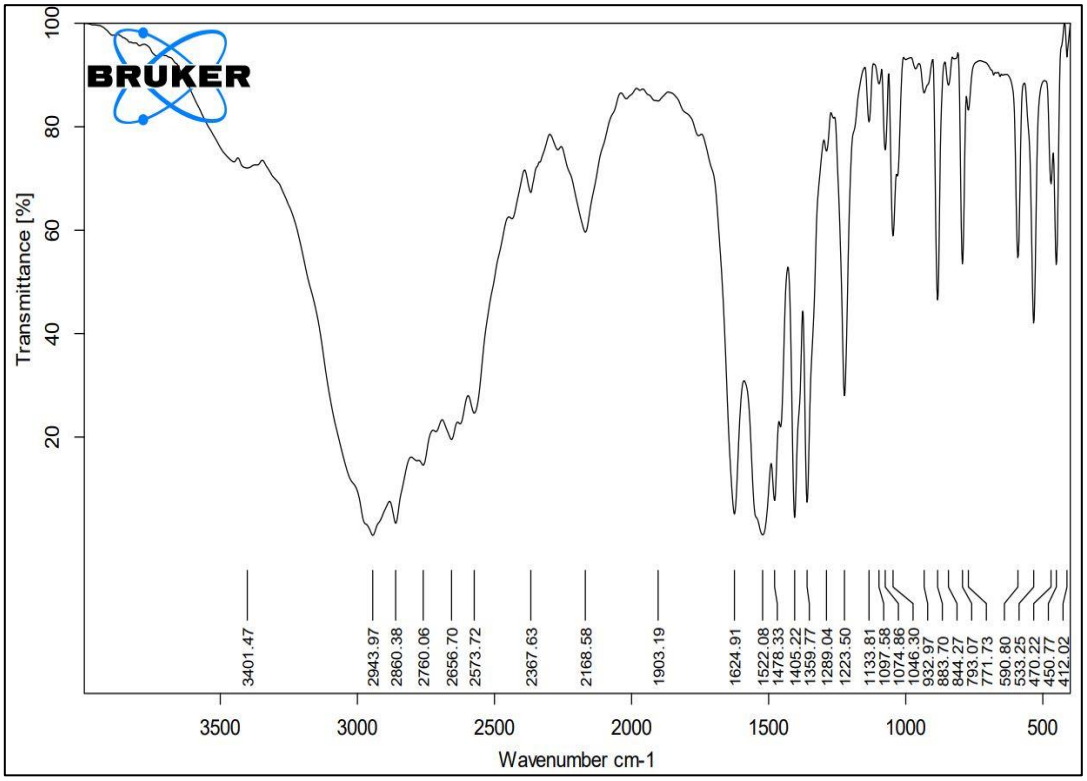
BRUKER
Transmittance [%]
100
80
60
40
20
3401.47
2943.97
2860.38
2760.06
2656.70
2573.72
2367.63
2168.58
1903.19
1624.91
1522.08
1478.33
1405.22
1359.77
1289.04
1223.50
1133.81
1097.58
1074.86
1046.30
932.97
883.70
844.27
793.07
771.73
590.80
533.25
470.22
450.77
412.02
3500
3000
2500
2000
1500
1000
500
Wavenumber cm-1

A1B11

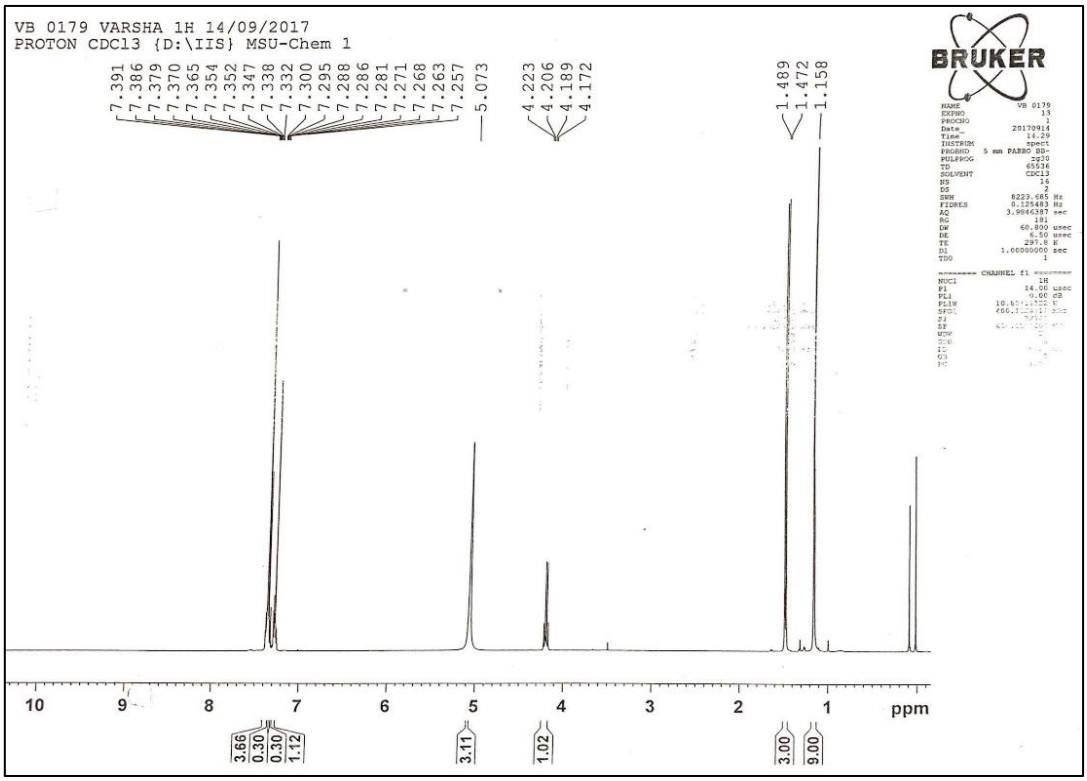
VB 0179 VARSHA 1H 14/09/2017
PROTON CDCl3 {D:\IIS} MSU-Chem 1
BRUKER
7.391
7.386
7.379
7.370
7.365
7.354
7.352
7.347
7.338
7.332
7.300
7.295
7.288
7.286
7.281
7.271
7.268
7.263
7.257
5.073
4.223
4.206
4.189
4.172
1.489
1.472
1.158
10
9
8
7
6
5
4
3
2
1
ppm
3.66
0.30
0.30
1.12
3.11
1.02
3.00
9.00

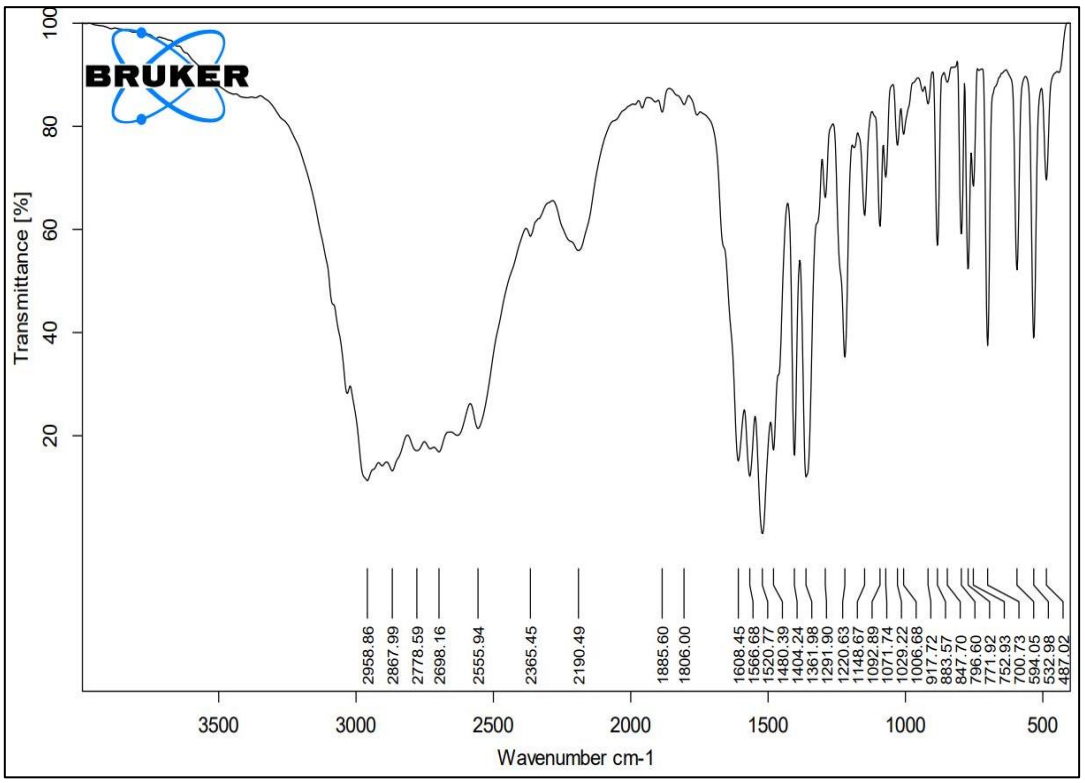
BRUKER
Transmittance [%]
100
80
60
40
20
2958.86
2867.99
2778.59
2698.16
2555.94
2365.45
2190.49
1885.60
1806.00
1608.45
1566.68
1520.77
1480.39
1404.24
1361.98
1291.90
1220.63
1148.67
1092.89
1071.74
1029.22
1006.68
917.72
883.57
847.70
796.60
771.92
752.93
700.73
594.05
532.98
487.02
3500
3000
2500
2000
1500
1000
500
Wavenumber cm-1

A1B12

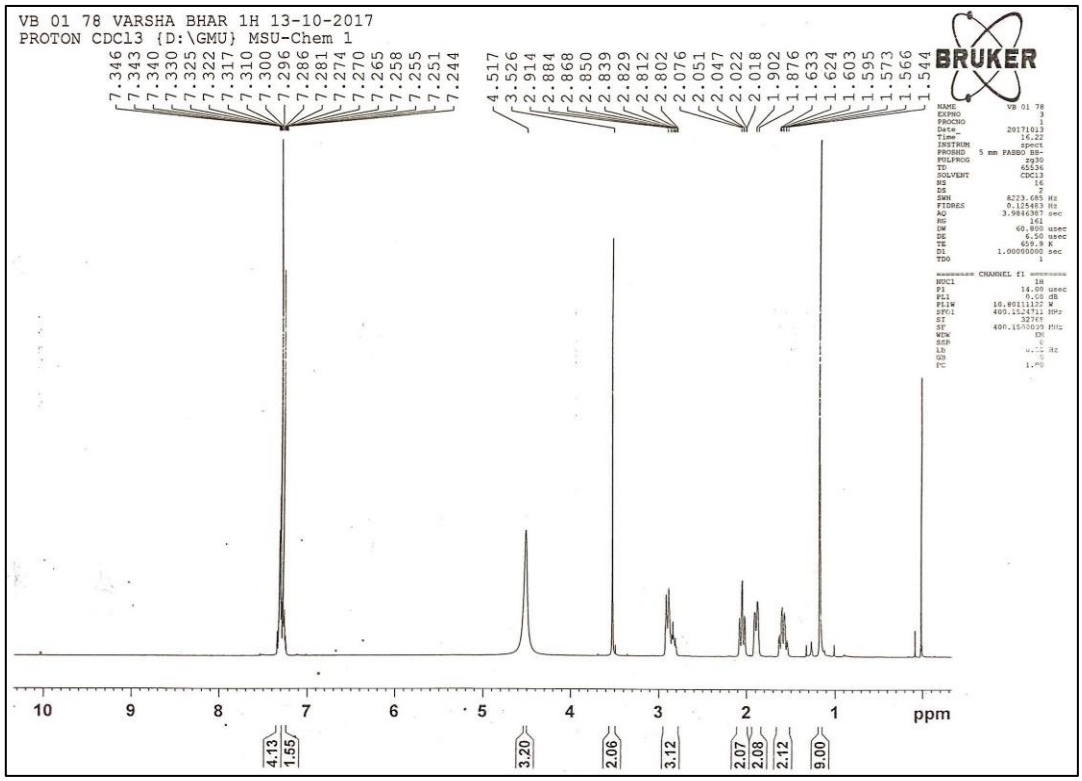
VB 01 78 VARSHA BHAR 1H 13-10-2017
PROTON CDCl3 {D:\GMU} MSU-Chem 1
BRUKER
7.346
7.343
7.340
7.330
7.325
7.322
7.317
7.310
7.300
7.296
7.286
7.281
7.274
7.270
7.265
7.258
7.255
7.251
7.244
4.517
3.526
2.914
2.884
2.868
2.850
2.839
2.829
2.812
2.802
2.076
2.051
2.047
2.022
2.018
1.902
1.876
1.633
1.624
1.603
1.595
1.573
1.566
1.544
10
9
8
7
6
5
4
3
2
1
ppm
4.13
1.55
3.20
2.06
3.12
2.07
2.08
2.12
9.00

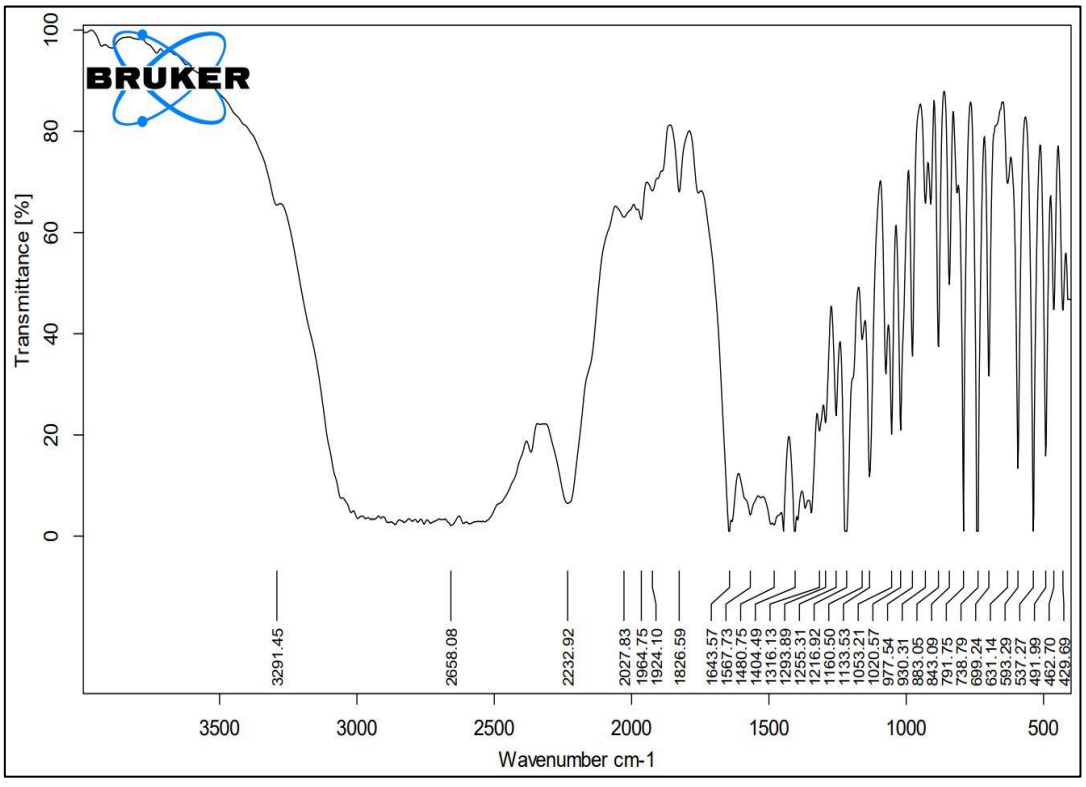
BRUKER
Transmittance [%]
100
80
60
40
20
0
3291.45
2658.08
2232.92
2027.83
1964.75
1924.10
1826.59
1643.57
1567.73
1480.75
1404.49
1316.13
1293.89
1255.31
1216.92
1160.50
1133.53
1053.21
1020.57
977.54
930.31
883.05
843.09
791.75
738.79
699.24
631.14
593.29
537.27
491.99
462.70
429.69
3500
3000
2500
2000
1500
1000
500
Wavenumber cm-1

A1B13

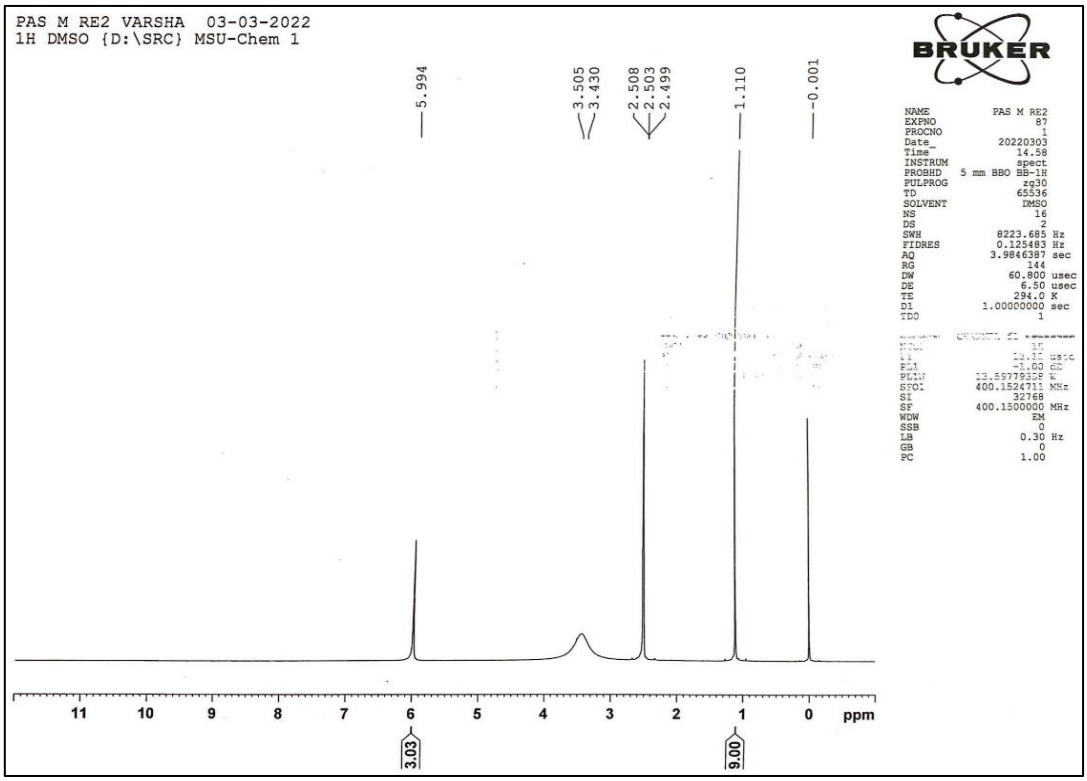
PAS M RE2 VARSHA 03-03-2022
1H DMSO {D:\SRC} MSU-Chem 1
BRUKER
5.994
3.505
3.430
2.508
2.503
2.499
1.110
-0.001
NAME PAS M RE2
EXPNO 87
PROCNO 1
Date_ 20220303
Time 14.58
INSTRUM spect
PROBHD 5 mm BBO BB-1H
PULPROG zg30
TD 65536
SOLVENT DMSO
NS 16
DS 2
SWH 8223.685 Hz
FIDRES 0.125483 Hz
AQ 3.9846387 sec
RG 144
DW 60.800 usec
DE 6.50 usec
TE 294.0 K
D1 1.00000000 sec
TD0 1
PL1 -1.00 dB
PL1W 13.59779358 W
SFO1 400.1524711 MHz
SI 32768
SF 400.1500000 MHz
WDW EM
SSB 0
LB 0.30 Hz
GB 0
PC 1.00
11 10 9 8 7 6 5 4 3 2 1 0 ppm
3.03
9.00

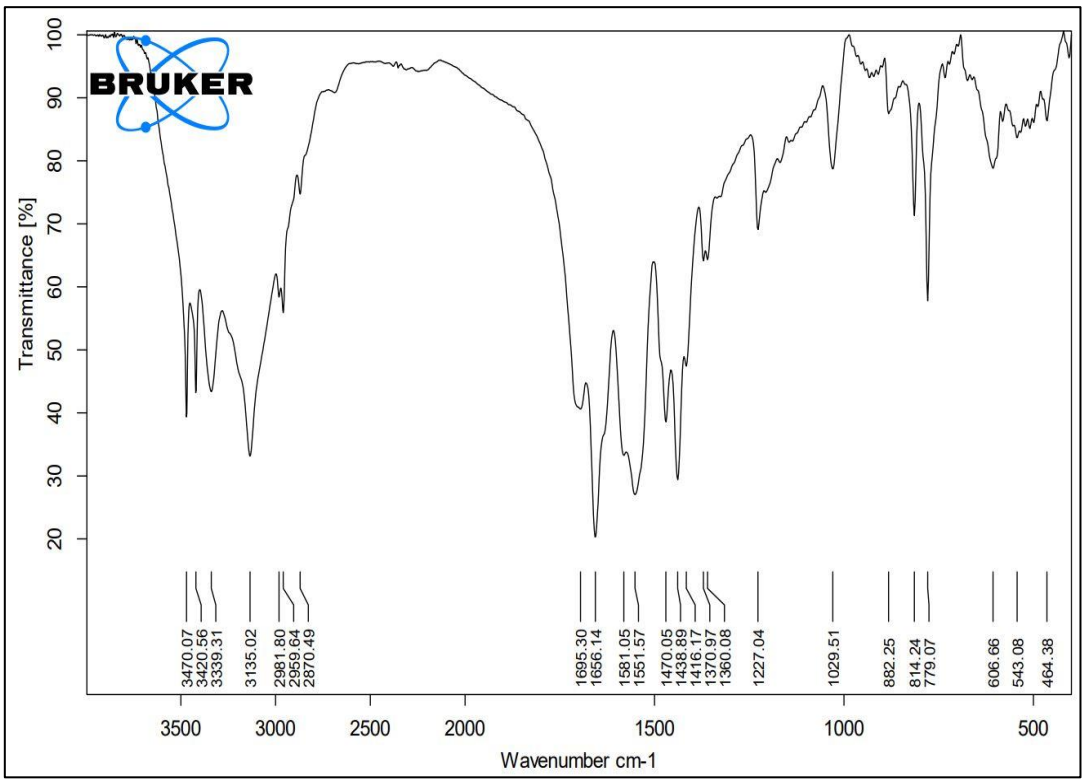
BRUKER
Transmittance [%]
100 90 80 70 60 50 40 30 20
3470.07
3420.56
3339.31
3135.02
2981.80
2959.64
2870.49
1695.30
1656.14
1581.05
1551.57
1470.05
1438.89
1416.17
1370.97
1360.08
1227.04
1029.51
882.25
814.24
779.07
606.66
543.08
464.38
3500 3000 2500 2000 1500 1000 500
Wavenumber cm-1

This page intentionally left blank.

Chapter 3B

Probing the role of weak interactions on gelation behavior of tert-butylacetic acid based multi-component systems

3.6 INTRODUCTION

Multi-component gels offer tremendous opportunities for preparing novel supramolecular materials with a wide range of applications. A 'bottom-up' approach can be utilized for the synthesis of programmable self-sorting supramolecular systems. We can also tune several properties like viscoelasticity, morphology, stability and response to desired stimuli with multi-component systems.[1–3] One of the key advantages they offer is ease of synthesis, where a large number of compounds can be screened before choosing the right fit.[4–6]

In the previous chapter, salts of pivalic acid were explored for their gelation behavior. A combinatorial library approach was utilized to screen the types of amines which favored gelation behavior. From the results obtained, it appears that the gelation systems contained a variety of backbones like alicyclic, aliphatic long chain, aromatic, etc. To delve into the plausible gelation mechanism, we decided to synthesize a new series of salts using *tert*-butylacetic acid (TBAA) with the same set of amines as in Chapter 3A.

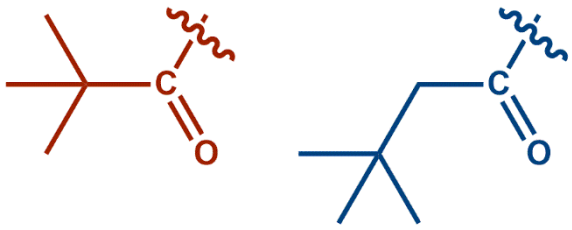

Figure 3.34 Structural backbone of pivalic acid and *tert*-butylacetic acid

Pivalic acid and TBAA happen to be structurally similar as they both contain terminal *tert*-butyl group (Figure 3.34). The presence of bulky group can contribute towards forcing the assembly to adopt a one-dimensional assembly, and hence can display gelation. Such concepts have allowed us to acquire better understanding of the assembly processes which allow us to use these directional non-covalent interactions (to promote one-dimensional organization of the molecules) and design more of such systems *de novo*.[7,8]

The two acids differ only by a methylene group which can increase the hydrophobicity of the system. It is believed that an intricate balance between the hydrophobic and hydrophilic interactions gives rise to the formation of fibrous assembly which can

immobilize solvent molecules by virtue of surface tension and capillary forces;[1,9–13] we believe this study could be helpful in putting some light in this direction and highlight the importance of non-covalent interactions in acid-amine systems.

3.7 EXPERIMENTAL PROCEDURES

3.7.1 Synthesis of Salts A2B1-A2B13

All the salts were synthesized by refluxing *tert*-butylacetic acid and amine taken in equimolar amounts ((1:1) and (2:1) for diamine) in methanol for 1 hour (Scheme 3.3). The solutions were then kept at RT (25ºC) for few days so that slow evaporation of solvent could lead to formation of crystalline solids. These compounds were then kept for recrystallization in various solvents. The salts so obtained were subjected to physico-chemical techniques such as NMR, FT-IR and gelation trials.

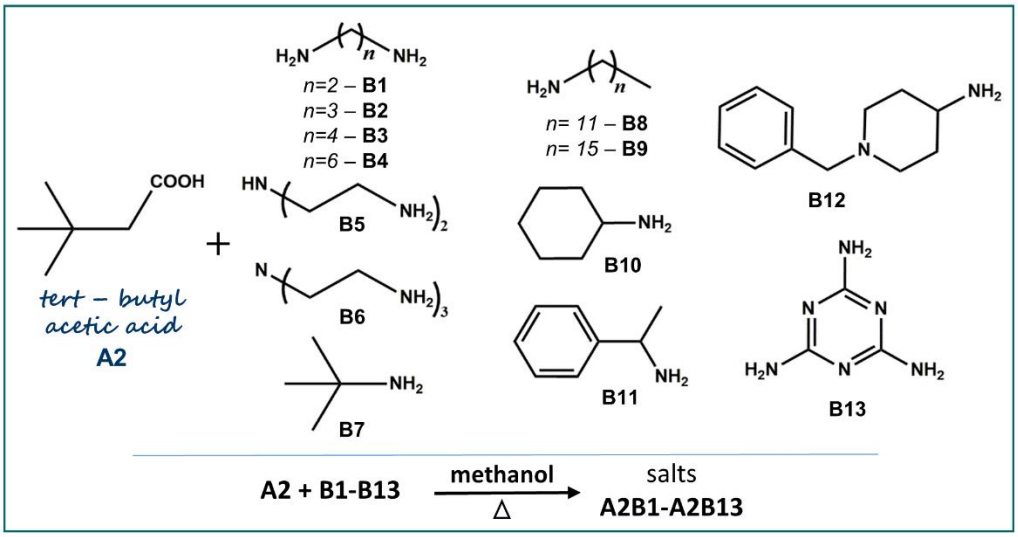

Scheme 3.3 Salts A2B1-A2B13 synthesized using *tert*-butylacetic acid and various amines

3.7.2 Gelation trials

All the salts were tested for their gelation behavior in various solvents of different polarities. 50 mg of sample of was taken in a glass vial to which solvent was added gradually and the vial heated in a temperature-controlled water bath till the solute dissolved completely. The solution was cooled to room temperature (~25ºC) and

allowed to stand overnight. The gel formation was confirmed by inverted vial method. The solvent was added till no more gelation was exhibited by the system.

T_{gel} (gel-to-sol conversion temperature) was also measured using the same inverted vial method. The vials containing the gels were heated in a temperature-controlled water bath at a steady rate of 0.5°C/min. The temperature at which first drop of gel melted was considered as $T_{gel.}$

3.7.3 Materials and Methods

All the chemicals were obtained from Sigma Aldrich and TCI and the solvents were obtained from SD Fine Chemicals, India and were used without any further purification.

3.7.3.1 NMR studies

NMR data was recorded on BRUKER AVANCE, 400 MHz spectrometer in $CDCl_3$ or DMSO-d6 with TMS as internal standard. The ^1H NMR spectra of all compounds can be found in Supplementary Data* at the end of the chapter.

3.7.3.2 FT-IR studies

FT-IR studies were performed on Bruker Alpha FT-IR spectrometer. The solid sample was ground together with anhydrous KBr using mortar pestle and the pellet so formed was subjected to FT-IR analysis. The FT-IR spectra of all compounds can be found in Supplementary Data* at the end of the chapter. Comparative FT-IR spectra of samples in gel and solution phase (with acetonitrile as solvent) were recorded using CaF_2 discs.

3.7.3.3 Polarizing Optical Microscopy studies

POM analyses were performed using LEICADM2500P polarizing microscope. Images were captured using LEICADFC295 camera which is attached with the instrument. Thin layer of gel was formed on glass slide and allowed to dry, forming xerogel whose images were captured.

3.7.3.4 SEM of gels

The samples for SEM were prepared by gently spreading the gel on the SEM stubs and freezing them under liquid nitrogen. These frozen gel samples were used directly for the viewing images using JEOL JSM-5610LV Scanning Electron Microscope instrument.

3.7.3.5 Rheology

Rheology studies of **A2B11** and **A2B13** were performed on an Anton Paar MCR 102 Modular Compact Rheometer at 38°C. The instrument has a parallel plate geometry with a plate diameter of 50 mm, maintained at a gap of 0.5 mm; the gel samples were subjected to oscillatory amplitude sweep range of 0 to 100 rad/s and values of G' (storage modulus) and G" (loss modulus) were evaluated.

3.7.3.6 Powder X-ray diffraction studies

Powder diffraction patterns of bulk (crystalline) gelator and xerogel (Acetonitrile, slowly evaporated) of **A2B11** and **A2B12** were recorded on an XPERT (Cu Kα radiation, λ = 1.54056 Å) diffractometer on a continuous scanning mode at 2θ value 5-90º.

3.7.4 Analytical Data

The salt formation was confirmed by Fourier Transform-Infra Red spectroscopy (FT-IR). All the synthesized salts showed characteristic bands for C=O stretching of carboxylate groups at (1690-1740 cm^{-1}), (1400-1450 cm^{-1}) indicating the formation of carboxylate salts of *tert*-butylacetic acid and N-H stretch of primary ammonium cations for the respective bases at (2700-2200 cm^{-1}), (3500-3300 cm^{-1}).

A comparative study of bulk and xero gels was also carried out using FT-IR was carried out (Section 3.8.5). The FT-IR spectra of all salts were found to be nearly matching with those of bulk indicating that the chemical nature of all the salts was retained after gel formation.

The ^{1}H NMR studies also confirmed salt formation.

Compound A2B1 (ethan-1,2-diaminium 3,3-dimethylbutanoate). M.P.= 138°C, ^{1}H NMR (400 MHz, DMSO-d6, TMS) = δ (ppm) 3.520 (*s*, 2H, CH_2), δ 2.815 (*s*, 2H, CH_2), δ 1.826 (*s*, 18H, 2 x 3(CH_3)), δ 1.274 (*s*, 4H, 2(CH_2)), δ 1.080 (*s*, 4H, 2(CH_2)).

FT-IR, cm^{-1} (KBr) – 3428, 2955, 2867, 2220, 1643, 1536, 1454, 1394, 1277, 1235, 1142, 1013, 735, 641, 497.

Compound A2B2 (propan-1,3-diaminium 3,3-dimethylbutanoate). M.P.= 144°C, ^{1}H NMR (400 MHz, DMSO-d6, TMS) = δ (ppm) 2.936 (NH), δ 2.161 (*s*, 2H, CH_2), δ

1.295-1.269 (*s*, 13H, 2(CH_2) + 3(CH_3)), δ 1.051 (*s*, 9H, 3(CH_3)), 0.912-0.878 (*s*, 4H, 2(CH_2)).

FT-IR, cm^{-1} (KBr) – 3402, 2954, 2217, 1628, 1572, 1527, 1391, 1298, 1277, 1141, 1042, 953, 911, 806, 772, 734, 636, 523.

Compound A2B3 (butan-1,4-diaminium 3,3-dimethylbutanoate). M.P.= 145°C, ^1H NMR (400 MHz, DMSO-d6, TMS) = δ (ppm) 2.750 (*s*, 2H, CH_2), δ 2.195-2.182 (*s*, 2H, CH_2), δ 1.736 (*s*, 18H, 2 x 3(CH_3)), δ 1.527 (*s*, 2H, CH_2), δ 1.267 (*s*, 2H, 2(CH_2)), δ 1.061 (*s*, 2H, 2(CH_2)), δ 0.895-0.877 (*m*, 2H, 2($C\underline{H}_2$)).

FT-IR, cm^{-1} (KBr) – 3424, 2960, 2216, 1632, 1524, 1396, 1272, 1235, 1168, 1138, 1089, 1056, 948, 904, 807, 754, 729, 646, 515.

Compound A2B4 (hexan-1,6-diaminium 3,3-dimethylbutanoate). M.P.= 120°C, ^1H NMR (400 MHz, DMSO-d6, TMS) = δ (ppm) 1.98 (*s*, 4H, 2(CH_2)), δ 1.371 (*s*, 6H, 3(CH_2)), δ 1.289 (*s*, 6H, 3(CH_2)), δ 0.989 (*s*, 18H, 2 x 3(CH_3)).

FT-IR, cm^{-1} (KBr) – 3423, 2955, 2865, 2201, 1629, 1535, 1393, 1298, 1238, 1148, 1044, 839, 733, 637, 531.

Compound A2B5 (2,2'-azanediyldiethanaminium 3,3-dimethylbutanoate). M.P.= 50°C, ^1H NMR (400 MHz, $CDCl_3$, TMS) = δ (ppm) 6.097 (*s*, 7H, NH), δ 2.962-2.923 (*m*, 8H, 2 x 2(CH_2)), δ 2.085 (*s*, 4H, 2 x 2(CH_2)), δ 1.020 (*s*, 18H, 2 x 3(CH_3)).

FT-IR, cm^{-1} (KBr) – 3182, 3050, 2975, 2924, 2440, 1871, 1686, 1559, 1450, 1377, 1333, 1302, 1283, 1235, 1150, 1073, 1046, 1008, 968, 882, 793, 707, 651.

Compound A2B6 (2,2',2''-nitrilotriethanaminium 3,3-dimethylbutanoate). M.P.= 122°C, ^1H NMR (400 MHz, $CDCl_3$, TMS) = δ (ppm) 5.808 (*s*, NH), 3.079 (*s*, 6H, 3(CH_2)), δ 2.740 (*s*, 6H, 3(CH_2)), δ 2.063 (*s*, 6H, 3 x 2(CH_2)), δ 1.014 (*s*, 27H, 3 x 3(CH_3)).

FT-IR, cm^{-1} (KBr) – 3397, 2953, 2362, 2186, 1634, 1560, 1396, 1299, 1237, 1142, 1099, 1043, 906, 806, 767, 731, 635.

Compound A2B7 (2-methylpropan-2-aminium 3,3-dimethylbutanoate). M.P.= 118°C, ^1H NMR (400 MHz, $CDCl_3$, TMS) = δ (ppm) 8.023 (NH), δ 2.074 (*s*, 2H, CH_2)), δ 1.343 (*s*, 9H, 3(CH_3)), δ 1.032 (*s*, 9H, 3(CH_3)).

FT-IR, cm^{-1} (KBr) – 3411, 2954, 2745, 2635, 2556, 2361, 2212, 2021, 1631, 1541, 1387, 1297, 1226, 1148, 732, 622.

Compound A2B8 (dodecan-1-aminium 3,3-dimethylbutanoate). M.P.= 41°C, ^1H NMR (400 MHz, $CDCl_3$, TMS) = δ (ppm) 7.48 (s, 3H, NH), δ 2.792 (*t*, 2H, CH_2), δ 2.06 (*s*, 2H, CH_2), δ 1.634 (*t*, 2H, CH_2), δ 1.255 (*s*, 20H, 10(CH_2)), δ 1.012 (*s*, 9H, 3(CH_3)), 0.899 (*t*, 3H, CH_3).

FT-IR, cm^{-1} (KBr) – 3440, 2955, 2182, 1632, 1528, 1482, 1405, 1355, 1222, 1043, 927, 883, 796, 735, 593, 537, 453.

Compound A2B9 (hexadecan-1-aminium 3,3-dimethylbutanoate). M.P.= 38°C, ^1H NMR (400 MHz, $CDCl_3$, TMS) = δ (ppm) 7.481 (s, 3H, NH), δ 2.792-2.753 (*t*, 2H, CH_2), δ 2.058 (*s*, 2H, CH_2), δ 1.651-1.616 (*t*, 2H, CH_2), δ 1.255 (*s*, 26H, 13(CH_2)), δ 1.012 (*s*, 9H, 3(CH_3)), 0.899-0.865 (*t*, 3H, CH_3).

FT-IR, cm^{-1} (KBr) – 3421, 2920, 2852, 2680, 2558, 2362, 2222, 1629, 1529, 1472, 1382, 1275, 1236, 1142, 1042, 955, 806, 734, 718, 638.

Compound A2B10 (cyclohexyl aminium 3,3-dimethylbutanoate). M.P.= 146°C, ^1H NMR (400 MHz, $CDCl_3$, TMS) = δ (ppm) 3.506 (3H, NH), δ 2.823 (*m*, 1H, CH), δ 2.195-2.135 (*d*, 2H, CH_2), δ 1.965 (*s*, 2H, CH_2), δ 1.783-1.754 (*m*, 2H, $C\underline{H}_2$), δ 1.266-1.47 (*m*, 6H, 3(CH_2)), δ 1.047 (*s*, 9H, 3(CH_3)).

FT-IR, cm^{-1} (KBr) – 3430, 2948, 2857, 2628, 2573, 2361, 2229, 1726, 1638, 1527, 1448, 1387, 1279, 1146, 1052, 915, 805, 733, 634, 551, 452.

Compound A2B11 (1-phenylethanaminium 3,3-dimethylbutanoate). M.P.= 98°C, ^1H NMR (400 MHz, $CDCl_3$, TMS) = δ (ppm) 7.416-7.303 (*m*, 5H, 5(CH)), δ 6.769 (*s*, 3H, NH), δ 4.235-4.184 (*m*, 1H, CH), δ 1.958 (*s*, 2H, CH_2), 1.527-1.510 (*d*, 3H, CH_3), δ 0.955 (*s*, 9H, 3(CH_3)).

FT-IR, cm^{-1} (KBr) – 3443, 2949, 2864, 2774, 2195, 1637, 1567, 1523, 1453, 1390, 1280, 1237, 1147, 1094, 1044, 912, 763, 702, 635.

Compound A2B12 (1-benzylpiperidin-4-aminium 3,3-dimethylbutanoate). M.P.= 130°C, ^1H NMR (400 MHz, $CDCl_3$, TMS) = δ (ppm) 7.328-7.282 (*m*, 5H, 5(CH)), δ 4.672 (*s*, 3H, NH), δ 3.527 (*s*, 2H, CH_2), δ 2.908-2.832 (*m*, 2H, 2(CH)), δ 2.821-2.805 (*m*, 1H, CH), δ 2.128 (*s*, 2H, CH_2), δ 1.906-1.880 (*m*, 2H, 2(CH)), δ 1.631-1.621 (*d*, 2H, 2(CH)), δ 1.600-1.532 (*m*, 2H, 2(CH)), δ 1.046 (*s*, 9H, 3(CH_3)).

FT-IR, cm^{-1} (KBr) – 3443, 2949, 2774, 2195, 1637, 1567, 1523, 1453, 1390, 1280, 1237, 1147, 1094, 912, 763, 702, 635, 538, 481.

Compound A2B13 (4,6-diamino-1,3,5-triazin-2-aminium 3,3-dimethylbutanoate). M.P >280°C, ^1H NMR (400 MHz, DMSO-d6, TMS) = δ (ppm) 6.011 (3H, 3(CH)), δ 3.5 (3H, NH), δ 2.083 (*s*, 2H, CH_2), δ 0.976 (*s*, 9H, 3(CH_3)).

FT-IR, cm^{-1} (KBr) – 3590, 3469, 2963, 1908, 1686, 1657, 1539, 1472, 1440, 1367, 1321, 1270, 1231, 1193, 1144, 1030, 792, 739, 579.

3.8 RESULTS AND DISCUSSION

All the salts were tested for their gelation behavior in the same set of solvents as mentioned in Table 3.2.

Table 3.9 Classification of all salts according to their gelation/non-gelation behavior

Gelators	Non-gelators
A2B2, A2B3 A2B8-A2B13	A2B1 A2B4-A2B7

3.8.1 Gelation studies and effect of amines on gelation

It was observed that out of the 13 salts, 8 turned out to be gelators (Table 3.9). We did not observe any gelation in alcohols (methanol, ethanol, etc.) and acetone. Gels were formed mainly in DMF, DMSO and acetonitrile. Moreover, the gelation performance was found to be sluggish in terms of mgc values and number of solvents gelled.

Table 3.10 Gelation behavior of salts in various solvents

	ACN	Acetone	EtOH	MeOH	DMF	DMSO	Water
A2B2	S	S	S	S	G (5.0)	G (5.0)	I
A2B3	S	S	S	S	G (5.5)	G (5.5)	I
A2B8	S	S	S	S	S	G (7.5)	I
A2B9	S	S	S	S	S	G (7)	I
A2B10	S	S	S	S	G (6.5)	G (7.0)	I
A2B11	G (5.5)	S	S	S	G (>10)	G (>10)	I
A2B12	G (6.0)	S	S	S	G (5)	G (5)	I
A2B13	I	I	I	I	I	G (7.5)	G (6.25)

Salts **A2B2** and **A2B3** formed gels in only DMF and DMSO and remained soluble in all the other tested solvents. A small hydrocarbon chain in di-/tri-amines along with the increased hydrophobicity of the acid moiety might be contributing to lack of hydrophilic character in this set of salts (**A2B1-A2B6**), which could be deterrent to the formation of fibrils required for entrapping the solvents. The salt of *tert*-butyl amine failed to give any gels (Table 3.10).

The salts of long chain amines, **A2B8** and **A2B9**, too, gave gels only in DMSO. A similar trend was observed in pivalic acid salts, **A1B8** and **A1B9** where gels were formed only in DMF and DMSO.

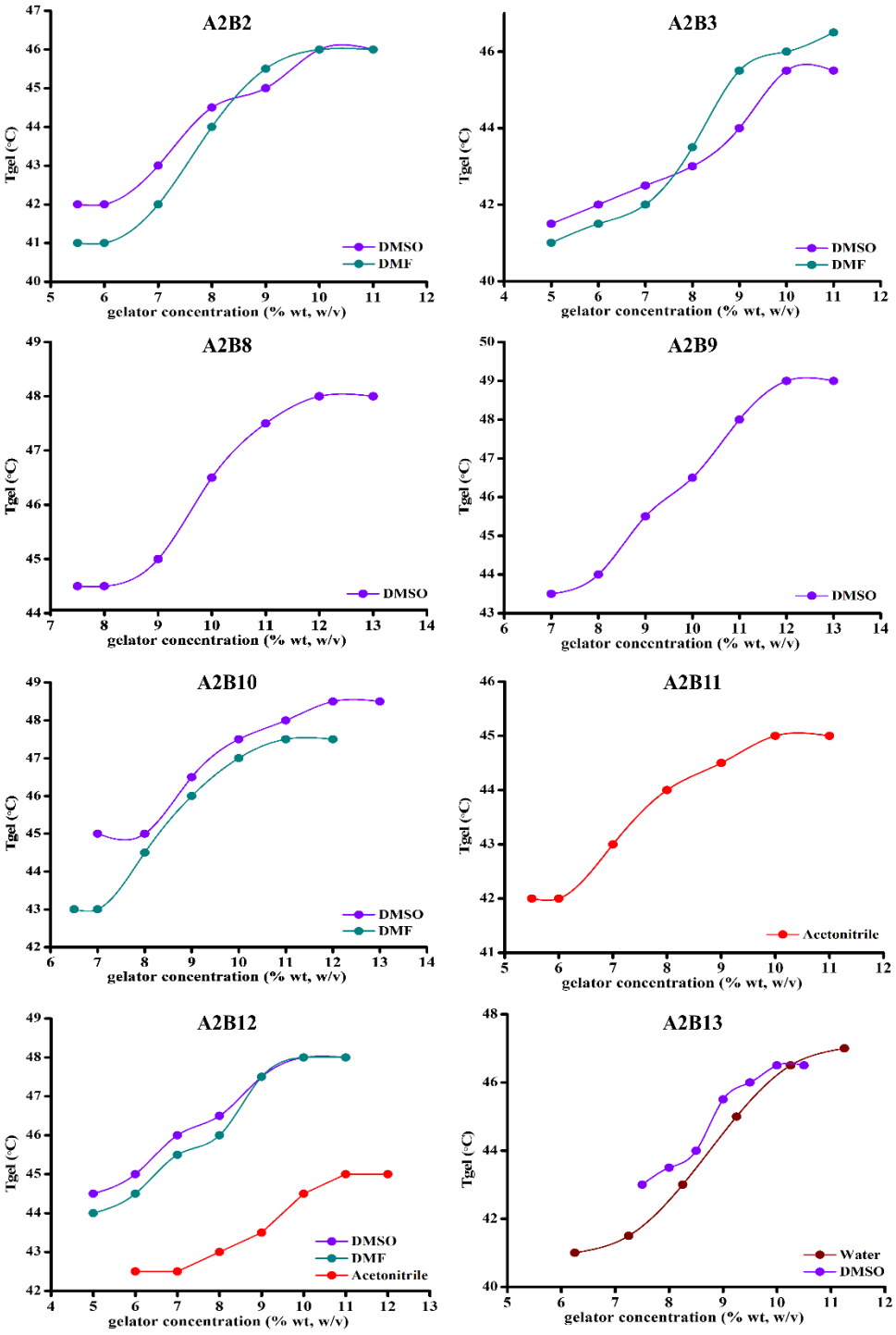

Figure 3.35 Variation of T_{gel} with increase in concentration of gelator

We also observed that in comparison to the pivalic acid salts, this set of salts could form gels at much higher mgc values which is indicative of their increased hydrophobicity and a disturbed balance of hydrophobic and hydrophilic character. The plots of T_{gel} vs. concentration follow nearly S-shaped behavior (Figure 3.35) where the T_{gel} values increased with increase in gelator concentration and become nearly constant when the solute reached a certain concentration.

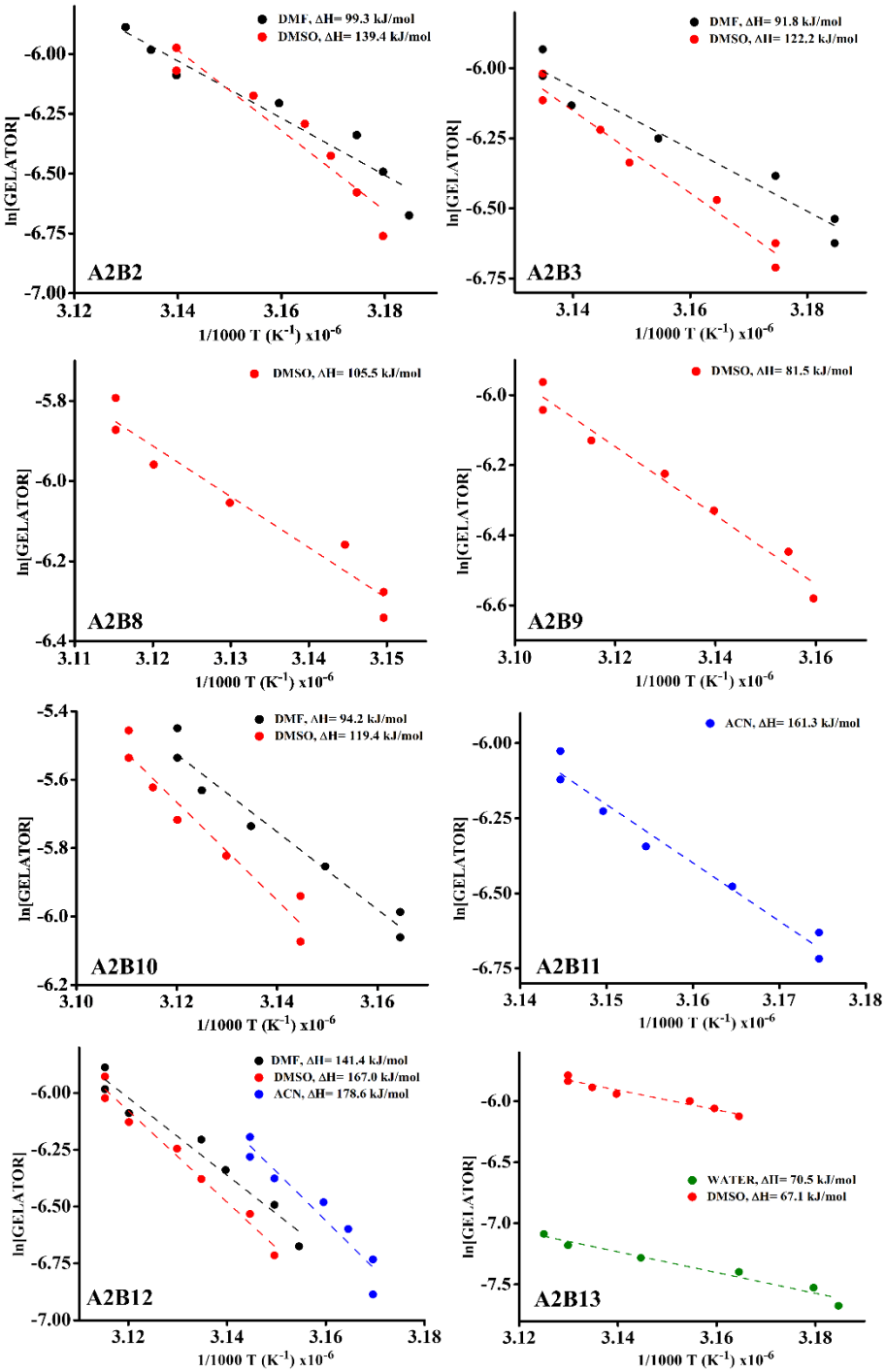

Figure 3.36 Structural backbone of pivalic acid and *tert*-butylacetic acid

Salts **A2B10-A2B12** also showed a similar gelation behavior, whereas their pivalic acid homologues were the most versatile gelators in the series. The melamine salt **A2B13** gave gels in water as well as in DMSO, **A1B13** could only form a hydrogel and remained insoluble in all the solvents tested, as rigid and planar molecules with such good hydrogen bonding functionalities are commonly very insoluble as a result of the

formation of very stable π-stacking and infinite hydrogen bonded chains in the solid state.

The semilog graph of mole fraction of gelator concentration plotted against 1/1000 T_{gel} (K^{-1}) for every gel gave a nearly linear relationship according to the Schroeder-van Laar equation (Figure 3.36) (where ΔH_m is the enthalpy of melting and T_{gel} is the transition temperature corresponding to gel-to-sol transition). ΔH_m values calculated from the plots fell within a range of 67-178 kJ/mol, which are considerably lower than those calculated for pivalic acid salts. This also proves that this set of salts has a more restrained gelation behavior than the pivalic acid ones.

3.8.2 Rheology

The mechanical strength and deformation behavior of the gels was evaluated using rheology (Figure 3.37). The plots of **A2B11** (acetonitrile gel) and **A2B13** (hydrogel) exhibited a nearly parallel throughout the amplitude sweep range of storage modulus, G' and loss modulus, G"; indicating a static interaction. The value of G' is almost an order greater than that of G", which demonstrate a degree of high elasticity in the gels.

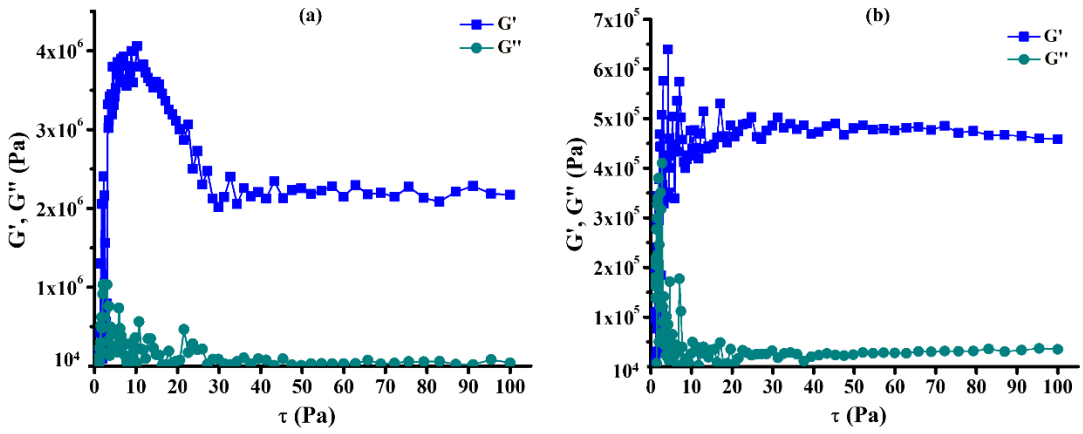

Figure 3.37 Rheological behavior of (a) A2B11 in acetonitrile gel and (b) A2B13 in hydrogel

3.8.3 Morphology

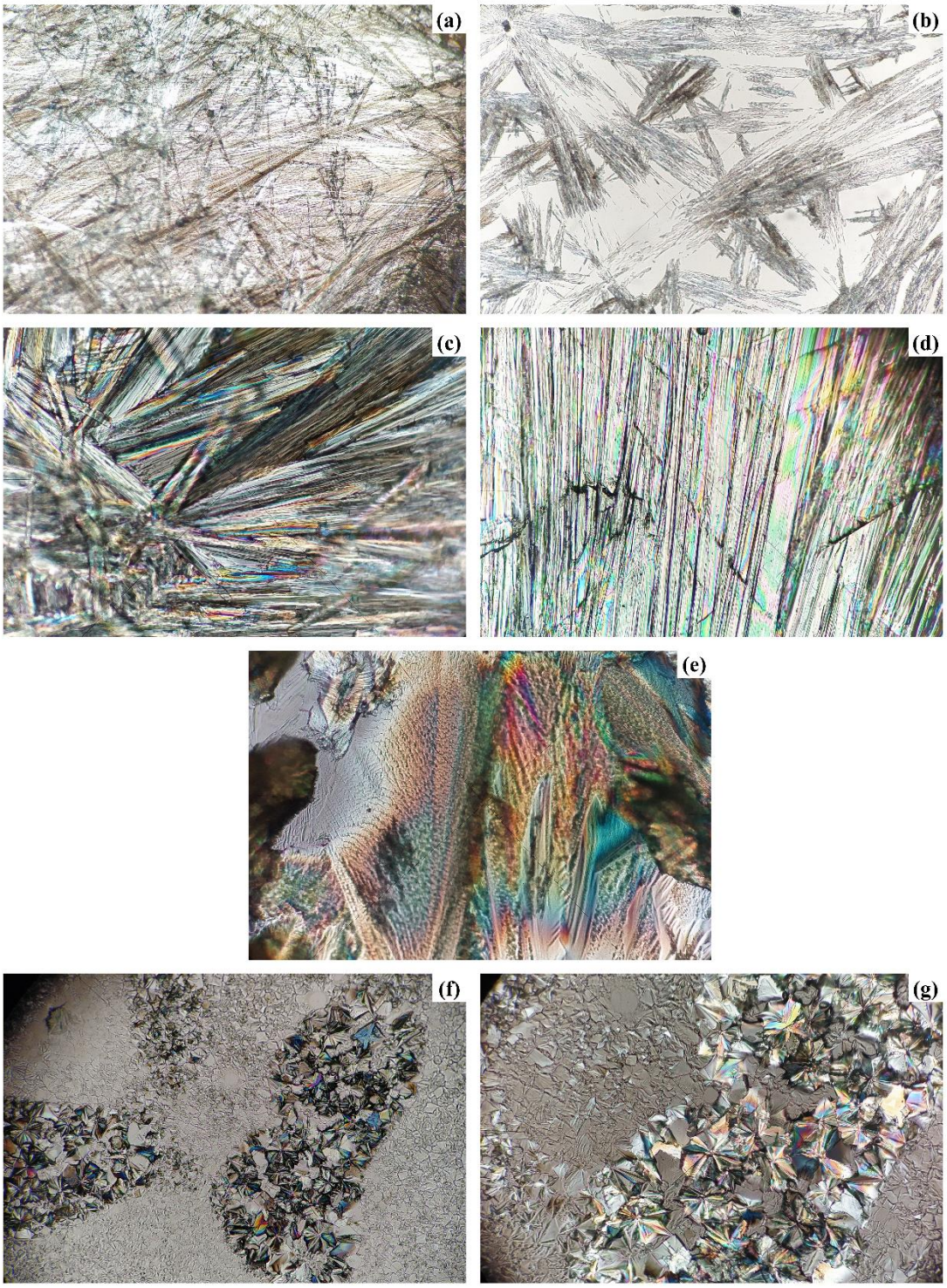

Figure 3.38 POM images of (a) A2B2 4x 45 deg (b) A2B8 20x 45 deg (c) A2B9 4x 90 deg (d) A2B10 10x 45 deg in DMSO GELS (e) A2B11 10x 90 deg and (f) 4x 45 deg (g) 10x 45 deg A2B12 in acetonitrile gels

The POM images show a fibrous and highly crystalline nature of the xerogels. The micrographs of **A2B11** show a highly birefringent texture, while those of **A1B12** show diamond-like crystalline fashion (Figure 3.38).

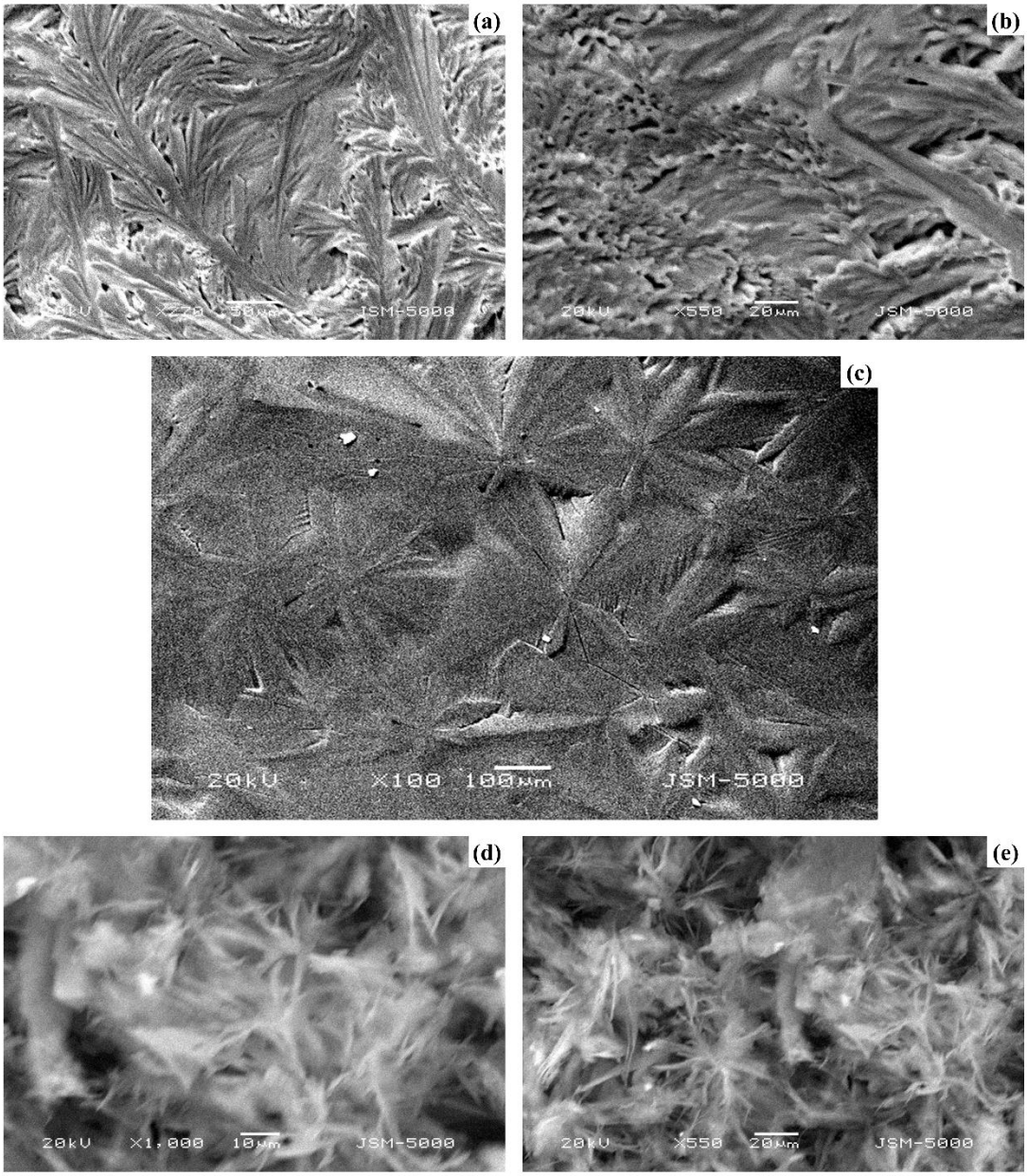

Figure 3.39 SEM images of frozen gels of (a) A2B9, (b) A2B9 in DMSO gel (c) A2B12 in acetonitrile gel and (d) A2B13 in hydrogel, at different magnifications

The SEM images of **A2B9** show a Cayley tree type morphology of the gels, whereas **A2B12** shows geometrical flower shaped patterns. However, the most interesting morphology was found in the melamine salt, **A2B13** where very thin thread-like fibers were observed in a flower-like pattern (Figure 3.39).

3.8.4 Powder X-ray diffraction studies

X-ray diffraction methods can provide useful information on the dimensions of the molecular fibrils and the morphologies responsible for gel formation. Generally, the X-ray studies of xerogels exhibit significantly more ordered arrangement than the solvated systems. The diffraction peaks for xerogels can directly give an idea about the d spacing, from the crystalline peaks observed in the spectrum.[14,15]

A comparative powder X-ray diffraction study was carried out to get an insight about the effect on the packing and morphology of the compounds after gelation. The XRD patterns of salts **A2B11 and A2B12** in bulk and xerogel (with Acetonitrile as solvent) were compared with the simulated patterns obtained from single crystal studies (Figures 3.40, 3.41).

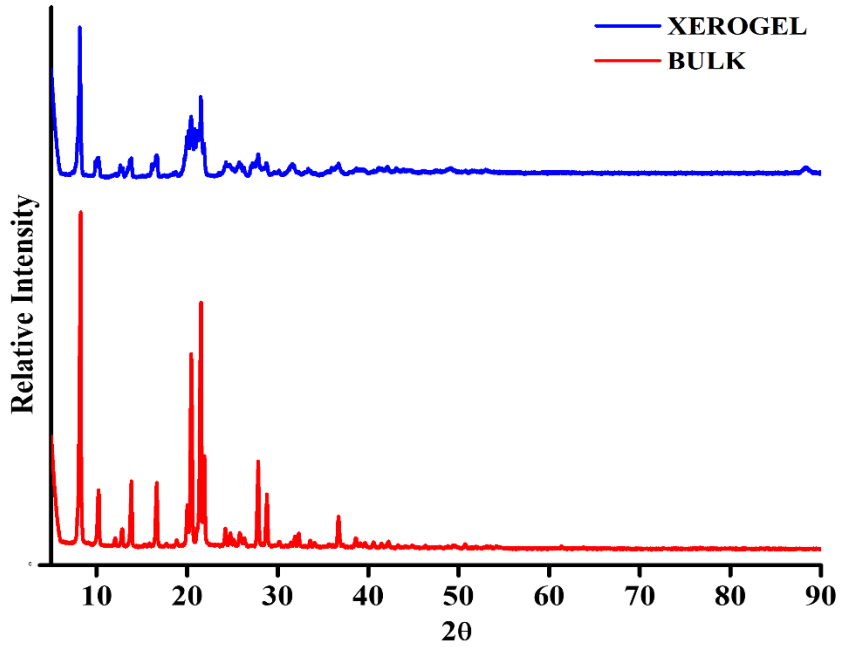

Figure 3.40 Comparison of PXRD patterns for salt A2B11

Majority of the peaks around 2θ values 8, 10, 13.8, 16.5, 20.5, 21.6, 24, 26, 27.8, 29 and 36.7 were found to overlapping in bulk and xerogel forms in the salt **A2B11**.

While in **A2B12**, the spectrum of xerogel displayed some new peaks at 2θ values 8.2, 10, 12, 12.6, 13.9. Several shoulder peaks between 2θ values 20-40 were also observed.

Generally, multiple hydrogen bonding interactions between complementary moieties (acid-amine in this case) lead to the formation of robust supramolecular gels. But

overall, nearly identical PXRD patterns were obtained, irrespective of gelator concentration and drying method.

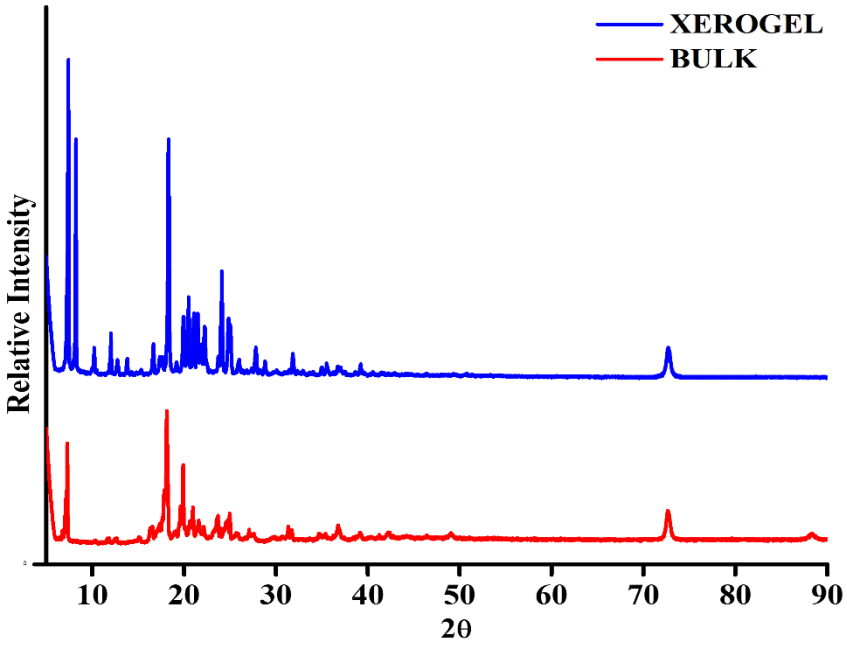

Figure 3.41 Comparison of PXRD patterns for salt A2B12

3.8.5 Comparative IR studies

FT-IR is a particularly useful tool for probing hydrogen bonded interactions in molecular self-assemblies. In particular, O–H, N–H and C=O stretches show distinctive responses to hydrogen bonding – with the bonds changing in strength as hydrogen bonds form resulting in a shift in wave number. van der Waals interactions can also be detected by looking for changes in C–H stretching interactions. Usually, it is required to compare the IR spectra of the gelator in both the sol and the gel forms in order to determine the key non-covalent interactions responsible for assembly.

On these grounds, comparative IR studies were carried out in bulk, xerogel, gel and solution forms for the same salts. (Figures 3.42, 3.43)

The major peaks were retained in the gel and solution phases with slight shifts, which can be attributed to intermolecular H-bonding. Moreover, the characteristic bands for C=O stretching of carboxylate groups around 1650 cm^{-1} and 1450 cm^{-1} and N-H stretch of primary ammonium cations for the respective bases at 2200 cm^{-1} and 3500 cm^{-1} was

retained in gel form as well the solution form for both the salts.

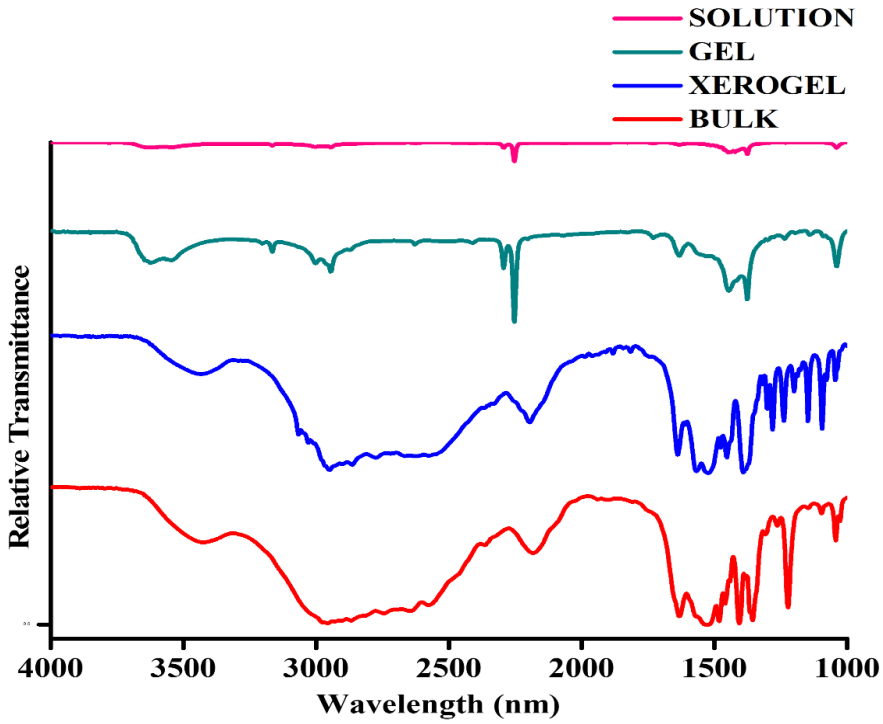

Figure 3.42 Comparative FT-IR patterns in bulk, xerogel, gel and solution phase in A2B11

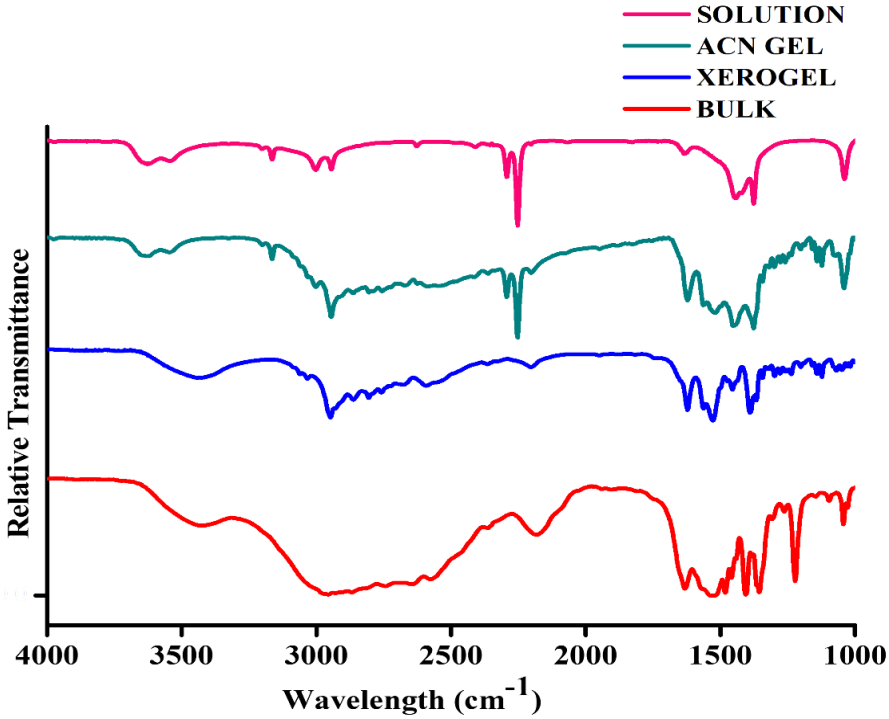

Figure 3.43 Comparative FT-IR patterns in bulk, xerogel, gel and solution phase in A2B12

A comparative FT-IR for the melamine salt of TBAA (**A2B13**) also displayed a similar pattern in bulk and xerogel, obtained from the hydrogel of the salt (Figure 3.44).

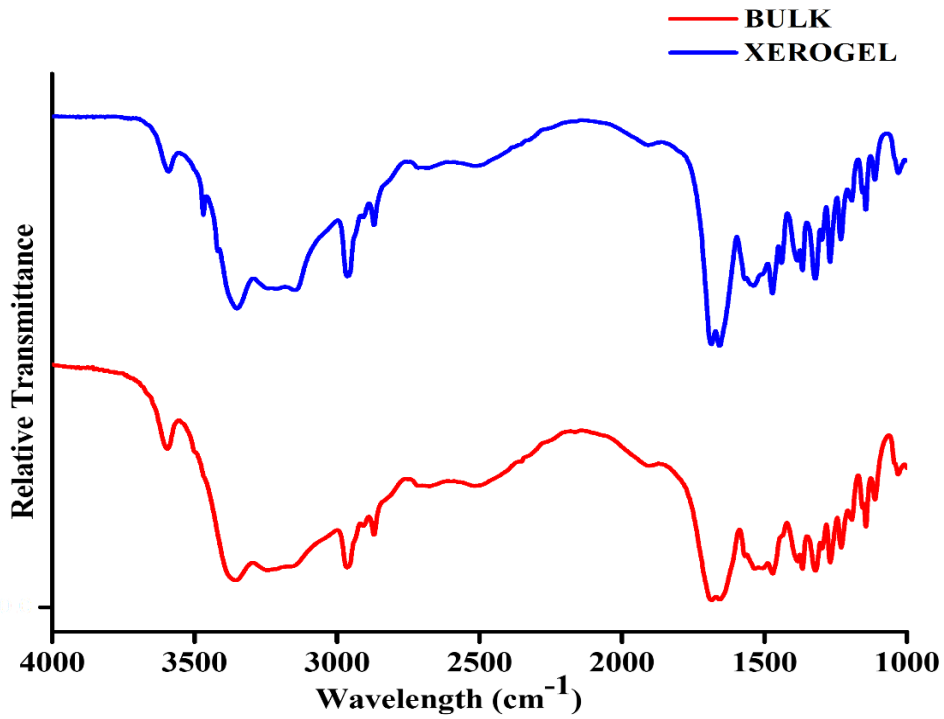

Figure 3.44 Comparative FT-IR patterns in A2B13

From these comparative PXRD and FT-IR studies, we can corroborate that the packing in gel phase (xerogel or dried gel) and the bulk form is similar for this series of salts. The basic morphology and internal arrangement remain very similar in both the phases for this set of compounds and the presence of additional peaks in the X-ray pattern of xerogel may be due to certain changes in the packing of the molecules after interacting with the solvent.

3.9 SUMMARIZING DISCUSSION AND CONCLUSIONS

The idea of synthesizing salts has emerged as a powerful strategy for development of soft functional materials with higher tunability, adaptability and better responsive properties than single component systems. This chapter is an effort to get a better understanding of the self-assembly processes and the role of directional non-covalent interactions in promoting one-dimensional organization of the molecules.

A series of *tert*-butylacetic acid based salts was synthesized to probe into the gelation performance and compare it with that of pivalic acid based salts. Since we obtained a set of versatile gelators in Chapter 3A, this study was carried out to analyze this behavior and scrutinize the plausible reasons behind it. This work was extended from pivalic acid salts in order to devise a working hypothesis as organic salts possess a number of advantages like ease of synthesis, high yield, stability, etc. A combinatorial library approach can be applied conveniently to create multi-component gelators. In retrospect, we believe that an additional methylene group fails to attain the delicate balance between hydrophobic and hydrophilic forces required for exhibiting gelation behavior. This is contradictory to the notion that an increased alkyl chain length enhances the van der Waals and similar hydrophobic interactions which allow the system to exhibit improved gelation properties.

In pivalic acid salts, gels were formed in solvents like acetone, acetonitrile, methanol, ethanol, etc. In TBAA analogues, gels were mainly formed in DMF and DMSO; only two salts formed gels in acetonitrile and no gels were formed in acetone, methanol and ethanol. Also, the mgc values in pivalic acid salts range mainly from (1-5) wt%, while in TBAA salts, the mgc values range between (5-10) wt%. The thermal stability also appeared to be lower than those of pivalic acid salts.

An increase in chain length by one methylene group proved to be deterrent to gel formation. The performance of the salts was found to be adversely affected. In nutshell, we can say that the inherent ability of TBAA as a molecule to prompt the system towards self-assembly is subdued. Despite a failed effort, we believe that such systems can guide our way to design molecular gelators by providing more insights into the self-assembly process of multi-component gelators. Even in absence of an *ab initio* approach, these studies significantly enhance our understanding functional of soft materials with tailor-made properties.

REFERENCES

1. Hirst, A. R., Escuder, B., Miravet, J. F. & Smith, D. K. High-tech applications of self-assembling supramolecular nanostructured gel-phase materials: From regenerative medicine to electronic devices. *Angew. Chemie - Int. Ed.* **47**, 8002–8018 (2008).
2. Zweep, N. & van Esch, J. H. Chapter 1. The Design of Molecular Gelators. in *Functional Molecular Gels* (eds. Escuder, B. & Miravet, J. F.) 1–29 (The Royal Society of Chemistry, 2014).
3. Amabilino, D. B., Smith, D. K. & Steed, J. W. Supramolecular materials. *Chem. Soc. Rev.* **46**, 2404–2420 (2017).
4. Panja, S. & Adams, D. J. Stimuli responsive dynamic transformations in supramolecular gels. *Chem. Soc. Rev.* **50**, 5165–5200 (2021).
5. Cornwell, D. J. & Smith, D. K. Photo-patterned multi-domain multi-component hybrid hydrogels. *Chem. Commun.* **56**, 7029–7032 (2020).
6. Draper, E. R. & Adams, D. J. Low-Molecular-Weight Gels: The State of the Art. *Chem* **3**, 390–410 (2017).
7. Draper, E. R. & Adams, D. J. How should multicomponent supramolecular gels be characterised ? *Chem. Soc. Rev.* **47**, 3395–3405 (2018).
8. Panja, S. & Adams, D. J. Chemical crosslinking in 'reactive' multicomponent gels. *Chem. Commun.* **23**, 5622–5625 (2022).
9. Cornwell, D. J. & Smith, D. K. Expanding the scope of gels – combining polymers with low-molecular-weight gelators to yield modi fi ed self-assembling smart materials with high-tech applications. *Mater. Horizons* **2**, 279–293 (2015).
10. Buerkle, L. E. & Rowan, S. J. Supramolecular gels formed from multi-component low molecular weight species. *Chem. Soc. Rev.* **41**, 6089–6102 (2012).
11. Patterson, A. K. & Smith, D. K. Two-component supramolecular hydrogel for controlled drug release. *Chem. Commun.* **56**, 11046–11049 (2020).
12. Friggeri, A., Bommel, K. J. C. Van & Shinkai, S. Chapter 25. Gels of low molecular-mass organic gelators as templates. in *Molecular Gels. Materials with Self-Assembled Fibrillar Networks* (eds. Weiss, R. G. & Terech, P.) 857–893 (Springer International Publishing, The Netherlands, 2006).
13. Yue, X., Subraveti, S. N., John, G. & Raghavan, S. R. Phase-Selective Gelation of the Water Phase in an Oil-Water Mixture: An Approach Based on Oil-Activated Nanoparticle Assembly in Water. *Langmuir* **37**, 8107–8114 (2021).
14. Nebot, V. J. & Smith, D. K. Chapter 2. Techniques for the Characterisation of Molecular Gels. in *Functional Molecular Gels* (eds. Escuder, B. & Miravet, J. F.) 30–66 (The Royal Society of Chemistry, 2014).
15. Anderson, K. M., Day, G. M., Paterson, M. J., Byrne, P., Clarke, N. & Steed, J. W. Structure Calculation of an Elastic Hydrogel from Sonication of Rigid Small Molecule Components. *Angew. Chemie Int. Ed.* **47**, 1058–1062 (2008).

*SUPPLEMENTARY DATA

Spectral Data – NMR and FT-IR

A2B1

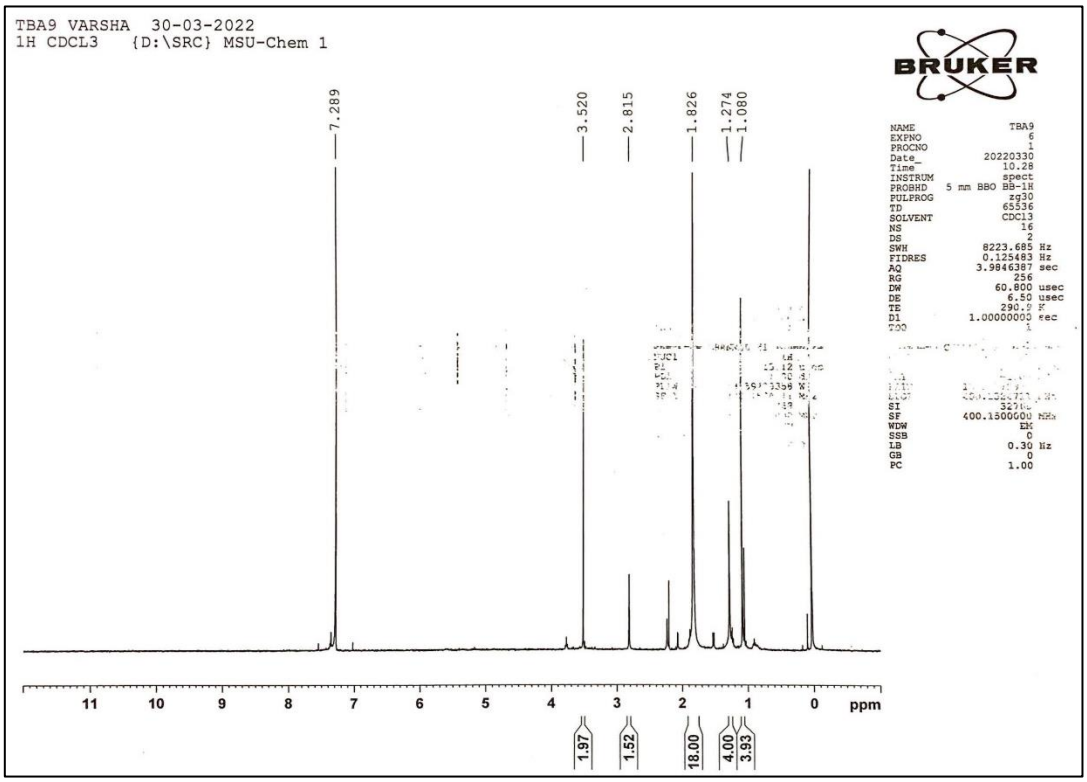

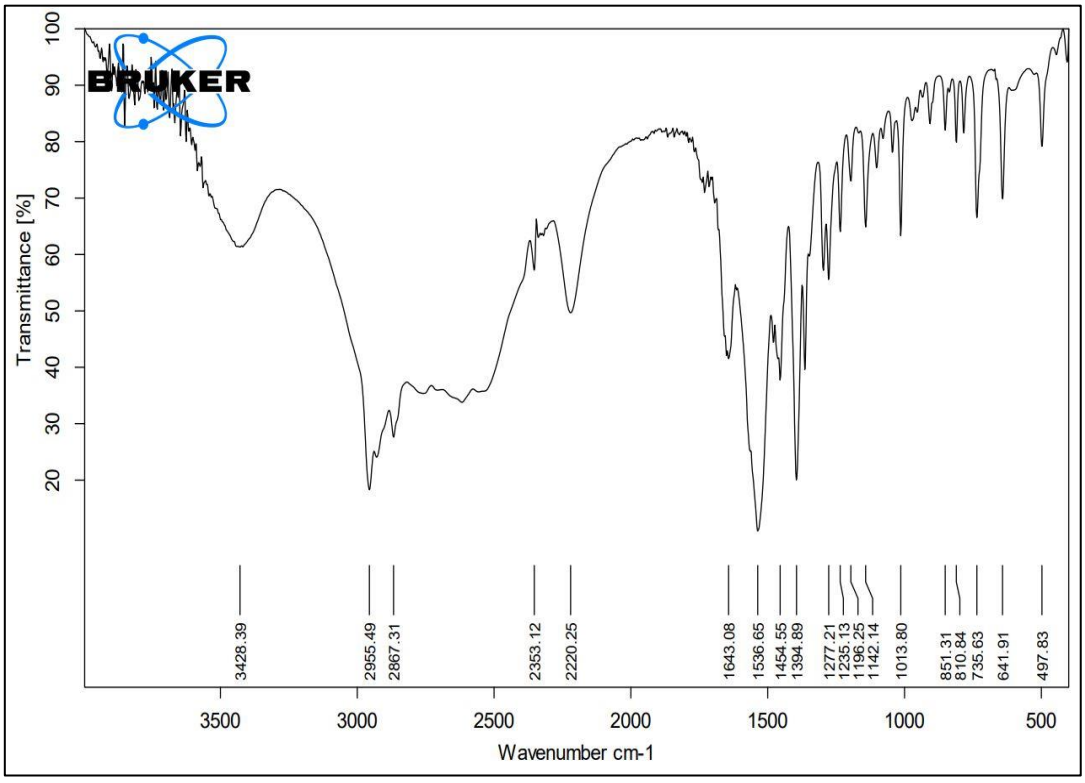

A2B2

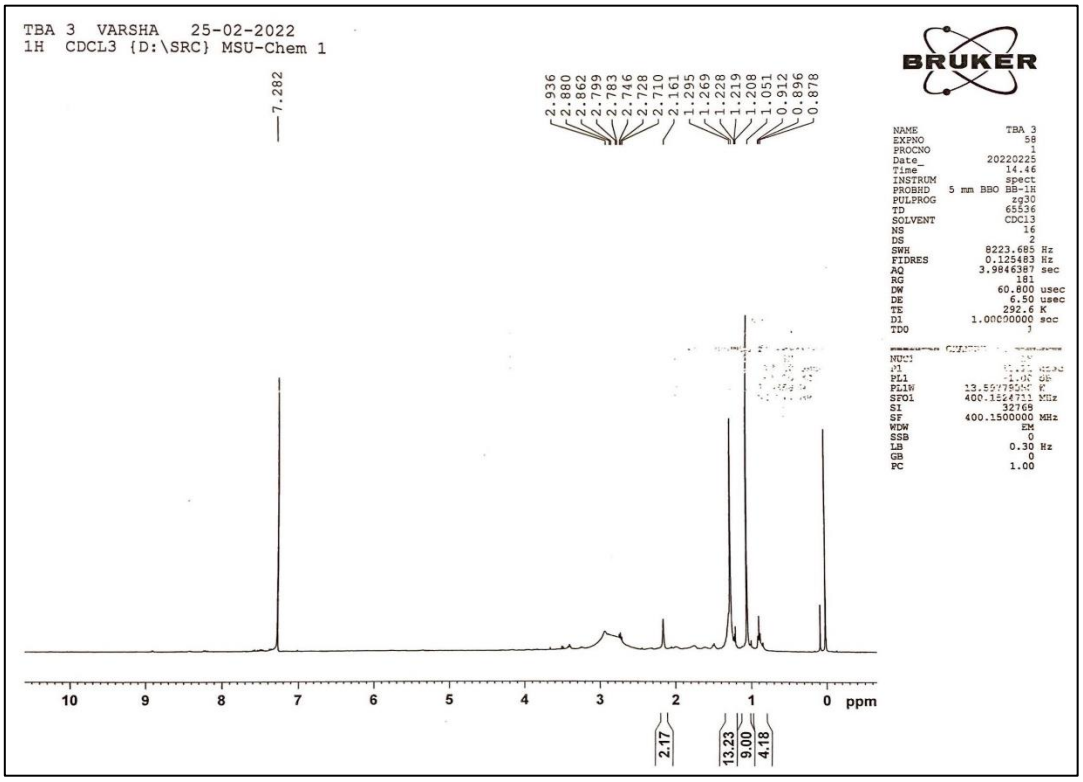
TBA 3 VARSHA 25-02-2022
1H CDCL3 {D:\SRC} MSU-Chem 1
BRUKER
7.282
2.936
2.880
2.862
2.799
2.783
2.746
2.728
2.710
2.161
1.295
1.269
1.228
1.219
1.208
1.051
0.912
0.896
0.878
NAME TBA 3
EXPNO 58
PROCNO 1
Date_ 20220225
Time 14.46
INSTRUM spect
PROBHD 5 mm BBO BB-1H
PULPROG zg30
TD 65536
SOLVENT CDCl3
NS 16
DS 2
SWH 8223.685 Hz
FIDRES 0.125483 Hz
AQ 3.9846387 sec
RG 181
DW 60.800 usec
DE 6.50 usec
TE 292.6 K
D1 1.00000000 sec
TD0 1
SFO1 400.1524711 MHz
SI 32768
SF 400.1500000 MHz
WDW EM
SSB 0
LB 0.30 Hz
GB 0
PC 1.00
10 9 8 7 6 5 4 3 2 1 0 ppm
2.17
13.23
9.00
4.18

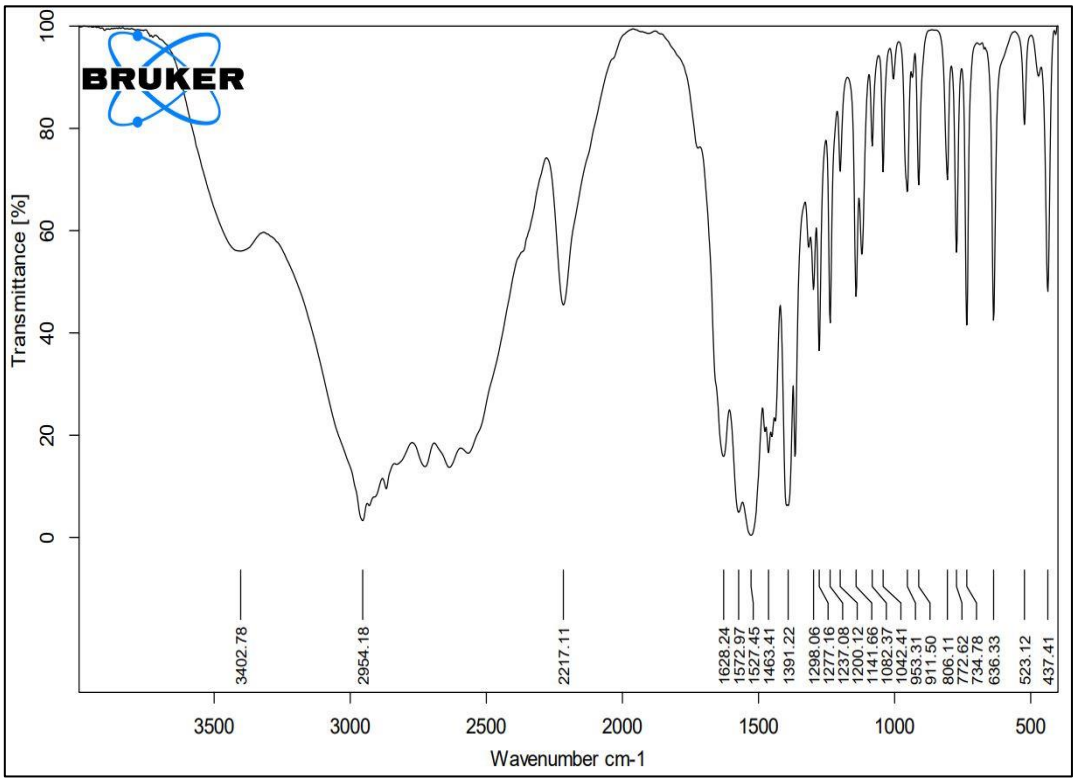
BRUKER
Transmittance [%]
0 20 40 60 80 100
3402.78
2954.18
2217.11
1628.24
1572.97
1527.45
1463.41
1391.22
1298.06
1277.16
1237.08
1200.12
1141.66
1082.37
1042.41
953.31
911.50
806.11
772.62
734.78
636.33
523.12
437.41
3500 3000 2500 2000 1500 1000 500
Wavenumber cm-1

A2B3

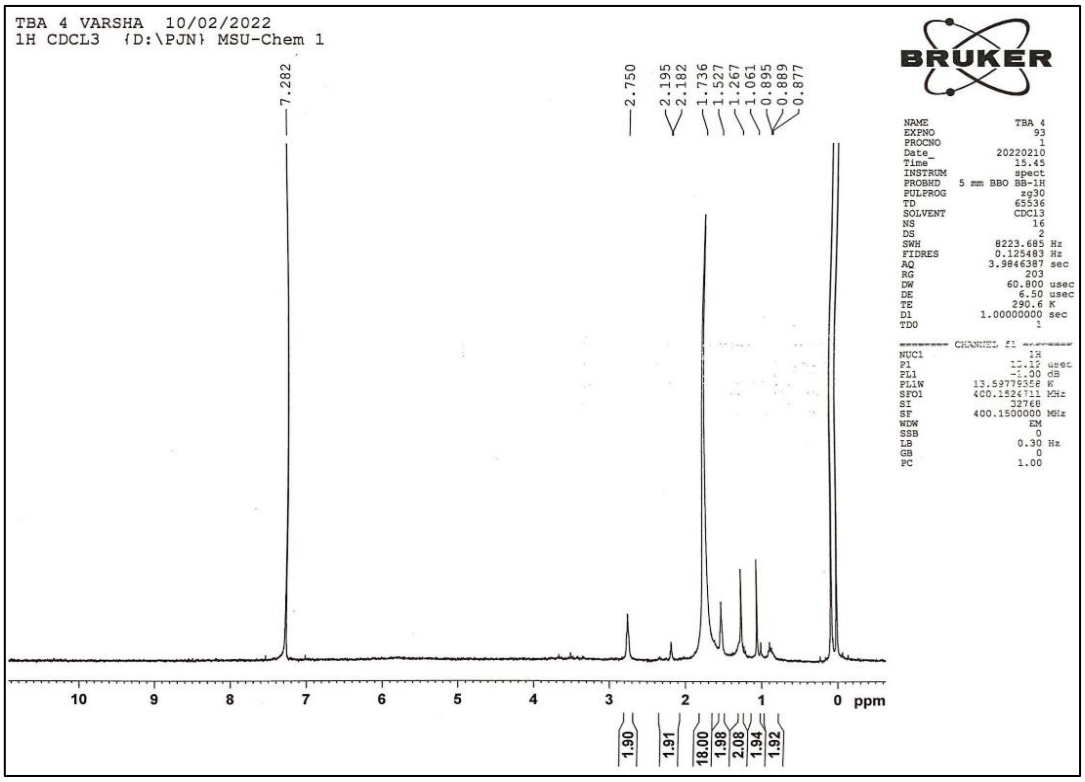
TBA 4 VARSHA 10/02/2022
1H CDCL3 {D:\PJN} MSU-Chem 1
BRUKER
7.282
2.750
2.195
2.182
1.736
1.527
1.267
1.061
0.895
0.889
0.877
10 9 8 7 6 5 4 3 2 1 0 ppm
1.90
1.91
18.00
1.98
2.08
1.94
1.92

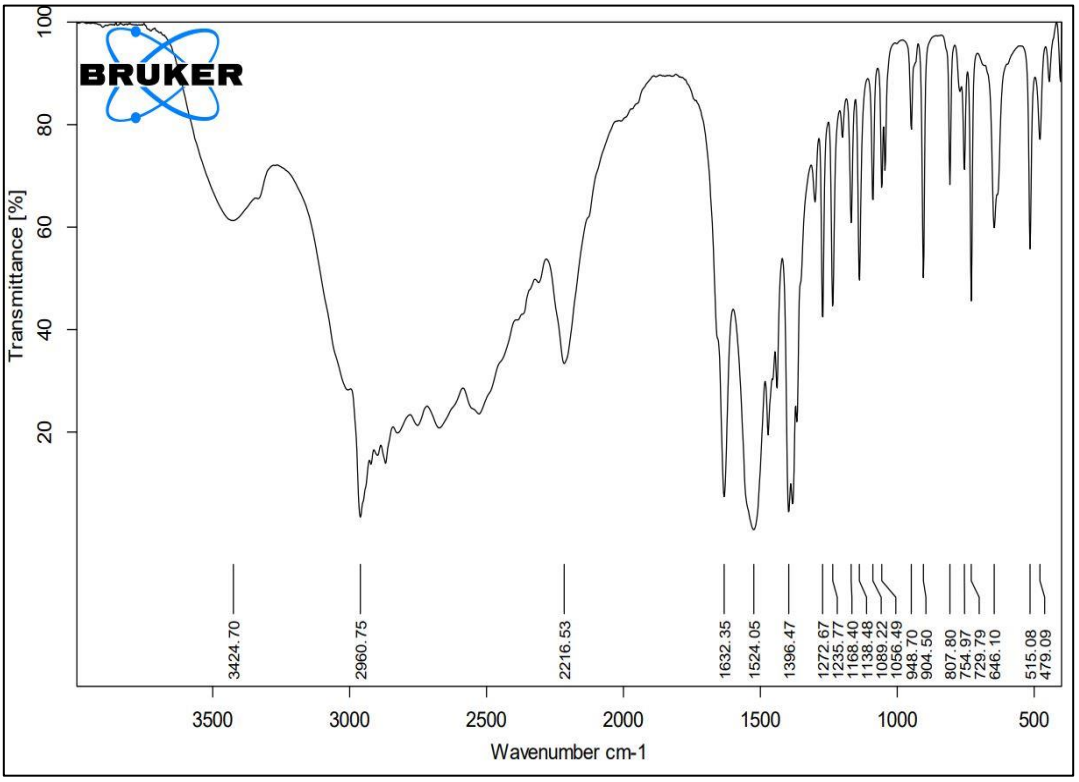
BRUKER
Transmittance [%]
100
80
60
40
20
3424.70
2960.75
2216.53
1632.35
1524.05
1396.47
1272.67
1235.77
1168.40
1138.48
1089.22
1056.49
948.70
904.50
807.80
754.97
729.79
646.10
515.08
479.09
3500 3000 2500 2000 1500 1000 500
Wavenumber cm-1

A2B4

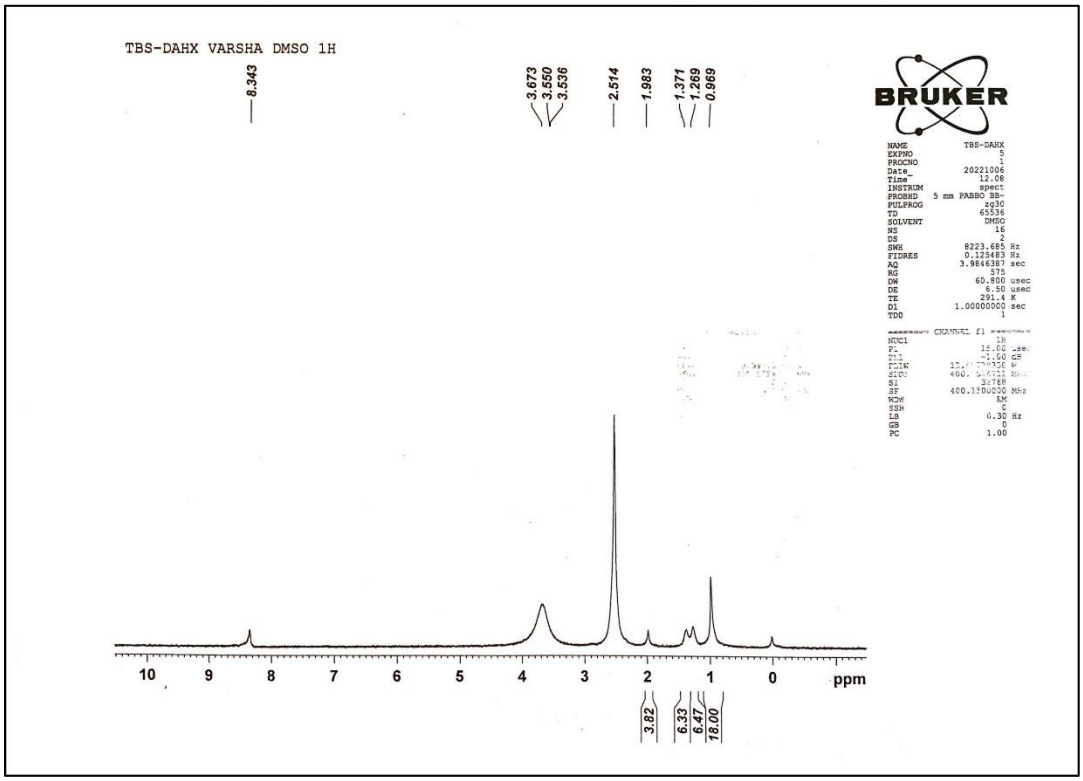
TBS-DAHX VARSHA DMSO 1H
8.343
3.673
3.550
3.536
2.514
1.983
1.371
1.269
0.969
BRUKER
10
9
8
7
6
5
4
3
2
1
0
ppm
3.82
6.33
6.47
18.00

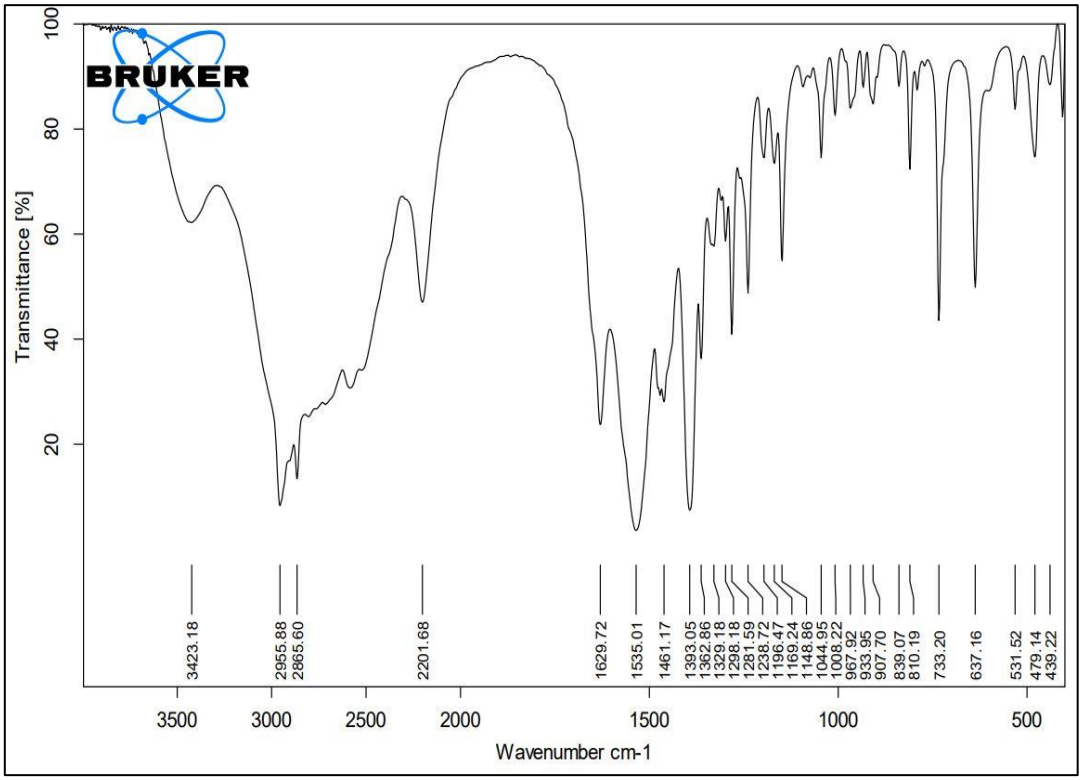
BRUKER
Transmittance [%]
100
80
60
40
20
3423.18
2955.88
2865.60
2201.68
1629.72
1535.01
1461.17
1393.05
1362.86
1329.18
1298.18
1281.59
1238.72
1196.47
1169.24
1148.86
1044.95
1008.22
967.92
933.95
907.70
839.07
810.19
733.20
637.16
531.52
479.14
439.22
3500
3000
2500
2000
1500
1000
500
Wavenumber cm-1

A2B5

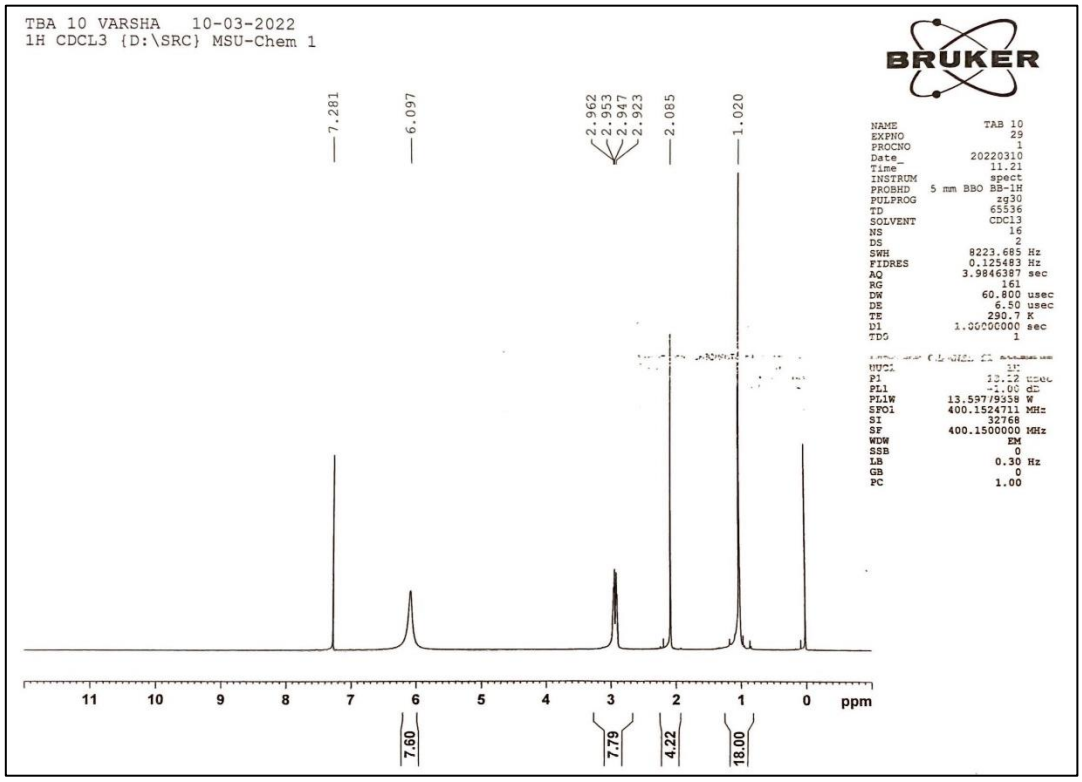
TBA 10 VARSHA 10-03-2022
1H CDCL3 {D:\SRC} MSU-Chem 1
BRUKER
7.281
6.097
2.962
2.953
2.947
2.923
2.085
1.020
NAME TAB 10
EXPNO 29
PROCNO 1
Date_ 20220310
Time_ 11.21
INSTRUM spect
PROBHD 5 mm BBO BB-1H
PULPROG zg30
TD 65536
SOLVENT CDCl3
NS 16
DS 2
SWH 8223.685 Hz
FIDRES 0.125483 Hz
AQ 3.9846387 sec
RG 161
DW 60.800 usec
DE 6.50 usec
TE 290.7 K
D1 1.00000000 sec
TDG 1
PL1 -1.00 dB
PL1W 13.597/9338 W
SFO1 400.1524711 MHz
SI 32768
SF 400.1500000 MHz
WDW EM
SSB 0
LB 0.30 Hz
GB 0
PC 1.00
11 10 9 8 7 6 5 4 3 2 1 0 ppm
7.60
7.79
4.22
18.00

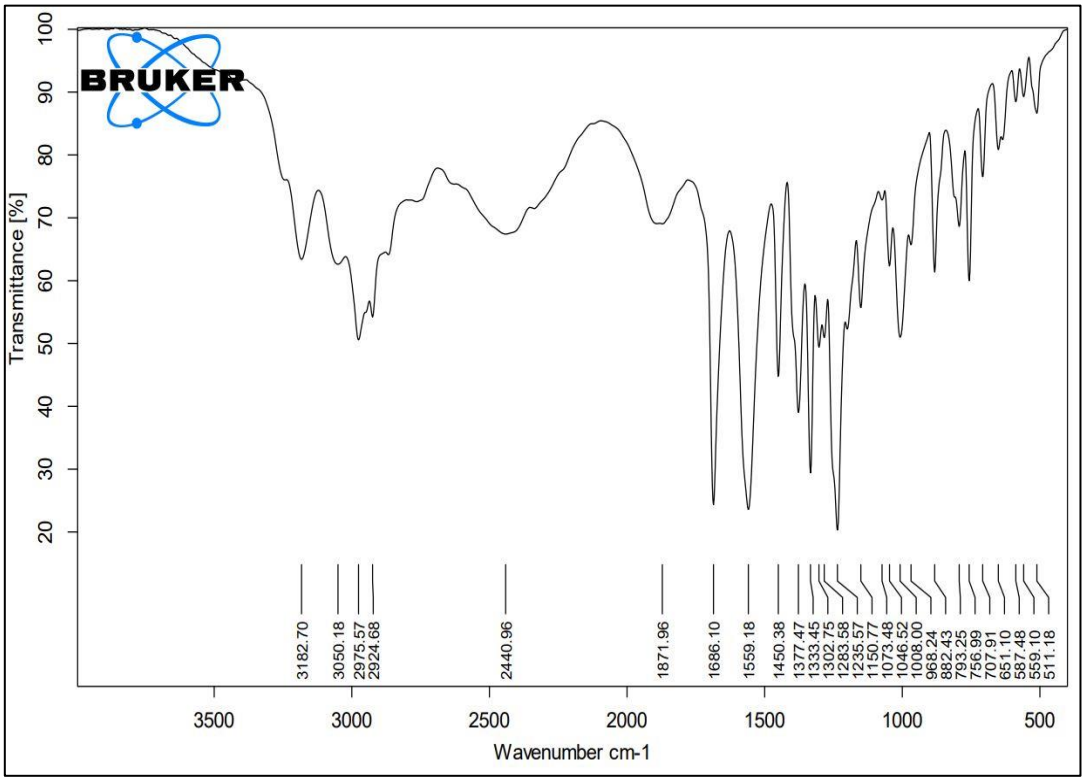
BRUKER
Transmittance [%]
100 90 80 70 60 50 40 30 20
3182.70
3050.18
2975.57
2924.68
2440.96
1871.96
1686.10
1559.18
1450.38
1377.47
1333.45
1302.75
1283.58
1235.57
1150.77
1073.48
1046.52
1008.00
968.24
882.43
793.25
756.99
707.91
651.10
587.48
559.10
511.18
3500 3000 2500 2000 1500 1000 500
Wavenumber cm-1

A2B6

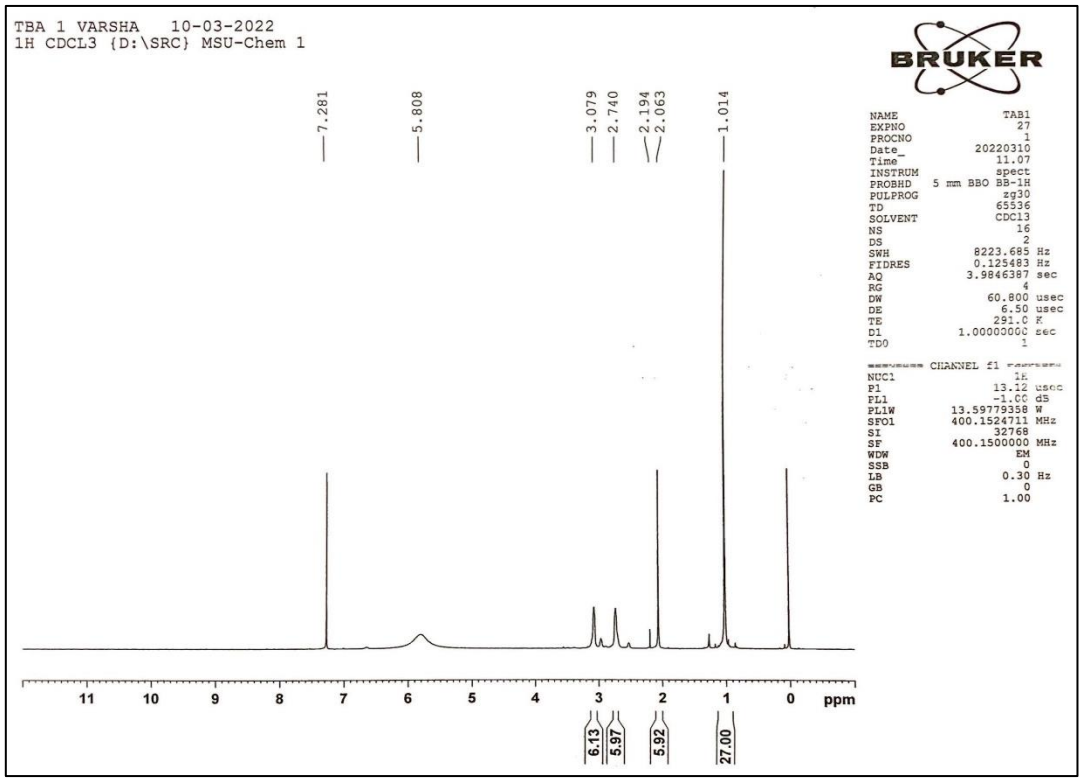
TBA 1 VARSHA 10-03-2022
1H CDCL3 {D:\SRC} MSU-Chem 1
BRUKER
7.281
5.808
3.079
2.740
2.194
2.063
1.014
NAME TAB1
EXPNO 27
PROCNO 1
Date_ 20220310
Time 11.07
INSTRUM spect
PROBHD 5 mm BBO BB-1H
PULPROG zg30
TD 65536
SOLVENT CDCl3
NS 16
DS 2
SWH 8223.685 Hz
FIDRES 0.125483 Hz
AQ 3.9846387 sec
RG 4
DW 60.800 usec
DE 6.50 usec
TE 291.0 K
D1 1.00000000 sec
TD0 1
CHANNEL f1
NUC1 1H
P1 13.12 usec
PL1 -1.00 dB
PL1W 13.59779358 W
SFO1 400.1524711 MHz
SI 32768
SF 400.1500000 MHz
WDW EM
SSB 0
LB 0.30 Hz
GB 0
PC 1.00
11 10 9 8 7 6 5 4 3 2 1 0 ppm
6.13
5.97
5.92
27.00

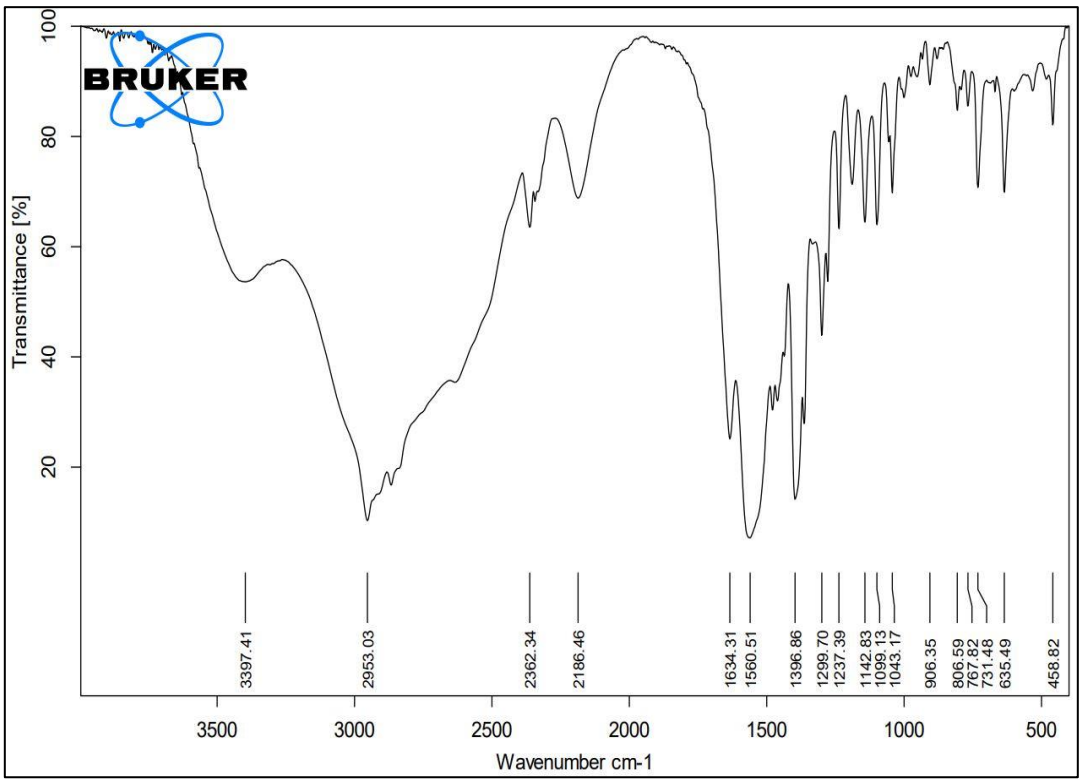
BRUKER
Transmittance [%]
100
80
60
40
20
3397.41
2953.03
2362.34
2186.46
1634.31
1560.51
1396.86
1299.70
1237.39
1142.83
1099.13
1043.17
906.35
806.59
767.82
731.48
635.49
458.82
3500 3000 2500 2000 1500 1000 500
Wavenumber cm-1

A2B7

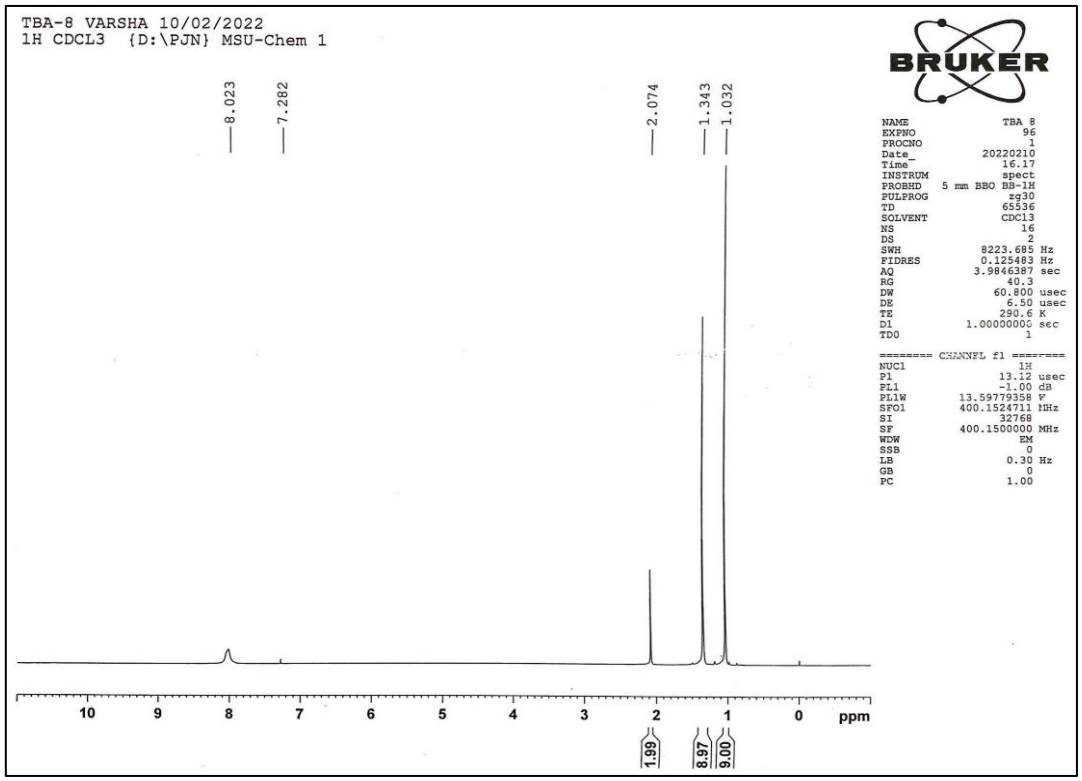
TBA-8 VARSHA 10/02/2022
1H CDCL3 {D:\PJN} MSU-Chem 1
BRUKER
8.023
7.282
2.074
1.343
1.032
NAME TBA 8
EXPNO 96
PROCNO 1
Date_ 20220210
Time 16.17
INSTRUM spect
PROBHD 5 mm BBO BB-1H
PULPROG zg30
TD 65536
SOLVENT CDCl3
NS 16
DS 2
SWH 8223.685 Hz
FIDRES 0.125483 Hz
AQ 3.9846387 sec
RG 40.3
DW 60.800 usec
DE 6.50 usec
TE 290.6 K
D1 1.00000000 sec
TD0 1
======== CHANNEL f1 ========
NUC1 1H
P1 13.12 usec
PL1 -1.00 dB
PL1W 13.59779358 W
SFO1 400.1524711 MHz
SI 32768
SF 400.1500000 MHz
WDW EM
SSB 0
LB 0.30 Hz
GB 0
PC 1.00
10 9 8 7 6 5 4 3 2 1 0 ppm
1.99
8.97
9.00

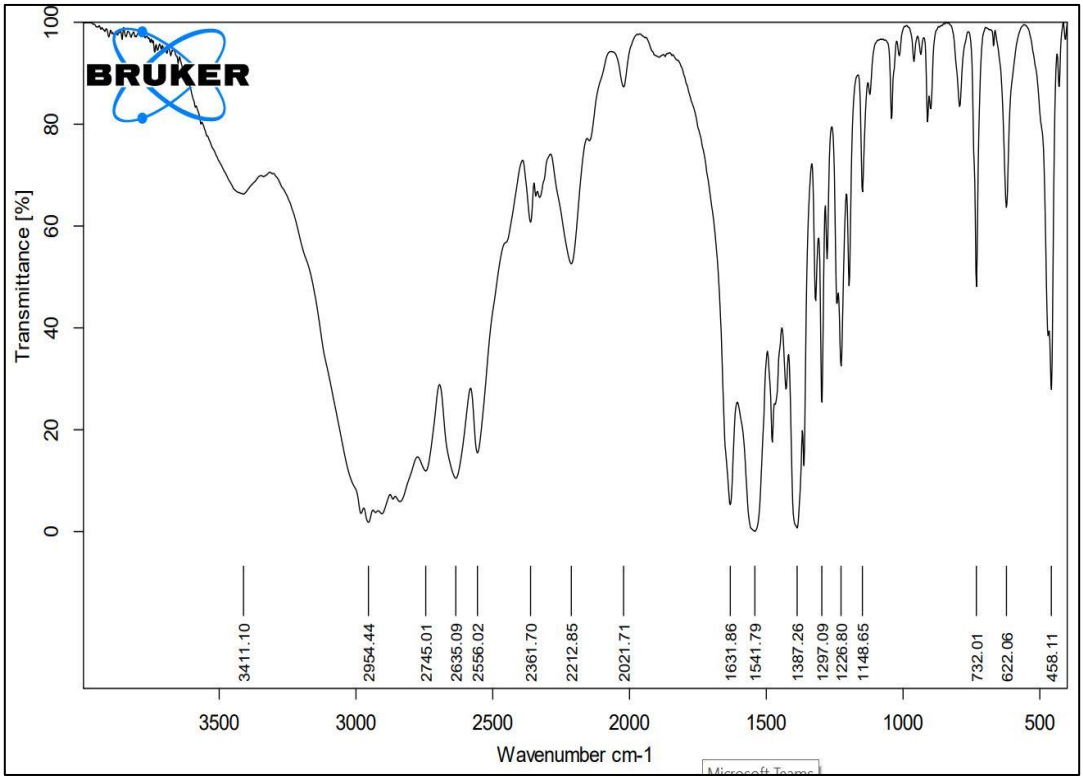
BRUKER
Transmittance [%]
0 20 40 60 80 100
3411.10
2954.44
2745.01
2635.09
2556.02
2361.70
2212.85
2021.71
1631.86
1541.79
1387.26
1297.09
1226.80
1148.65
732.01
622.06
458.11
3500 3000 2500 2000 1500 1000 500
Wavenumber cm-1

A2B8

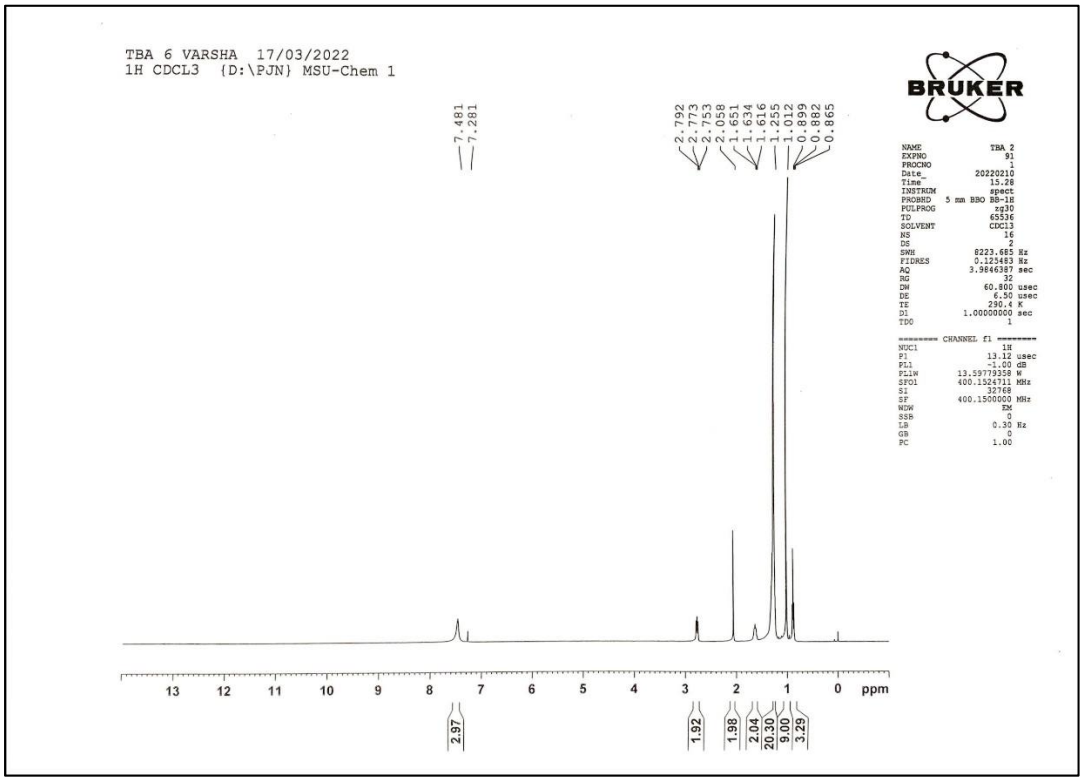
TBA 6 VARSHA 17/03/2022
1H CDCL3 {D:\PJN} MSU-Chem 1
BRUKER
7.481
7.281
2.792
2.773
2.753
2.058
1.651
1.634
1.616
1.255
1.012
0.899
0.882
0.865
13 12 11 10 9 8 7 6 5 4 3 2 1 0 ppm
2.97
1.92
1.98
2.04
20.30
9.00
3.29

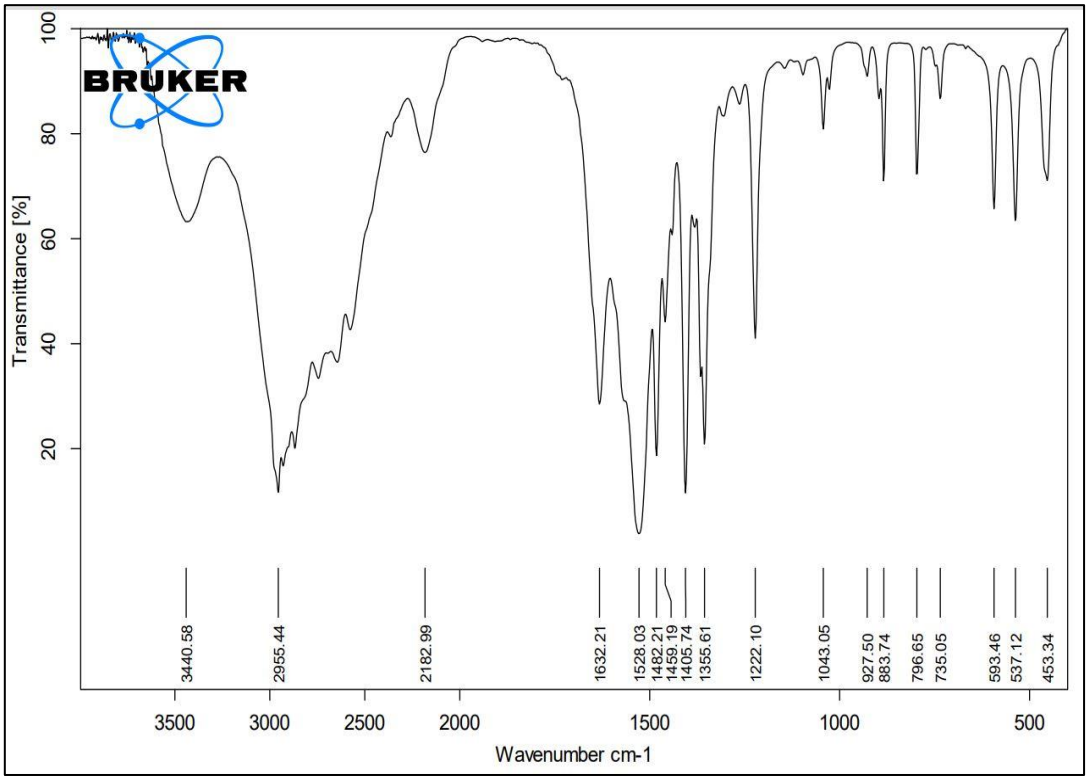
BRUKER
Transmittance [%]
100
80
60
40
20
3440.58
2955.44
2182.99
1632.21
1528.03
1482.21
1459.19
1405.74
1355.61
1222.10
1043.05
927.50
883.74
796.65
735.05
593.46
537.12
453.34
3500 3000 2500 2000 1500 1000 500
Wavenumber cm-1

A2B9

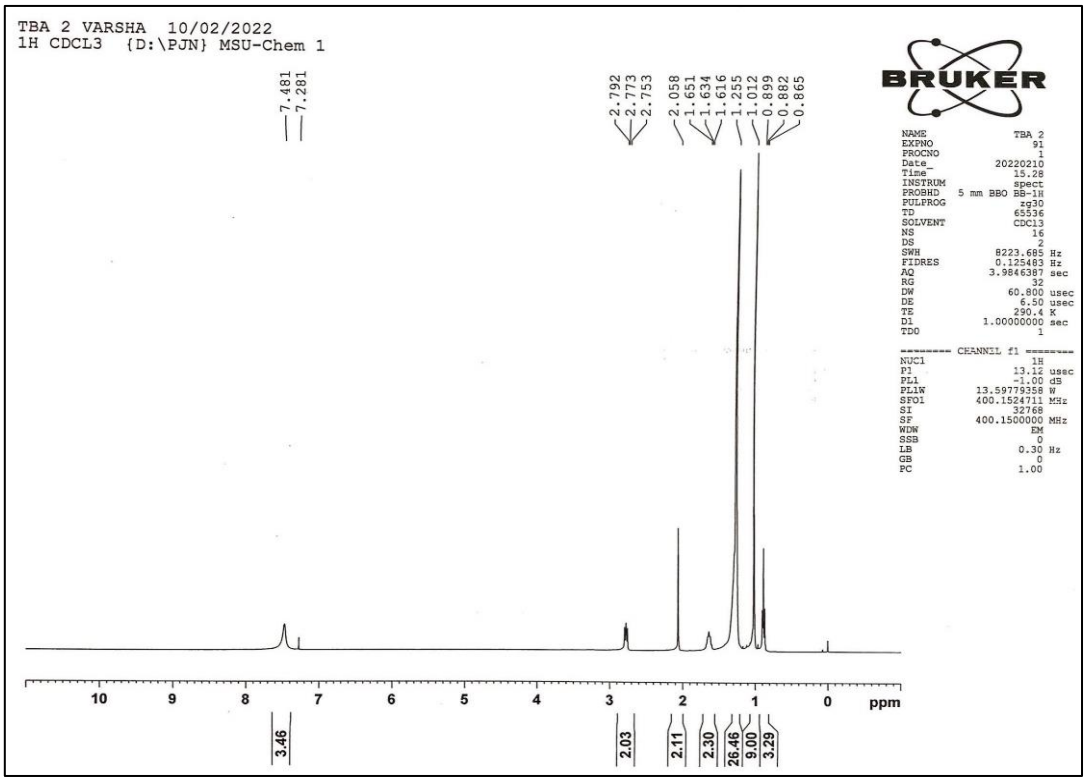
TBA 2 VARSHA 10/02/2022
1H CDCL3 {D:\PJN} MSU-Chem 1
7.481
7.281
2.792
2.773
2.753
2.058
1.651
1.634
1.616
1.255
1.012
0.899
0.882
0.865
BRUKER
NAME TBA 2
EXPNO 91
PROCNO 1
Date_ 20220210
Time 15.28
INSTRUM spect
PROBHD 5 mm BBO BB-1H
PULPROG zg30
TD 65536
SOLVENT CDCl3
NS 16
DS 2
SWH 8223.685 Hz
FIDRES 0.125483 Hz
AQ 3.9846387 sec
RG 32
DW 60.800 usec
DE 6.50 usec
TE 290.4 K
D1 1.00000000 sec
TD0 1
======== CHANNEL f1 ========
NUC1 1H
P1 13.12 usec
PL1 -1.00 dB
PLIW 13.59779358 W
SFO1 400.1524711 MHz
SI 32768
SF 400.1500000 MHz
WDW EM
SSB 0
LB 0.30 Hz
GB 0
PC 1.00
10
9
8
7
6
5
4
3
2
1
0
ppm
3.46
2.03
2.11
2.30
26.46
9.00
3.29

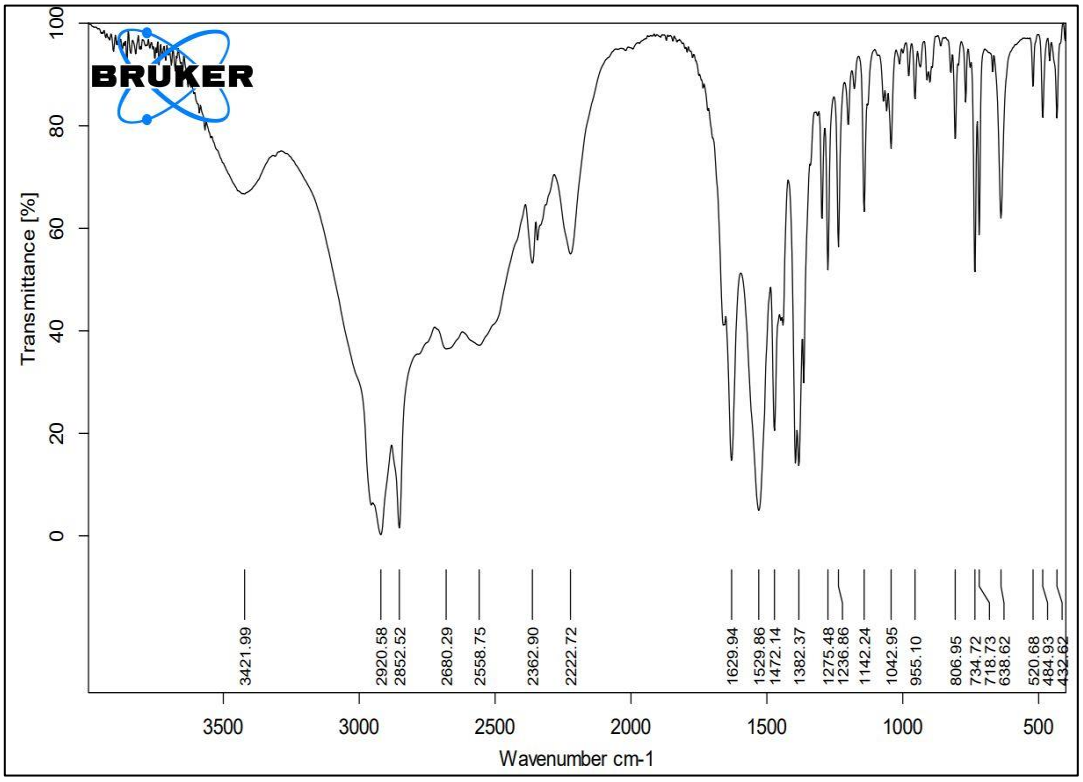
BRUKER
Transmittance [%]
100
80
60
40
20
0
3421.99
2920.58
2852.52
2680.29
2558.75
2362.90
2222.72
1629.94
1529.86
1472.14
1382.37
1275.48
1236.86
1142.24
1042.95
955.10
806.95
734.72
718.73
638.62
520.68
484.93
432.62
3500
3000
2500
2000
1500
1000
500
Wavenumber cm-1

A2B10

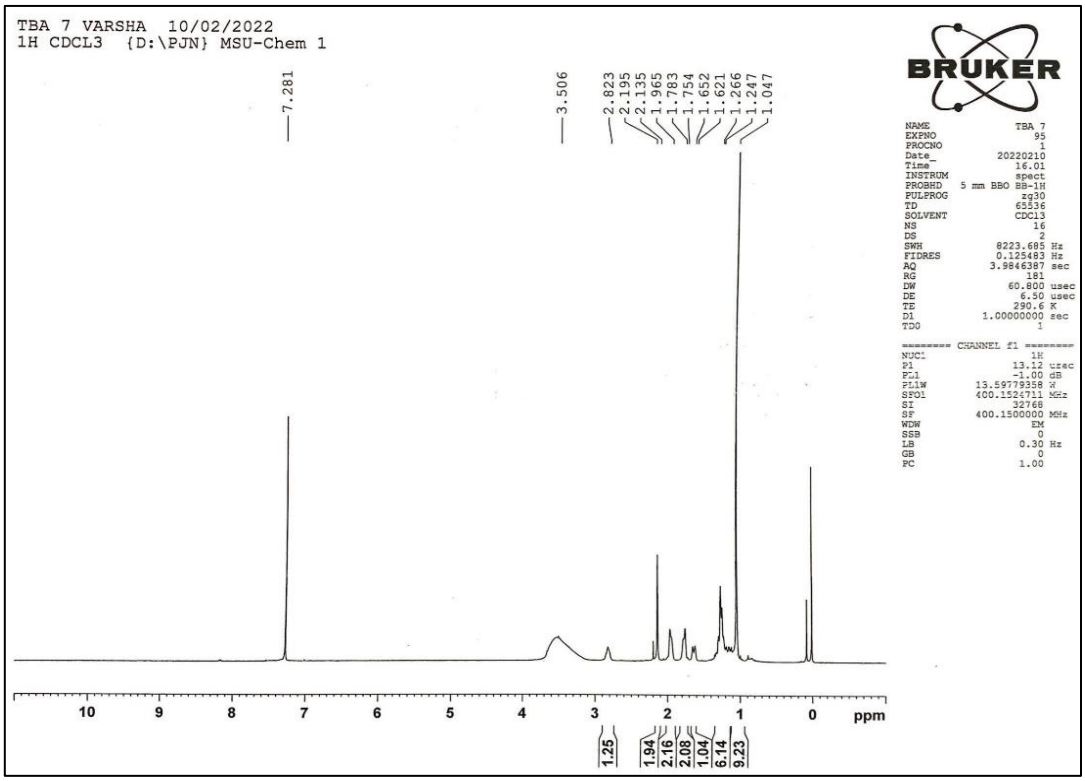
TBA 7 VARSHA 10/02/2022
1H CDCL3 {D:\PJN} MSU-Chem 1
BRUKER
7.281
3.506
2.823
2.195
2.135
1.965
1.783
1.754
1.652
1.621
1.266
1.247
1.047
10 9 8 7 6 5 4 3 2 1 0 ppm
1.25
1.94
2.16
2.08
1.04
6.14
9.23

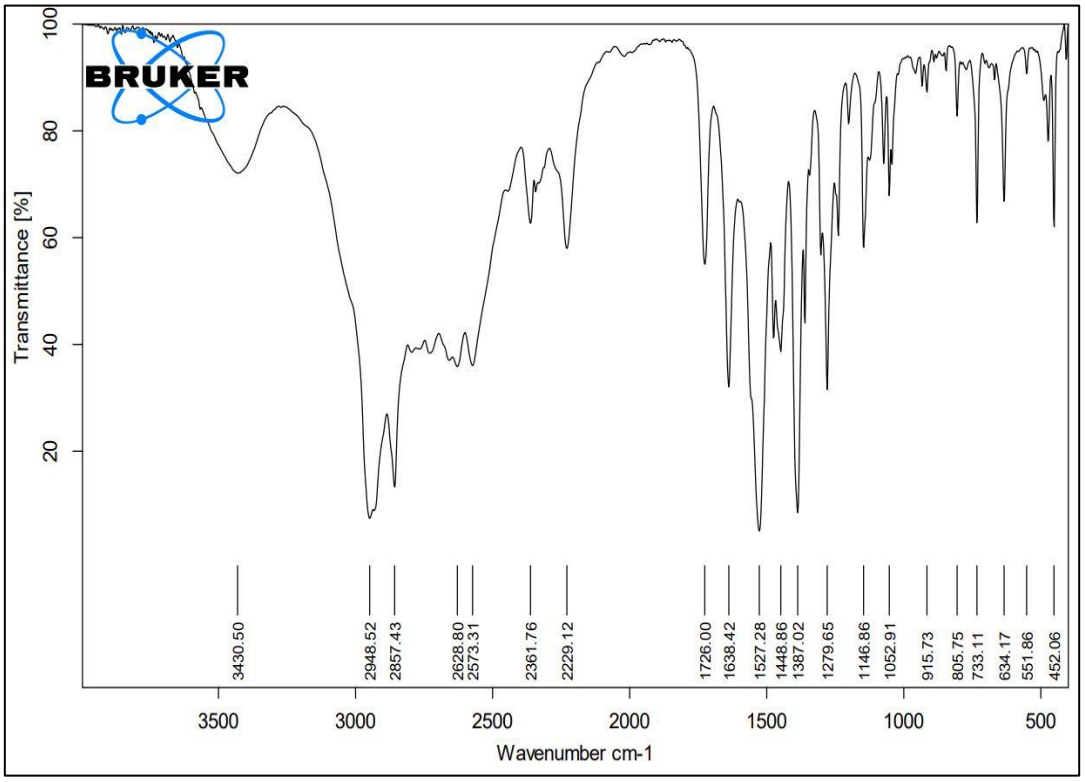
BRUKER
Transmittance [%]
100
80
60
40
20
3430.50
2948.52
2857.43
2628.80
2573.31
2361.76
2229.12
1726.00
1638.42
1527.28
1448.86
1387.02
1279.65
1146.86
1052.91
915.73
805.75
733.11
634.17
551.86
452.06
3500 3000 2500 2000 1500 1000 500
Wavenumber cm-1

A2B11

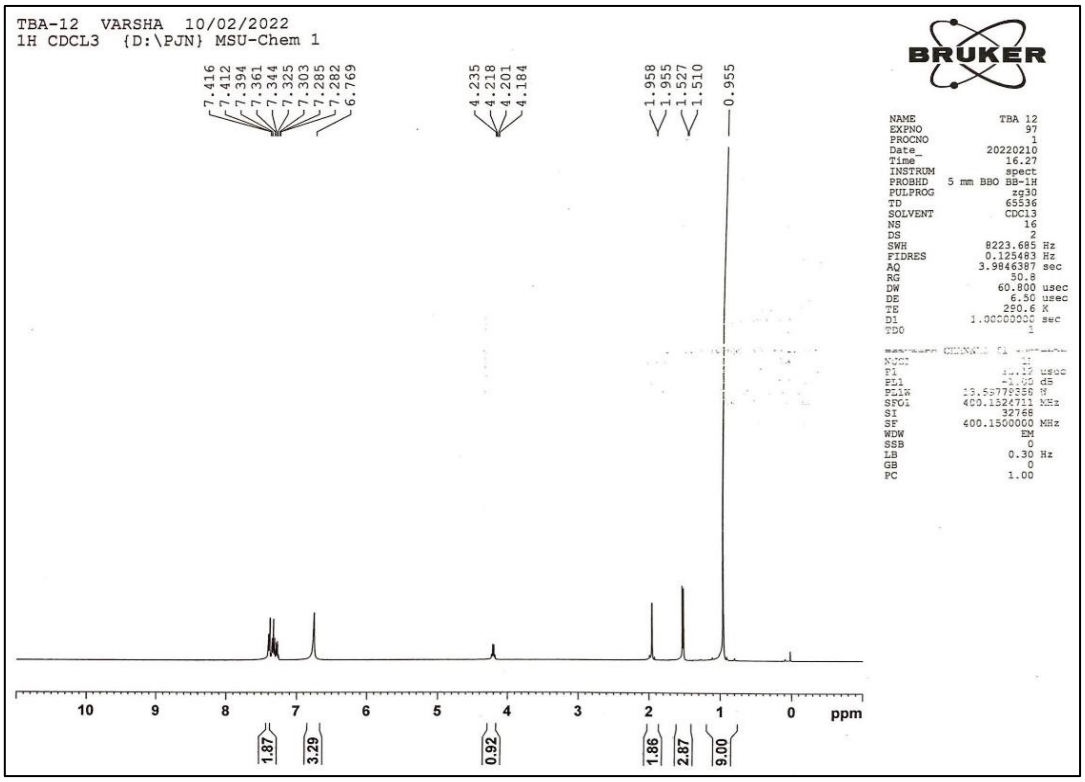
TBA-12 VARSHA 10/02/2022
1H CDCL3 {D:\PJN} MSU-Chem 1
BRUKER
7.416
7.412
7.394
7.361
7.344
7.325
7.303
7.285
7.282
6.769
4.235
4.218
4.201
4.184
1.958
1.955
1.527
1.510
0.955
NAME TBA 12
EXPNO 97
PROCNO 1
Date_ 20220210
Time_ 16.27
INSTRUM spect
PROBHD 5 mm BBO BB-1H
PULPROG zg30
TD 65536
SOLVENT CDCl3
NS 16
DS 2
SWH 8223.685 Hz
FIDRES 0.125483 Hz
AQ 3.9846387 sec
RG 50.8
DW 60.800 usec
DE 6.50 usec
TE 290.6 K
D1 1.00000000 sec
TD0 1
SFO1 400.1524711 MHz
SI 32768
SF 400.1500000 MHz
WDW EM
SSB 0
LB 0.30 Hz
GB 0
PC 1.00
10 9 8 7 6 5 4 3 2 1 0 ppm
1.87
3.29
0.92
1.86
2.87
9.00

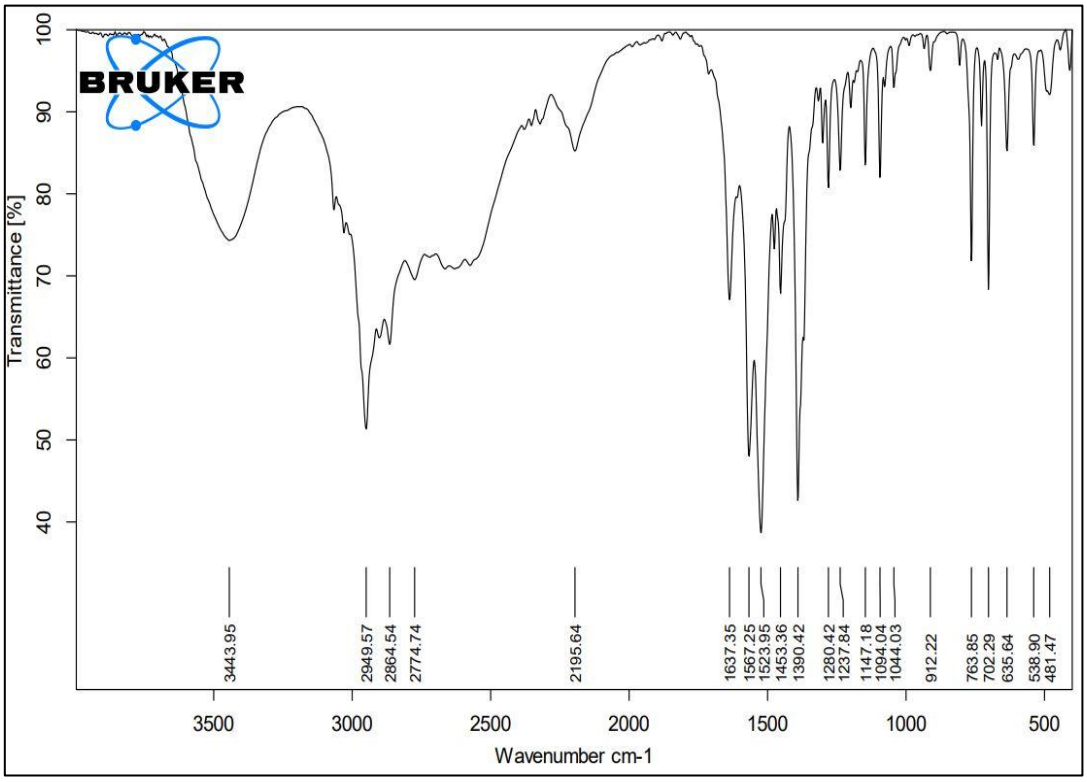
BRUKER
Transmittance [%]
100
90
80
70
60
50
40
3443.95
2949.57
2864.54
2774.74
2195.64
1637.35
1567.25
1523.95
1453.36
1390.42
1280.42
1237.84
1147.18
1094.04
1044.03
912.22
763.85
702.29
635.64
538.90
481.47
3500
3000
2500
2000
1500
1000
500
Wavenumber cm-1

A2B12

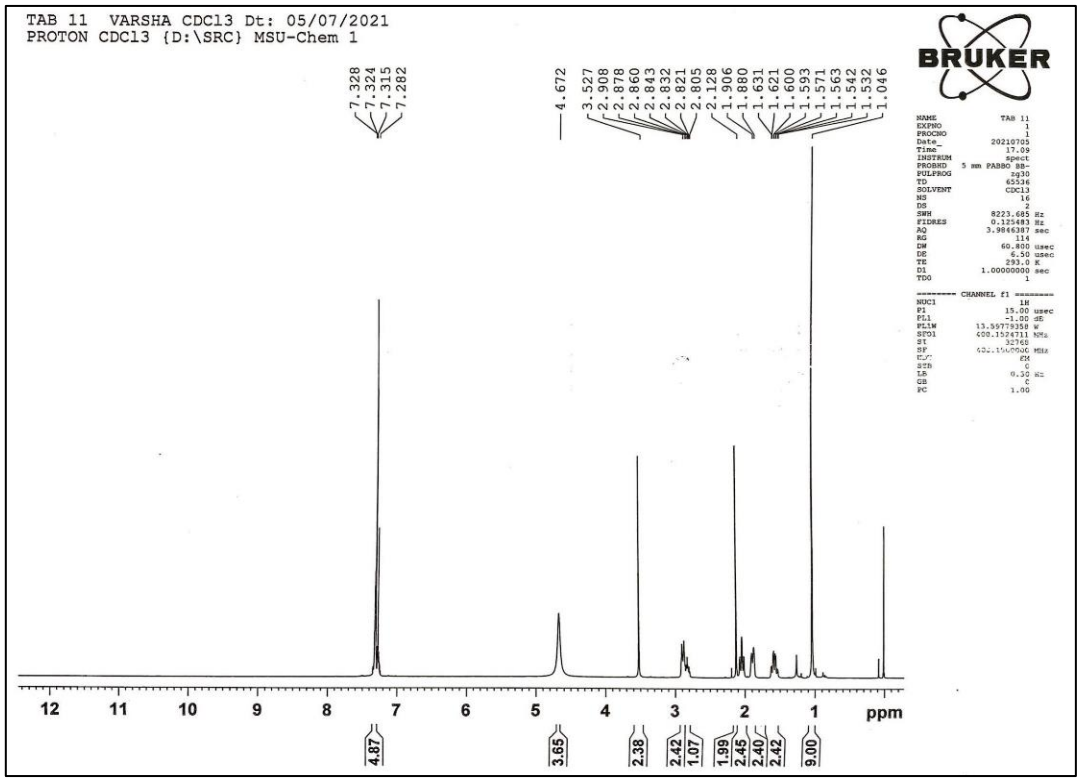
TAB 11 VARSHA CDCl3 Dt: 05/07/2021
PROTON CDCl3 {D:\SRC} MSU-Chem 1
BRUKER
7.328
7.324
7.315
7.282
4.672
3.527
2.908
2.878
2.860
2.843
2.832
2.821
2.805
2.128
1.906
1.880
1.631
1.621
1.600
1.593
1.571
1.563
1.542
1.532
1.046
12 11 10 9 8 7 6 5 4 3 2 1 ppm
4.87
3.65
2.38
2.42
1.07
1.99
2.45
2.40
2.42
9.00

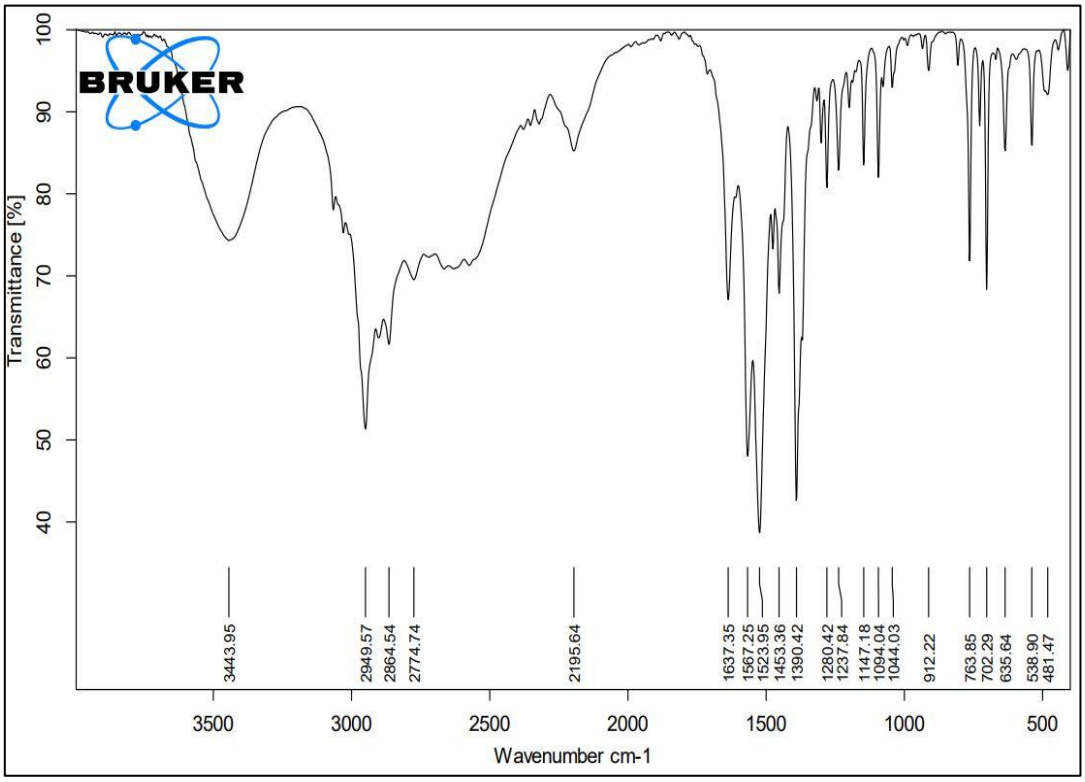
BRUKER
Transmittance [%]
100
90
80
70
60
50
40
3443.95
2949.57
2864.54
2774.74
2195.64
1637.35
1567.25
1523.95
1453.36
1390.42
1280.42
1237.84
1147.18
1094.04
1044.03
912.22
763.85
702.29
635.64
538.90
481.47
3500
3000
2500
2000
1500
1000
500
Wavenumber cm-1

A2B13

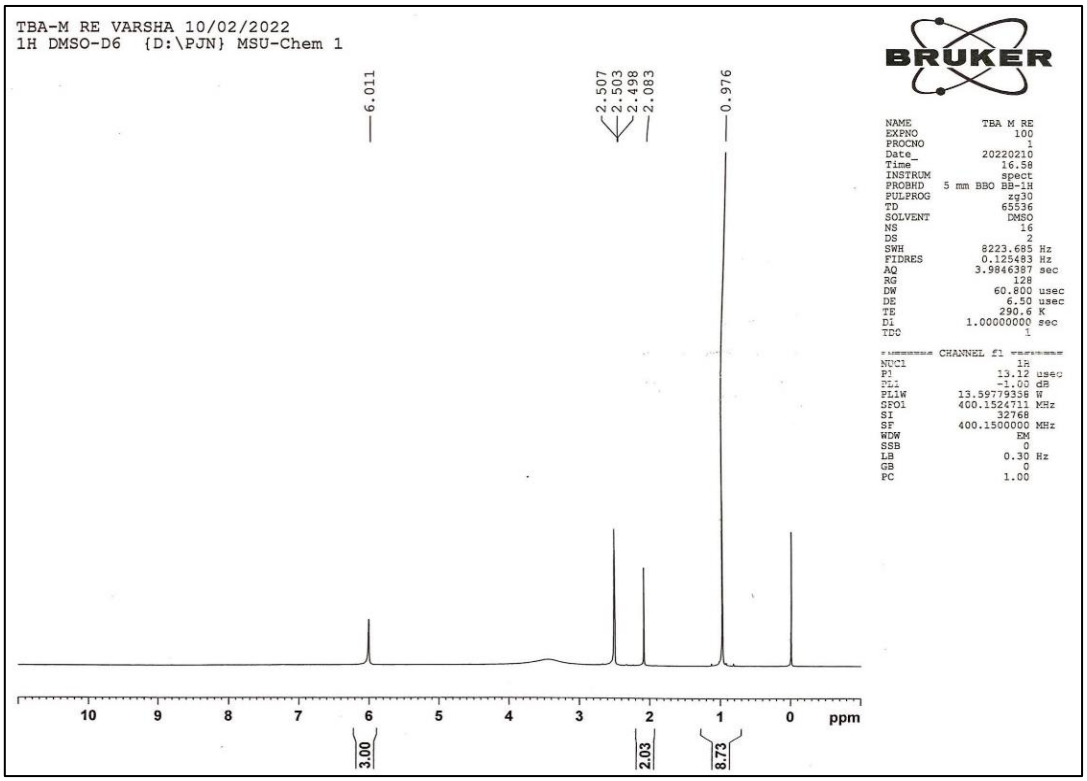
TBA-M RE VARSHA 10/02/2022
1H DMSO-D6 {D:\PJN} MSU-Chem 1
BRUKER
6.011
2.507
2.503
2.498
2.083
0.976
NAME TBA M RE
EXPNO 100
PROCNO 1
Date_ 20220210
Time 16.58
INSTRUM spect
PROBHD 5 mm BBO BB-1H
PULPROG zg30
TD 65536
SOLVENT DMSO
NS 16
DS 2
SWH 8223.685 Hz
FIDRES 0.125483 Hz
AQ 3.9846387 sec
RG 128
DW 60.800 usec
DE 6.50 usec
TE 290.6 K
D1 1.00000000 sec
TDC 1
CHANNEL f1
NUC1 1H
P1 13.12 usec
PL1 -1.00 dB
PL1W 13.59779358 W
SFO1 400.1524711 MHz
SI 32768
SF 400.1500000 MHz
WDW EM
SSB 0
LB 0.30 Hz
GB 0
PC 1.00
10 9 8 7 6 5 4 3 2 1 0 ppm
3.00
2.03
8.73

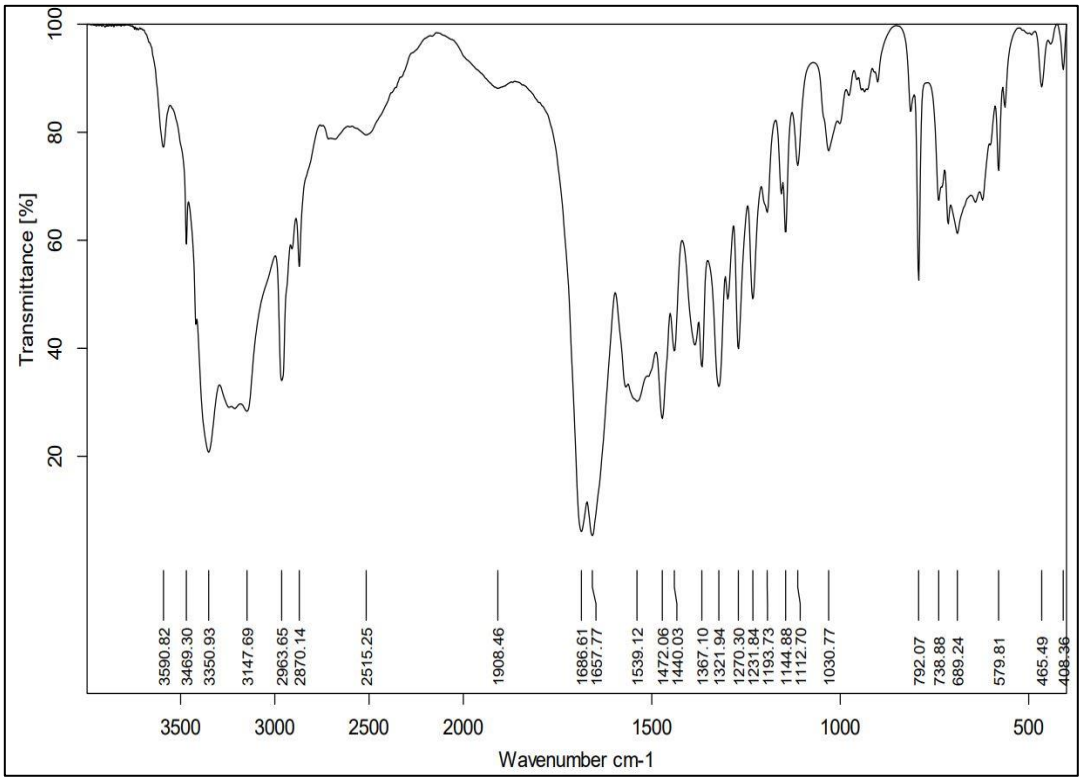
Transmittance [%]
100
80
60
40
20
3590.82
3469.30
3350.93
3147.69
2963.65
2870.14
2515.25
1908.46
1686.61
1657.77
1539.12
1472.06
1440.03
1367.10
1321.94
1270.30
1231.84
1193.73
1144.88
1112.70
1030.77
792.07
738.88
689.24
579.81
465.49
408.36
3500
3000
2500
2000
1500
1000
500
Wavenumber cm-1

●

This page intentionally left blank.